TABLE OF CONTENTS

Nanoporous silica-based materials for sorption of pharmaceuticals and biomolecules

Karolina Gdula[a] and Mariusz Barczak[b]

Department of Theoretical Chemistry, Faculty of Chemistry,
Maria Curie-Skłodowska University
Maria Curie-Skłodowska Sq. 3, 20-031 Lublin
[a]karolina.gdula@poczta.umcs.lublin.pl
[b]mbarczak@poczta.umcs.lublin.pl

Our concern in this paper is to review four kinds of mesoporous silica materials which can be used as potential sorbents for pharmaceuticals. It is known that a continuous development of science, medicine and food industry has an effect on contamination of the natural environment. Moreover, many impurities, such as drugs, vitamins or proteins etc., which get into environment from urban and hospital wastes, can also influence on human organisms. Thus, there is a need to control an amount of those compounds, especially in the natural waters and wastewaters [1-4]. In this work, we present four types of silica materials which can be helpful in water purification by using adsorption process.

Keywords: nanoporous silica-based materials, adsorption, pharmaceuticals, biomolecules, environmental protection

1. INTRODUCTION

Nowadays, an increased interest of the adsorption process of pharmaceuticals and biomolecules, such as drugs, enzymes or proteins, from solutions onto solid surfaces is observed [5,6]. It is due to their increasing amount in the natural environment and human bodies. The

adsorption process is taking into account due to its promising results in water purification. Above-mentioned biocompounds have a huge influence on living organisms. Beyond the positive effects they can also (in high concentrations) cause damage in some organs or tissues, e.g. some proteins can facilitate adsorption of fibrous proteins causing adverse biological consequences [7-9], such as increased blood clotting or heart disease [10]. Therefore, it is necessary to control the amount of those biocompounds and other pharmaceuticals in the surrounding hydro- and biosphere. Thus, the new methods and new materials as potential sorbents have been searched. This is due to the fact that efficient adsorption techniques have huge commercial importance and find applications in different fields, such as biotechnology, biocatalysis, medicine, and controlled drug delivery systems.

Nanoporous Silica-based Materials (NSM) are attractive as adsorbents due to their simplicity of synthesis, facility of surface functionalization and biocompatibility. Each group have a different particle morphology, porous structure and surface composition. These above-mentioned groups of nanoporous silica materials are:

– OMS – Ordered Mesoporous Silicas,
– MCF – Meso-Cellular Silica Foams,
– ASX – Amorphous Silica Xerogels,
– PSN – Porous Silica Nanotubes.

The ordered mesoporous silica materials were synthesized in early 90s by Mobil researches [11, 12]. This group of silicas was named as M41S and it was the first group belonging to the other, bigger group – OMS. This discovery initiated the beginning of interest of mesoporous silicas, which has led to further studies on MCF, ASX and PSN.

In the next paragraph, the structural properties and surface chemistry of four of the above-mentioned materials, in related to their sorption properties, will be described.

2.   GENERAL CONSIDERATIONS

The organosilicas are considered as good materials for adsorption, immobilization, separation and encapsulation of pharmaceuticals for many reasons. Silica is safe and non-toxic relative to the living organisms and resistant to microbial attack, and not swell in water like many organic polymers. It is also chemically and mechanically stable compound. Moreover, excellent properties of nanoporous silica materials, such as

high specific surface area, high total pore volume and well defined pores with narrow pore size distribution, are very attractive for the adsorption of pharmaceuticals and other biocompounds. Due to ordered porous structure physical adsorption onto nanoporous silica surface is possible. However, to make adsorption process more efficient the surfaces of sorbents have to be modified with basic (amine or aminopropyl [13-15]) or acid (thiol [14-17]) functional groups by co-condensation [18, 19] or post-grafting [20] processes. In this paragraph, four of the above-mentioned groups of NMS in regard to their use as efficient sorbents for pharmaceuticals and biomolecules, will be described.

Consideration on OMS will be introduced only in description of MCM-41 and SBA-15. MCM-41 was synthesized in 1992 by a group of scientists employed by the Mobile Corporation [11, 12]. This was the first synthesized silica-based material characterized by hexagonally ordered structure with cylindrical mesopores without any connections between them. Its specific surface are reaches 1200 m^2/g, while average pore size and total pore volume reach 10 nm and 1.2 cm^3/g, respectively [11]. SBA-15 material was synthesized in 1998 [21,22] by American's researches at Santa Barbara's University. SBA-15 is characterized by ordered structure, with high specific surface area range 690-1040 m^2/g, pore size and total pore volume reach 30 nm and 2.5 cm^3/g, respectively [22]. SBA-15 shows hexagonal arrays of cylindrical mesopores connected by micropores. Both, MCM-41 and SBA-15, are the most popular silica materials used in many fields of industry, such as biotechnology, biocatalysis, medicine, biosensors and bioreactors and controlled drug delivery systems [23, 24].

It is known that the sorption capacities strongly depend on number of sorption sites and pores size. Thus, such porous structure makes MCM-41 and SBA-15 very attractive materials for capturing (or immobilizing) pharmaceuticals and biomolecules. Diaz et al. [25] showed that the sorption capacities of various enzymes, cytochrome c, papain and trypsin onto MCM-41 depend on the molecule size. Anderson co-workers [26] proved that the degree of ibuprofen loading was strongly dependent on the specific surface area and the pore diameter of the host matrix. The bigger surface area is the most effective is adsorption process [27]. Qu et al. tested the dependence between average pore size and efficiency of captopril adsorption onto SBA-15 and MCM-41 [28]. The obtained results showed that the bigger pores are the higher is amount of adsorbed biomolecule onto silicas.

A lot of pharmaceuticals have been tried to capture by pristine MCM-41 and SBA-15 materials. For example, Wang et al. [29] used above-mentioned materials as suitable sorbents for immobilizing catalase, while Doadrio co-workers tested the mesoporous silica SBA-15 for adsorption of gentamicin [30] and erythromycin [31]. Vallet-Regi et al. [32] adsorbed antibiotic amoxicillin onto pristine SBA-15 and discovered that the sorption capacities depend on pH and amoxicillin concentration.

It is worth to mention, that for pure SBA-15 only silanol groups exist on its surface. To make it more effective for capturing biocompounds, the surface modification with various functional groups should be done [33]. Recently, there is observed a huge interest of use functionalized SBA-15 as efficient sorbents for biomolecules from liquid phase. Nanoporous silicas have been tested as adsorbents for amino acids and proteins. For example, Gao and co-workers [34] examined SBA-15 and modified SBA-15 as potential sorbents for arginine, glutamic acid, phenylalanine, leucyne and demonstrated that the sorption capacities strongly depend on pH and nature of particular amino acids. O'Connor et al. [35] proved that adsorption of amino acid onto MCM-41 also depends on ionic strength. MCM-41 materials were used for the immobilizing glutamic acid, phenylalanine and lysine by Ernst et al. [36,37]. Zhao et al. [38] used functionalized SBA-15 materials for separation of proteins by using chromatography technique. Deere et al. [39,40]. Washmon-Kriel et al. [41] and Humphrey et al. [42] examined different mesoporous sorbents as potential materials for capture cytochrome c. Vinu and co-workers investigated the influence of the solution pH on the adsorption of cytochrome c [43,44]. Other biocompounds, such as conalbumin, bovine serum albumin, trypsin, ovalbumin, myoglobin and β-lactoglubulin were also successfully adsorbed onto SBA-15 and thiol-functionalized SBA-15 [42]. Song et al. used pristine SBA-15 and amine-functionalized [45] SBA-15 as efficient sorbents for ibuprofen and bovine serum albumin. There was observed a huge difference on sorption capacities between pristine and modified adsorbents. The better sorption capacities are obtained for modified silica materials. Ibuprofen was also adsorbed onto MCM-41 [26,45-47] and Al-modified MCM-41 [48]. The adsorption of riboflavin (vitamin B2) was studied by Kisler et al. [49] and the obtained adsorption capacities were satisfied. Bilirubin adsorption process was tested, both onto pristine and amine-modified SBA-15 [13,50]. The obtained results showed that the better adsorption capacities were observed onto SBA-15 with amine groups.

The OMS is the best known and the most often used (in a broad range) group of silica sorbents. Their practical applications in many fields are still being extended.

MCFs were synthesized by Schmidt-Winkel et al. in 2000 [51]. The route of the synthesis is very similar to synthesis of SBA-15, but in this case pore-expander is involved. The most popular used expanders are 1,3,5-trimethylbenzene (TMB) and 1,3,5-triethylbenzene (TEB). Thus, MCFs have larger pore volumes than SBA-15. MCFs consist of spherical voids (22-42 nm in diameter) interconnected by "windows" of 10 nm with tunable sizes [51-53]. Such structure of pores can be described as "ink-bottled" [54]. Their surfaces areas reach 800 m^2/g and strongly depend on aging time and concentration of HCl [51, 54].

Specialist literature reports that Meso-Cellular Silica Foams can be successfully used as efficient sorbents for L-tryptophan, lysozyme from chicken egg and bovine serum albumin (BSA) [54-56]. Russo et al. [57] investigated the influence of surface functionalization on adsorption capacities of BSA and lysozyme onto MCFs. Pandaya et al. [58] carried out immobilization of α-amylase onto MCM-41, SBA-15 and MCF. The obtained results showed that adsorption onto SBA and MCM takes place on external, while onto MCF on internal, pores. Modified Fe_3O_4-MCF was used as potential sorbents for cytochrome c, BSA and aspirin by Huang and co-workers and Yang et al. [59, 60]. The obtained adsorption capacities were bigger for BSA than aspirin. BSA was also adsorbed by Sezoes et al. [61]. Zhao et al. [62] used amine-modified MCF for the immobilization of penicillin G acylase (PGA). Ibuprofen was also adsorbed onto pristine and polyizoprene (PI) modified MCF by Zhu et al. [63]. The obtained results clearly showed that better sorption capacities have been received for PI-MCF. Laccase [64, 65], lactase and papain [66] were also immobilized on MCF.

ASXs in contrast to OMSs are characterized by well-developed but disordered porous structure. To synthesis Amorphous Silica Xerogels the sol-gel method connected with slowly evaporation of solvent is employed. Their specific surface areas range from 50 to 1000 m^2/g obtained by Kumara et al. [67]. The pore size and total pore volume obtained by Kumara et al. ranged from 1 to 50 nm and 0.2-0.4. cm^3/g, respectively. L. A. de Miranda et al. investigated the influence of extraction processes amount on porous structure of obtained xerogels [68]. They demonstrated that with increasing number of extraction total pore volume and pore size also increase. C.A. Aerts and co-workers [69] examined how silica source and type of solvent influence on porous

structure of final material. They tested as-obtained materials as potential sorbents for ibuprofen. Tortajada et al. [70] successfully adsorbed lysozyme and α-L-arabinofuranosidase onto ASXs.

The Porous Silica Nanotubes (PSNs) have structure similar to carbon nanotubes [71] and pore diameter ranging 10-20 nm. The first Porous Silica Nanotubes were synthesized by Nakamura and co-workers in 1995 [72]. Like other silica materials, PSNs are also characterized by high hydrothermal resistance and biocompatibility. Their specific surface area can reach 800 m^2/g [73] and obtained pore size reach 20 nm [74]. The porous structure of PSN was precisely described by Wang et al. [75]. They obtained PSN with specific surface area reach to 1000 m^2/g, with total pore volume and average pore size 0.92 cm^3/g and 3.5 nm, respectively.

PSN is a relatively new group of silica materials and their potential applications as sorbents are not sufficient. There are only a few papers regard to adsorption biomolecules onto PSN. For example, Yang and co-workers [76] tested PSN in control doxorubicin release, while Ding et al. [77] immobilized lysozyme onto PSN. Xiao and co-workers [73] used PSNs in immobilization of glucose oxidase.

There is still a large gap in professional literature about MCFs, ASXs and PSNs as efficient sorbents for pharmaceuticals and other biocompounds. Thus, a lot of scientific groups have focused on those materials due to their attractive properties which could be used in sorption processes.

Parameters of porous structure of obtained materials depend on synthesis conditions, e.g. temperature, time of aging, pore expander addition etc. The better morphology, chemistry composition and porous structure of sorbents are the more effective is adsorption process. Therefore, there is a need to control above-mentioned parameters to obtain efficient materials which can be successfully used in adsorption process from the liquid phase. The capture properties with regards to pharmaceuticals will differ, because each of these groups can have different particles morphology, porosity and chemistry of the surface. The last one is the most important factor influence on the efficiency of the adsorption process of various pharmaceuticals and biomolecules onto NSMs structure.

3. CONCLUSIONS

An overview of organosilica materials with emphasis of their use as efficient sorbents for environmental pollutants, such as pharmaceuticals and biomolecules has been provided. Recent advances make possible to create selective sorbents by controlling pore size and tailoring surface chemistry by modifying the surface with the appropriate functional group. Thus, it is possible to design the desired properties of the final materials for a targeted application.

Adsorption of bioactive compounds becomes necessary due to their increasing amounts in the natural environment. Moreover, the biocompounds and pharmaceuticals are considered as new impurities which have to be removed from waters and wastewaters. Therefore, it is necessary to control their concentration in hydrosphere, biosphere, and so on. It is also very important to develop new methods which will be helpful in purification of the above-mentioned fields.

Summing up, porous structure, chemistry surface and other properties makes NSM good sorbents of biomolecules and pharmaceuticals.

ACKNOWLEDGEMENTS

REFERENCES

[1]   J. Tolls, *Environmental Science and Technology*, **35**, 3397, (2001).

[2]   A. Joss, F. Keller, A. Alder, A. Goebel, C. McArdel, T. A. Ternes and H. Siegrist, *Water Research*, **39**, 3139, (2005).

[3]   B. Halling Sorensen, S. Nors Nielsen, P.F. Lanzky, F. Ingersiev, H.C. Holten Lutzheft and S.E. Jorgensen, *Chemosphere*, **36**, 357, (1997).

[4]   C. Tixier, H.P. Singer, S. Oellers and S.R. Müller, *Environmental Science and Technology*, **37**, 1061, (2003).

[5]   T.X. Bui and H. Choi, *Journal of Hazardous Materials*, **168**, 602, (2009).

[6]   C.H. Lee, T.S. Lin and C.Y. Mou, *Nano Today*, **4**, 165, (2009).

[7]   C. Sandu and R.K. Singh, Food Technology, **45**, 84, (1991).

[8]   J.A. Hubbel, *Biotechnology*, **13**, 565, (1995).

[9]   K. Ishihara, H. Oshida, Y. Endo, T. Ueda, A. Watanabe and N. Nakabayashi, *Journal of Biomedical Materials Research*, **26**, 1543, (1992).

[10]   M. Feng, A.B. Morales, T. Beugeling, A. Bantjes, K. Vanderwerf, G. Gosselink, B. Degrooth and J. Greve, *Journal of Colloid and Interface Science*, **177**, 364, (1996).

[11]   C.T. Kresge, M.E. Leonowicz, W.J. Roth, J.C. Vartuli and J.S. Beck, *Nature*, **359**, 710, (1992).

[12]   J.S. Beck, J.C. Vartuli, J.W. Roth, M.E. Leonowicz, C.T. Kresge, K.D. Schmitt, C.T.-W. Chu, D.H. Olson, E.W. Sheppard, S.B. McCullen, J.B. Higgins and J.L. Schlenker, *Journal of the American Chemical Society*, **114**, 10834, (1992).

[13]   T. Tang, Y. Zhao, Y. Xu, D. Wu, J. Xu and F. Deng, *Applied Surface Science*, **257**, 6004, (2011).

[14]   M. Barczak, A. Dąbrowski, S. Pikus, J. Ryczkowski, P. Borowski and M. Kozak, *Adsorption*, **16**, 457, (2010).

[15]   E.I. Basaldella and M.S. Legnoverde, *Journal of Sol-Gel Science and Technology*, **56**, 191, (2010).

[16]   A. Walcarius, M. Etienne and B. Lebeau, *Chemistry of Materials*, **15**, 2161, (2003).

[17]   A.M. Liu, K. Hidajat, S. Kawi and D.Y. Zhao, *Chemical Communications*, 1145, (2000).

[18]   S.L. Burkett, S.D. Sims and M. Mann, *Chemical Communications*, **11**, 1367, (1996).

[19]   A.S. Maria Chong and Z.S. Zhao, *Journal of Physical Chemistry B*, **107**, 12650, (2003)

[20]   X.S. Zhao and G.Q. Lu, *Journal of Physical Chemistry B*, **102**, 1556, (1998).

[21]   D.Y. Zhao, J.L. Feng, Q.S. Huo, N. Melosh, G.H. Fredrickson, B.F. Chmelka and G.D. Stucky, *Science*, **279**, 548, (1998).

[22]   D.Y. Zhao, Q.S. Huo, J.L. Feng, B.F. Chmelka and G.D. Stucky, *Journal of the American Chemical Society*, **120**, 6024, (1998).

[23]   A. Popat, S.B. Hartono, F. Stahr, J. Liu, S.-Z. Qiao, G.-X. Lu, *Nanoscale*, **3**, 2801, (2011).

[24]   M. Hartmann, *Chemistry of Materials*, **17**, 4577, (2005).

[25]   J.F. Diaz and K.J. Balkus, *Journal of Molecular Catalysis B*, **2**, 115, (1996).

[26] J. Andersson, J. Rosenholm, S. Areva and M. Linden, *Chemistry of Materials*, **16**, 4160, (2004).

[27] M. Vallet-Regí, F. Balas and D. Arcos, *Mesoporous Materials for Drug Delivery*, Angew. Chem. Int. Ed. 2007, 46, 7548 – 7558

[28] F. Qu, G. Zhu, S. Huang, S. Li, J. Sun, D. Zhang and S. Qiu, *Microporous and Mesoporous Materials*, **92**, 1, (2006).

[29] Y. Wang and F. Caruso, *Chemistry of Materials*, **17**, 953, (2005).

[30] A.L. Doadrio, E.M.B. Sousa, J.C. Doadrio, J. Perez-Pariente, I. Izquierdo-Barba and M. Vallet-Regi, *Journal of Controlled Release*, **97**, 125, (2004).

[31] J.C. Doadrio, E.M.B. Sousa, I. Izquierdo-Barba, J. Perez-Pariente and M. Vallet-Regi, *Journal of Materials Chemistry*, **16**, 462, (2006).

[32] M. Vallet-Regi, J.C. Doadrio, A.L. Doadrio, I. Izquierdo-Barba and J. Perez-Pariente, *Solid State Ionics*, **172**, 435, (2004).

[33] J.C. Doadrio, E.M.B. Sousa, I. Izquierdo-Barba, J. Perez-Pariente and M. Vallet-Regi, *Journal of Materials Chemistry*, **16**, 462, (2006).

[34] Q. Gao, W. Xu, Y. Xu, D. Wu, Y. Sun, F. Deng and W. Shen, *The Journal of Physical Chemistry B*, **112**, 2261, (2008).

[35] A.J. O'Connor, A. Hokura, J.M. Kisler, S. Shimazu, G.W. Stevens, Y. Komatsu, *Separation and Purification Technology*, **48**, 197, (2006).

[36] S. Ernst, M. Hartmann and S. Munsch, *Studies in Surface Science and Catalysis*, **135**, 4566, (2001).

[37] S. Munch, M. Hartmann and S. Ernst, *Chemical Communications*, 1978, (2001).

[38] J. Zhao, F. Gao, Y. Fu, W. Jin, P. Yang and D.D. Zhao, *Chemical Communications*, **7**, 752, (2002).

[39] J. Deere, E. Magner, J.G. Wall and B.K. Hodnett, *Chemical Communications*, 465, (2001).

[40] J. Deere, E. Magner, J.G. Wall and B.K. Hodnett, *Studies in Surface Science and Catalysis*, **135**, 3694, (2001).

[41] L. Washmon-Kriel, V.L. Jimenez and K.J. Balkus Jr., *Journal of Molecular Catalysis B*, **10**, 453, (2000).

[42] H.H.P. Humphrey, C.H. Botting, N.P. Botting and P.A. Wright, *Physical Chemistry Chemical Physics*, **3**, 2983, (2001).

[43] [43] A. Vinu, V. Murugesan, O. Tangerman and M. Hartmann, *Chemistry of Materials*, **16**, 6056, (2004).

[44] A. Vinu, C. Sterb, V. Murugesan and M. Hartmann, *The Journal of Physical Chemistry B*, **107**, 8297, (2003).

[45] M. Vallet-Regi, A. Ramila, R.P. del Real and J. Perez-Pariente, *Chemistry of Materials*, **13**, 308, (2001).

[46] B. Munoz, A. Ramila, J. Perez-Pariente, I. Diaz and M. Vallet-Regi, *Chemistry of Materials*, **15**, 500, (2003).

[47] Y.F. Zhu, J.L. Shi, H.R. Chen, W.H. Shen and X.P. Dong, *Turret Materials*, **84**, 218, (2005).

[48] G. Cavallaro, P. Pierro, F.S. Palumbo, F. Testa, L. Pasqua and R. Aiello, *Drug Delivery*, **11**, 41, (2004).

[49] J.M. Kisler, A. Dahler, G.W. Stevens and A.J. O'Connor, *Microporous Mesoporous Materials*, **44-45**, 769, (2001).

[50] T. Tang, X. Li, Y. Xu, D. Wu, Y. Sun, J. Xu and F. Deng, *Colloids and Surfaces B*, **84**, 571, (2011).

[51] P. Schmidt-Winkel, W.W. Lukens Jr., P. Yang, D.I. Margolese, J.S. Lettow and J.Y. Ying, *Chemistry of Materials*, **12**, 686, (2000).

[52] P. Schmidt-Winkel, W.W. Lukens Jr., D. Zhao, P. Yang, B.F. Chmelka and G.D. Stucky, *Journal of the American Chemical Society*, **121**, 254, (1999).

[53] J.S. Lettow, Y.J. Han, P. Schmidt-Winkel, P. Yang, D. Zhao, G.D. Stucky and J.Y. Ying, *Langmuir*, **16**, 8291, (2000).

[54] J. Kim, R.J. Desch, S.W. Thiel, V.V. Guliants and N.G. Pinto, *Microporous and Mesoporous Materials*, **149**, 60, (2012).

[55] J. Kim, R.J. Desch, S.W. Thiel, V.V. Guliants and N.G. Pinto, *Journal of Chromatography A*, **1218**, 7796, (2011).

[56] J. Kim, J. Desch, S.W. Thiel, V.V. Guliants and N.G. Pinto, *Journal of Chromatography A*, **1218**, 6697, (2011).

[57] P.A. Russo, M.M.L. Ribeiro Carrott, P.A.M. Mourao and P.J.M. Carrott, *Colloids and Surfaces A*, **386**, 25, (2011).

[58] P.H. Pandya, R.V. Jasra, B.L. Newalkar and P.N. Bhatt, *Microporous and Mesoporous Materials*, **77**, 67, (2005).

[59] S. Huang, Ch. Li, Zi. Cheng, Y. Fan, P. Yang, C. Zhang, K. Yang and J. Lin, *Journal of Colloid and Interface Science*, **376**, 312, (2012).

[60] J. Yang, F. Zhang, W. Li, D. Gu, D. Shen, J. Fan, W. Zhang and D. Zhao, *Chemical Communications*, **50**, 713, (2014).

[61] F. Sezoes, M.M.L. Ribeiro Carrott, P.A.M. Mourao and P.J.M. Carrott, *Adsorption Science & Technology*, **28**, 777, (2011).

[62] J. Zhao, Y. Wang, G. Luo and S. Zhu, *Bioresource Technology*, **101**, 7211, (2010).

[63] S. Zhu, D. Zhang and N. Yang, *Journal of Nanoparticle Research*, **11**, 561, (2009).

[64] M. Zhao, Y. Wang, Z. Liu, D. Cui and X. Bian, *Journal of Macromolecular Science, Part A*, **48**, 447, (2011).

[65] J. Bryjak, K. Szymańska and A.B. Jarzębski, *Chemical and Process Engineering*, **33**, 611 (2012).

[66] Z. Gu, Y. Han, F. Pan, X. Wang, D. Weng and S. Zhou, *Materials Science and Engineering*, **610**, 109, (2009).

[67] D. Kumar, K. Schumacher, C. du Fresne von Hohenesche, M. Grün and K.K. Unger, *Colloids and Surfaces A*, **187-188**, 109, (2001).

[68] L.A. de Miranda, N.D.S. Mohallemb and Welington F. de Magalhaes, *Applied Surface Science*, **252**, 3466, (2006).

[69] C.A. Aerts, E. Verraedt, R. Mellaerts, A. Depla, P. Augustijns, J. Van Humbeeck, G. Van den Mooter and J.A. Martens, *The Journal of Physical Chemistry C*, **111**, 13404, (2007).

[70] M. Tortajada, D. Ramon, D. Beltran and Pedro Amoros, *Journal of Materials Chemistry*, **15**, 3859, (2005).

[71] Z.H. Yin, X. Liu and Z.X. Su, Bulletin of Material Science, 33, 351, (2010).

[72] H. Nakamura and Y. Matsui, *Journal of the American Chemical Society*, **117**, 2651, (1995).

[73] Q.Xiao, X. Tao and J.Chen, *Industrial & Engineering Chemistry Research*, **46**, 459, (2007).

[74] X. Pe, J. Zhang, S. Wang, Y. Chen, X. Wu, Y. Li, B. Li and Y. Yang, *Journal of Sol-Gel Science and Technology*, **50**, 397, (2009).

[75] J.X. Wang, L.X. Wen, R.J. Liu and J.F. Chen, *Journal of Solid State Chemistry*, **178**, 2383, (2005).

[76] Y. Yang, X, Tao, Q. Hou, Y. Ma, X. Chen and J. Chen, *Acta Biomaterialia*, **6**, 3092, (2010).

[77] H. Ding, L. Shao, R. Liu, Q. Xiao and J. Chen, *Journal of Colloid and Interface Science*, **290**, 102, (2005).

CURRICULA VITAE

Karolina Gdula was born in Lubartów in Poland in 1988. She studied Chemistry of Bioactive Substances and Cosmetics at Maria Curie-Skłodowska University in Lublin. In 2012 she obtained M.Sc. degree based on master thesis entitled: "Synthesis and characterization of hybrid materials composed of silica and nanotubes" (supervisor: dr Mariusz Barczak). During her studies she held a short-term (4 months) stay in the Faculty of Physics, in the Granada University (Spain). After graduation from the Faculty of Chemistry, Maria Curie-Skłodowska University in August 2012, she started Ph.D. studies in Department of Theoretical Chemistry, M.C.S. University in Lublin. Since 2012 she is a member of the Polish Chemical Society.

Mariusz Barczak was born in Świdnik in Poland in 1978. After graduation from the Faculty of Chemistry, Maria Curie-Skłodowska University in 2004, he was employed in the Department of Theoretical Chemistry as an assistant. In 2007 he obtained Ph.D. degree on the basis of desideration entitled: "Synthesis, characterization and adsorption properties of bridged polysilsesquio-xanes function-nalized with amine and thiol groups". Since 2007 he has been held a position of adjunct in the Department of Theoretical Chemistry, M.C.S. University. He is a co-author over 40 papers. Main fields of scientific interest are: synthesis, functionalization and of porous silica, carbon and hybrid nanomaterials and their application as sorbents of heavy metal ions, phenols and biomolecules.

ANNALES
UNIVERSITATIS MARIAE CURIE-SKŁODOWSKA
LUBLIN – POLONIA

Two-dimensional structures composed of cross-shaped molecules adsorbed on solid surfaces – a computational model

Adam Kasperski[a] and Paweł Szabelski[b]

Department of Theoretical Chemistry, Faculty of Chemistry,
Maria Cure-Sklodowska University
3 Maria Curie-Slodowska Sq., 20-031 Lublin, Poland
[a]*adam@vega.umcs.lublin.pl*
[b]*szabla@vega.umcs.lublin.pl*

      The ability of simple molecular building blocks to form extended ordered patterns by adsorption and self-assembly on solid substrates is an advantageous property that has been widely used to create nanostructured surfaces. In this contribution we demonstrate how the lattice Monte Carlo simulation method can be used to predict morphology of adsorbed overlayers comprising simple functional cross-shaped molecules resembling phthalocyanines and porphyrins. In particular, we focus on the influence of the distribution of active interaction centers within a model cross-shaped molecule on the structure of the resulting molecular networks. Additionally, we investigate how using racemic mixtures of input prochiral molecules affects the chirality and porosity of the corresponding ordered patters. The obtained results show that suitable manipulation of the chemistry of cross-shaped building block allows for the controlled creation of largely diversified molecular porous networks.

      Keywords: adsorption, self-assembly, computer simulations, porous overlayers.

1. INTRODUCTION

Designing two-dimensional porous networks by controlled self-assembly of organic molecules on solid substrates is a quickly developing area which links individual characteristics of molecular building blocks and physico-chemical properties of the resulting 2D porous material. Most experimental results related to bottom-up synthesis of such materials are based on the self-assembly on graphite or metal surfaces in ultra-high vacuum conditions and from liquid phase. It has been shown that self-assembled porous networks can be sustained not only by directional hydrogen bonds [1-4] and metal-organic coordination bonds [5-7] but also via van der Waals interactions, for example by interdigitation of long alkyl chains of the adsorbed, star-shaped molecules, such as alkyl-substituted phthalocyanines [8], dehydro-benzoannulenes (DBAs) [9,10] and stilbenoid compounds [11]. The advantageous feature of nanoporous networks is the presence of nanometer-sized cavities with uniform well-defined shape [12,13], which can be filled by foreign molecules, e.g. thiols, coronenes and fullerenes [14-16], having required chemical, biological, magnetic or optical properties. Moreover, tuning of chemistry and geometry of such building bricks allows for custom fabrication of 2D nanomaterials for adsorption, separation and catalytic processes.

Controlling and directing the on-surface patterning requires the optimal choice of shape and functionality of the building block. However, it appears that the structure of the porous networks depends mostly on the geometry and distribution of interaction centers in the input-molecule and not on its specific chemistry, limiting the number of necessary parameters needed to describe such systems. In consequence, the self-assembly can be effectively predicted by theoretical modeling. Among computational methods, Monte Carlo lattice approach seems to be the most effective, allowing for investigation of system with large number of molecules under variable conditions, where the geometry of building blocks as well as interactions can be described with relatively low number of adjustable parameters [17-26]. This simple coarse-grained MC model was recently used by us to explore the effect of aspect ratio and relative position of molecular arms in cross-shaped molecules [25] and the role of the number and position of the interaction centers on the morphology of the corresponding 2D assemblies. In this contribution we use the adopted approach to investigate the effect of intramolecular distribution of active centers in an asymmetric building block on the superstructures formation

in adsorbed overlayers. In particular, we explore the self-assembly of racemic mixtures of prochiral molecules with no symmetry elements in which three interaction centers were activated.

2. THE MODEL AND SIMULATIONS

The self-assembling molecules were modeled as flat, rigid structures composed of identical discrete segments, each of which occupies one site on a square lattice. Selected segments were activated to represent different intramolecular distribution of the active centers. The interactions between the activated segments were described by a short range segment-segment interaction potential limited to nearest neighbors on a square lattice and characterized by $\varepsilon = -1$ expressed in kT units [25, 26]. Fig. 1. shows an exemplary molecule on the lattice with the corresponding interactions. In all simulations we used a square $L \times L$ lattice with $L = 200$ representing the underlying surface. Periodic boundary conditions in both planar directions were imposed to eliminate edge effects. To simulate the on-surface self-assembly we use the Monte Carlo method in canonical ensemble with orientationally biased sampling [26]. The simulation algorithm can be described in the following way. At the beginning of the simulation N molecules of the same type (or $2 \times N / 2$ in case of racemic mixtures) were randomly distributed over the surface. Next, up to 10^6 MC steps were performed, with the MC step being defined as an attempt to move and rotate each of the molecules in the system. Each trial to change the configuration began with a random choice of a molecule and the associated displacement. Then, by rotating the molecule around its central segment, four trial orientations $\{b_{n1}, b_{n2}, b_{n3}, b_{n4}\}$ in the new position were generated. By summing up the interactions between the active segments of the selected molecule and neighboring molecules, the potential energy in each trial orientation $U(b_{ni})$, for $I = 1, 2, 3, 4$ was calculated. Then, the Rosenbluth factor in the new position $W(n)$, was determined as:

$$W(n) = \sum_{j=1}^{4} \exp[-\beta U(b_{nj})] \tag{1}$$

where $\beta = kT$, k is the Boltzmann factor and T is temperature. Out of these four orientations one, denoted b_{nk}, was selected with a probability:

$$p(b_{nk}) = \exp[-\beta U(b_{nk})] / \sum_{j=1}^{4} \exp[-\beta U(b_{nj})] \tag{2}$$

The same procedure was repeated for the old position, by generating three trial orientations $\{b_{o2}, b_{o3}, b_{o4}\}$ and calculating the corresponding potential energies $U(b_{oi})$, for i = 2, 3, 4. The Rosenbluth factor in the old position was given as:

$$W(o) = \exp[-\beta U(b_{01})] + \sum_{j=2}^{4} \exp[-\beta U(b_{0j})] \qquad (3)$$

where b_{o1} refers to the initial orientation of the molecule.

To decide if the move was successful, the transition probability P was calculated:

$$P = \min(1, W(n)/W(o)) \qquad (4)$$

and compared with a random number $r \in (0,1)$. If r < p the move was accepted and otherwise the molecule was left in the original position. Additionally, we used the annealing procedure [27], slowly cooling the overlayer from $T = 1$ to target temperature $T = 0.1$, minimizing the risk of trapping the system in metastable states. In all of the simulations, the number of molecules correspond to submonolayer coverage, allowing for unrestricted development of ordered domains.
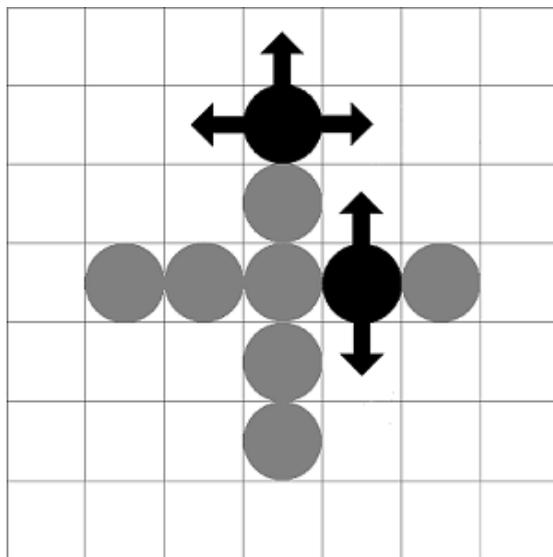

Fig. 1. Schematic drawing of the model molecule adsorbed on a square lattice. The active segments are shown in black. The arrows indicate directions and range of intermolecular interactions allowed in the model.

3. RESULTS AND DISCUSSION

To explore how the distribution of active segments in the input molecule affects the pattern formation, we consider a few selected simple cases. In particular, we focus on racemic mixtures of prochiral molecules. Two shapes of building blocks were taken into account, which were obtained by elongating one arm or two orthogonal arms of the parent C_4 molecule. In addition, selected molecular segments were activated. To explore pattern formation in the racemic mixtures we used four types of molecules, (presented in Fig. 2.) and their opposite enantiomers (not shown).
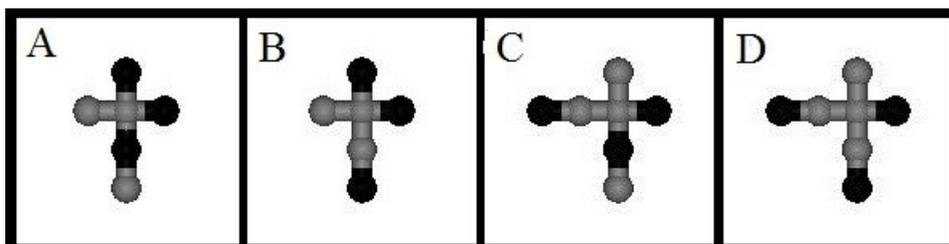

Fig. 2. Types of molecules used in the simulations. Only one enantiomer of each structure is shown. Black segments correspond to the interaction centers.

Let us first discuss the structures simulated for the molecules with one longer arm. Fig. 3. shows the results obtained for the molecule of type **A**. The interaction centers in this building block are located on two orthogonal short arms and on the middle segment of the longer arm of the molecule. The performed calculations show that such an arrangement leads to the formation of small dispersed clusters, randomly distributed over the surface and comprising four molecules each, as can be seen in Fig. 3a. Because the described molecule is chiral in 2D, it is possible to simulate phase behavior of the racemic mixture. In this case, mirror images of the clusters observed previously are present on the surface (Fig. 3b) and the introduction of the other enantiomer does not induce substantial changes in the morphology.
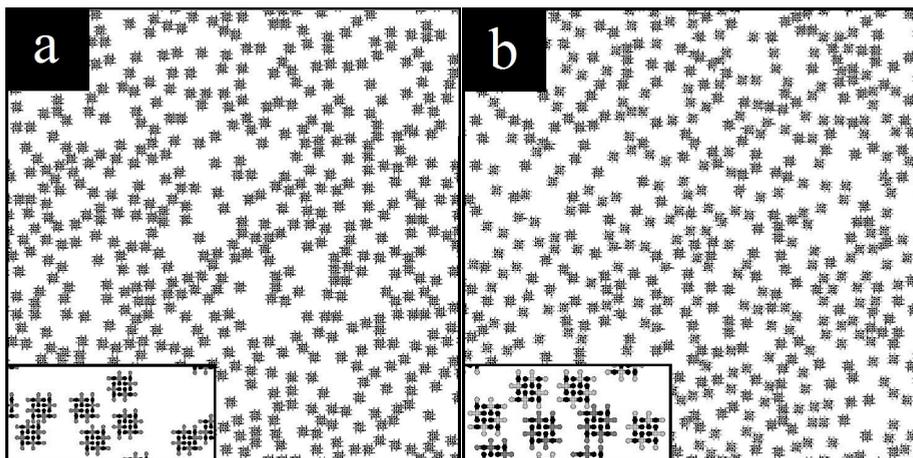
Fig. 3. Adsorbed structures formed by a) 2134 molecules of type A b) 2134 molecules of molecules A and their mirror images (racemic mixture). The insets show magnified fragments of the simulated snapshots. Black segments represent the active centers.

The molecular building-block denoted by **B** differs from molecule **A** only in the position of the activated segment in the longer arm. Namely, now this segment is moved to the terminal position of the longer arm. Fig. 4. presents the pattern formed by the molecules of **B**.
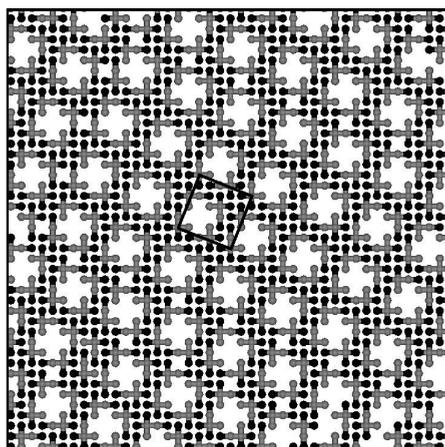

Fig. 4. Magnified fragment of the porous phase observed in the simulations performed for 2134 molecules of type B. The solid black line delimits the corresponding unit cell.

The molecules of **B** form an extended, periodic pattern, composed of a large number of interlocked subdomains characterized by square $\sqrt{29}\times\sqrt{29}$ unit cell. Moreover, we can observe cross-shaped nano-cavities in the structure, as well as, smaller unitary pores surrounded by four active segments.

We also investigated the patterns formed by the molecules with two orthogonal longer arms and mixed racemic structures comprising these molecules. A molecule of type **C** has three active centers located on the ends of two collinear arms (one- and two-membered) and one center on the segment close to the core of the other two-membered arm. Fig. 5. presents the results of the simulations carried out for molecule **C** and for the corresponding racemic mixture.
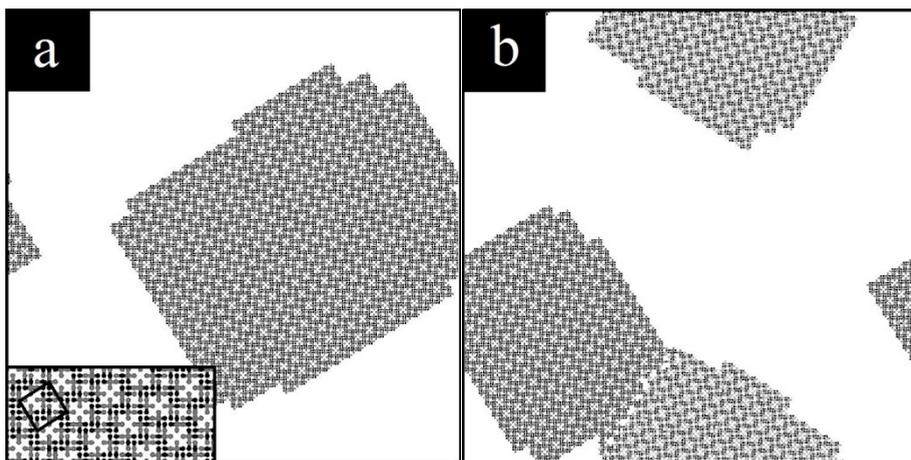

Fig. 5. Ordered chiral patterns formed by a) 1828 molecules of type C; b) corresponding racemic mixture of enantiomers. The inset shows magnified part of the structure. The unit cell is delimited by the black lines.

The arrangement of interaction centers in molecule **C** promotes the formation of ideally periodic, chiral domains with complex structure comprising five pores of unitary area (i.e. one lattice site) per $\sqrt{34}\times\sqrt{34}$ square unit cell. In the case of the corresponding racemic mixture, we can observe the chiral resolution of enantiomers into two equally large domains, one being mirror image of the other. This situation changes significantly when all of the three active segments occupy terminal positions in the molecular building brick, forming the molecule of type **D**.

In this last example, shown in Fig. 6., the presence of a single enantiomer in the system leads to the creation of one large homochiral domain, characterized by parallelogram $\sqrt{26} \times \sqrt{10}$ unit cell. Although this behavior is similar to that observed already for **C**, the self-assembly of the corresponding racemic mixture results in the formation of a mixed crystal with $\sqrt{101} \times \sqrt{34}$ unit cell. Moreover, the mixed molecular network of **D** comprises three kinds of cavities: 1×1, 1×2, and S-shaped ones, versus only one type (2×2) observed for the enantiopure structure from Fig. 6a. Apparently, these results demonstrate how the small change in the functionality of the building block can result in a substantial difference in the morphology of the self-assembled networks.
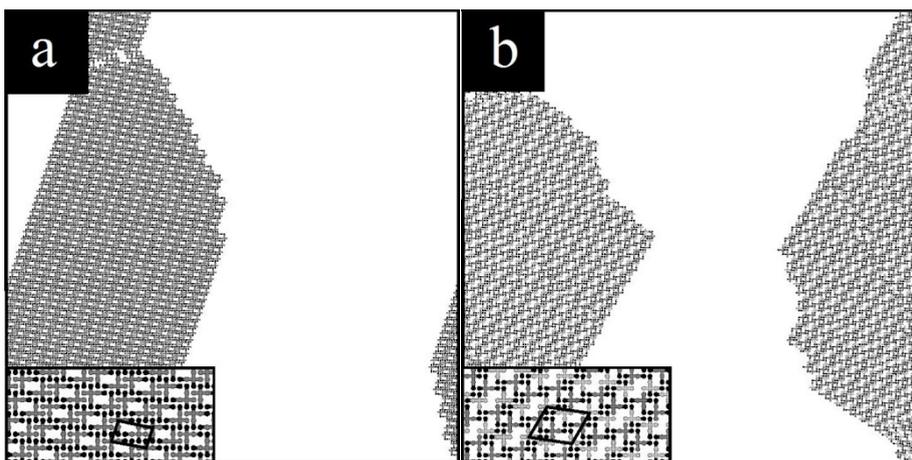
Fig. 6. Porous molecular networks formed by 1828 molecules of type D a) and by the molecules of the corresponding racemate b). The insets show magnified parts of the structures, while the solid black lines delimit the unit cells.

4. CONCLUSIONS

The results presented in this contribution show that the simple lattice MC model can be helpful in finding the relation between the intramolecular distribution of active centers in the cross-shaped input molecule and the architecture of the resulting adsorbed structures. In particular it is demonstrated how by using racemic mixtures of functional building blocks it is possible to direct the self-assembly towards separated chiral porous networks or mixed surface crystals with diversified pore

structure. The findings reported in this work can be used for designing surface overlayers sustained by intermolecular interactions between cross-shaped building blocks resembling derivatized porphyrins or phthalocyanines. The proposed methodology can reduce the number of necessary test syntheses needed to obtain the optimal building molecule.

5. ACKNOWLEDGMENT

REFERENCES

[1] H. Zhou, H. Dang, Y. Ji-Hyun, A. Nanci, A. Rochefort, J. D. Wuest, *J. Am. Chem. Soc.,* **129,** 13774, (2007).
[2] M. Blunt, X. Lin, M. Gimenez-Lopez, M. Schröder, N.R. Champness, P. H. Beton, *Chem. Commun.*, **20,** 2304, (2008).
[3] M. Lackinger, W. M. Heckl, *Langmuir*, **25**, 11307, (2009).
[4] A. Ciesielski, P. Szabelski, W. Rżysko, A. Cadeddu, T. R. Cook, P. J. Stang, P. Samori, *J. Am. Chem. Soc.,* **135,** 6942, (2013).
[5] P. Messina, A. Dmitriev, N. Lin, H. Spillmann, M. Abel, J.V. Barth, K. Kern, *J. Am. Chem. Soc.,* **124**, 14000, (2002).
[6] A. Dmitriev, H. Spillmann, M. Lingenfelder N. Lin, J.V. Barth, K. Kern, *Langmuir* **20**, 4799, (2004).
[7] Z. Shi, N. Lin, *J. Am. Chem. Soc.,* **131**, 5376, (2009).
[8] K. Miyake, Y. Hori, T. Ikeda, M. Asakawa, T. Shimizu, S. Sasaki, *Langmuir*, **24**, 4708, (2008).
[9] K. Tahara, S. Furukawa, H. Uji-i, T. Uchino, T. Ichikawa, J. Zhang, W. Mamdouh, M. Sonoda, F.C. De Schryver, S. De Feyter, Y. Tobe, *J. Am. Chem. Soc.,* **128**, 16613, (2006).
[10] S. Furukawa, H. Uji-i, K. Tahara, T. Ichikawa, M. Sonoda, F.C. De Schryver, Y. Tobe, S. De Feyter, *J. Am. Chem. Soc.*,**128**, 3502, (2006).
[11] D. Bléger, D. Kreher, F. Mathevet, A.-J. Attias, G. Schull, A. Huard, L. Douillard, C. Fiorini-Debuischert, F. Charra, *Angew. Chem. Int. Ed.,* **46**, 7404, (2007).
[12] R. Gutzler,   H. Walch, G. Eder, S. Kloft,, W. Hecklab, M.. Lackinger, *Chem. Commun.,* **29,** 4456, (2009).

[13] T. Kudernac, S. Lei, J. A .A. W. Elemans, S. De Feyter, *Chem. Soc. Rev.,* **38**, 402, (2009).

[14] R. Madueno, M. T. Räisänen, C. Silien, M. Buck, *Nature,* **454**, 618, (2008).

[15] L. Piot, F. Silly, L. Tortech, Y. Nicolas, P. Blanchard, J. Roncali, D. Fichou, *J. Am.Chem. Soc.,* **131,** 12864, (2009).

[16] S. Lei, K. Tahara, X. Feng, S. Furukawa, F. C. De Schryver, K. Müllen, Y. Tobe, S. De Feyter, *J. Am. Chem. Soc.,* **130,** 7119, (2008).

[17] K. U. Weber, V. M. Burlakov, L. M. A. Perdigão, R. H. J. Fawcett, P. H. Beton, N. R. Champness, J. H. Jefferson, G. A. D. Briggs, D. G. Pettifor, *Phys. Rev. Lett.,* **100,** 156101, (2008).

[18] F. Silly, U. K. Weber, A. Q. Shaw, V. M. Burlakov, M. R. Castell, G. A. D. Briggs, D. G. Pettifor, *Phys. Rev. B,* **77,** 201408, (2008).

[19] P. Szabelski, S. De Feyter, M. Drach, S. Lei, *Langmuir,* **26,** 9506, (2010).

[20] P. Szabelski, A. Kasperski, *Top. Catal.,* **54,** 1368, (2011).

[21] A. Ibenskas, E. E. Tornau, *Phys. Rev. E,* 86, 051118, (2012).

[22] T. Misiunas, E. E.Tornau, *J. Phys. Chem. B,* **116,** 2472, (2012).

[23] T. J. Roussel, L. F. Vega, *J. Chem. Theory Comput.,* **9,** 2161, (2013).

[24] J. Adisoejoso, K. Tahara, S. Lei, P. Szabelski, W. Rżysko, K. Inukai, M.O. Blunt, Y. Tobe, S. De Feyter, *ACS Nano,* **6,** 897, (2012).

[25] A. Kasperski, P. Szabelski, *Adsorption*, **19,** 283, (2013).

[26] D. Frenkel, B. Smit, *Understanding Molecular Simulation From Algorithms to Applications,*, Academic Press 2002.

[27] K. Tahara, E. Ghijsens, M. Matsushita, P. Szabelski, S. De Feyter, Y. Tobe, *Chem. Commun*., **47**, 11459 (2011).

CURRICULA VITAE

Adam Kasperski. Born in 1988 in Lublin. Graduated from the Faculty of Chemistry of Maria Curie-Sklodowska University in Lublin in 2012. After graduation he started Ph. D. studies in Department of Theoretical Chemistry of the same university. In 2012 awarded the Diamond Grant stipend by the Polish Ministry of Science and Higher Education. His research interests: adsorption, computer simulations, nanoporous molecular networks.

Paweł Szabelski. Born in Lublin, Poland in 1972. In 1996 graduated from the Faculty of Chemistry of Maria Curie-Skłodowska University in Lublin. In 2000 received Ph.D. from the same university. Employed as an assistant lecturer (2000) and next as an assistant professor (2001) in the Department of Theoretical Chemistry, UMCS. Post doctoral studies (2000-2001) at the University of Tennessee, Knoxville, TN, USA. In 2003 and 2004 awarded the stipend for young scientists from the Foundation for Polish Science. In 2006 awarded Fulbright Advanced Research Grant at Carnegie Mellon University, Pittsburgh, PA, USA. Employed as an associate professor since 2012. Main research interests: statistical mechanics of adsorption, computer simulations, chiral surfaces and molecules.

ANNALES
UNIVERSITATIS MARIAE CURIE-SKŁODOWSKA
LUBLIN – POLONIA

FT-IR/PAS study of surface EDTA-ZnO interactions

Marcin Kuśmierz[a] and Sylwia Pasieczna-Patkowska[b]

[a]*Department of Environmental Chemistry,*
[b]*Department of Chemical Technology,*
Faculty of Chemistry, Maria Curie-Sklodowska University,
pl. M. Curie-Skłodowskiej 3, 20-031 Lublin, Poland
[a]*marcin.kusmierz@poczta.umcs.lublin.pl*

The interaction of EDTA disodium salt with zinc oxide was investigated by photoacoustic (PA) FT-IR. It was demonstrated that EDTA-III adsorbs on ZnO, and the process mimics behaviour of EDTA-oxide systems, in which IEPS of oxide catalytic supports is higher than 9. Model of the interaction, described in literature, was discussed.

1. INTRODUCTION

Ethylenediaminetetraacetic acid (EDTA) and its sodium salts are often used in preparation of catalysts by double impregnation method (DIM). In the first stage of the preparation a chelating compound (usually disodium EDTA salt) is deposited on a surface of metal oxide, which serves as a support. After drying, so-called "activated carrier" is impregnated with a solution of a catalyst precursor. This method is well suited for preparing supported catalysts characterized with high metallic phase dispersion [1].

Understanding the interactions between EDTA and support oxides is essential for obtaining catalysts with desired properties. Most of the literature data devoted to this preparation technique is focused on EDTA–Al_2O_3 [2–5], EDTA–$AlPO_4$ [6] and EDTA–MgO/Al_2O_3 systems [7].

Contrary to SiO_2 or Al_2O_3, zinc oxide is a partially reducible support [8–10] and therefore reduced Zn may form alloys with main metallic phase. In some cases such binary catalyst performs better than a single-phase one: Iwasa [11] reported that in the reaction of CO_2 hydrogenation on Pd-Zn/ZnO catalysts showed higher activities and selectivities towards methanol than pure palladium based ones.

The DIM method facilitates high dispersion of catalyst metallic phase, thus forming alloys is easier. This study focuses on phenomena occurring during the first stage of the process: interactions between EDTA and ZnO.

2. EXPERIMENTAL

Two samples of ZnO (supplied by INS Puławy, Poland) were calcined in air at 823 K using muffle furnace for 8 hours (sample S8) and 4 hours (sample S4). According to calcination curve supplied by producer this thermal treatment lowered their surface areas to about 5 m^2/g and 15m^2/g, respectively. EDTA and it salts strongly chelates metal ions (which charge is at least +2). It even may leach them from oxide and hydroxide solids [12–15]. High surface area of metal oxides facilitates this phenomena and in consequence may hinder investigations of EDTA adsorption. In the case when this phenomena would have been observed for S4 samples, strongly calcined S8 samples have been prepared.

Both S8 and S4 samples were divided into subsamples S8H, S8E and S4H, S4E, respectively. Subsamples S8E and S4E were impregnated with 0.1M EDTA-III (EDTA disodium salt, Na_2H_2Y, supplied by POCh, Gliwice) solution at 343 K for 20 minutes. For the reference purposes subsamples S8H and S4H were treated in the same manner with distilled water. All the subsamples were then dried at 391 K overnight.

FT-IR/PAS spectra of investigated materials (S8H, S4H, S8E, S4E) were recorded using Bio-Rad spectrometer equipped with MTEC300 photoacoustic detector, over the 4000–400 cm^{-1} range. The spectra were measured at RT at 4 cm^{-1} resolution and normalized by computing the ratio of a sample spectrum to the spectrum of a MTEC carbon black standard. Prior to measurements the PA cell was purged with dry helium for 5 minutes. Interferograms of 512 scans were average for each spectrum. Spectra of untreated ZnO samples (S8 and S4) were also recorded.

3. RESULTS AND DISCUSSION

Spectra of S8, S8H and S8E samples are presented in Figure 1. Peaks at 3065, 2957, 2922 and 2854 cm^{-1} (small chart) are characteristic for surface carbon species [18]. Their presence is caused by incomplete removal of graphite, which is used as a grease during production of ZnO pellets. This implies that flow furnance and oxygen atmosphere should be used, rather than muffle one and air.

Band at 1640 cm^{-1}, present in spectra S8 and S8H is ascribed to oxide surface hydroxyl groups. In spectrum S8E this peak is covered by features at 1626 and 1670 cm^{-1} (very weak shoulder), which can be assigned to ν_{as}–COO$^-$ and –COOH vibrations of EDTA-III carboxyl groups, respectively [16–18]. Bands associated with strong symmetric vibrations of –COO$^-$ groups appear at 1400 and 1323 cm^{-1}, and the peak at 1280 cm^{-1} corresponds to vibrations of –CH$_2$COOH chains [16–18].
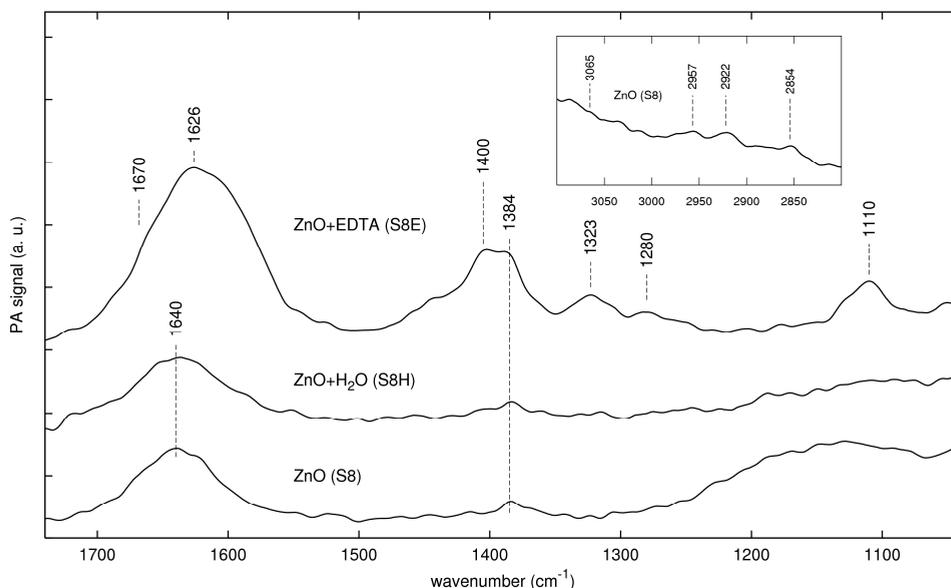
Fig 1. FT-IR/PAS spectra of S8E, S8H and S8 samples.

The presence of EDTA adsorbed on the ZnO surface is confirmed by relatively intensive band at 1110 cm^{-1}, which is attributed to stretching of C–N bond [16–18]. Spectra of S4, S4H and S4E samples were almost identical to those described above, and therefore they are not shown.

Interactions between adsorbates and metal oxides strongly depends on surface composition of the latter. Hydroxyl groups and their

distribution are of special importance. In the case of impregnation from water solutions, the population of these species depends on isoelectric point of solid surface (IEPS) and pH of the solution [19]. Equations describing protonation, deprotonation and state of the oxide surface in water solution are included in papers [20,21]. Their more general form is presented in paper [5], and can be applied to various oxides:

$$\equiv M - O^- \qquad pH > IEPS \qquad (1)$$

$$\equiv M - OH \qquad pH \approx IEPS \qquad (2)$$

$$\equiv M - OH^+_2 \qquad pH < IEPS \qquad (3)$$

In publication [5] models of interactions between EDTA disodium salt and various inorganic oxides are shown. For magnesium oxide the proposed reaction is as follows:

$$(4)$$
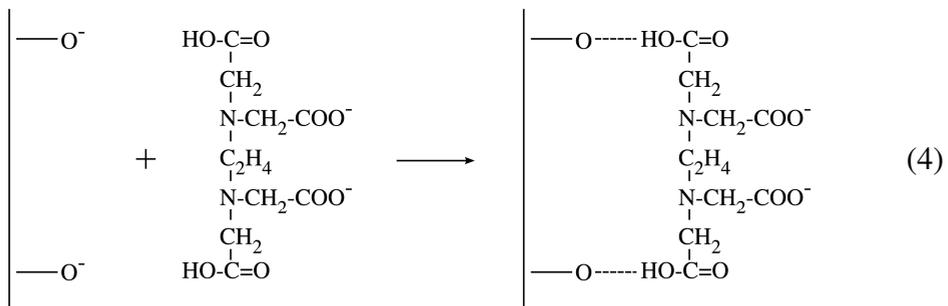
According to scheme (4) EDTA salt interacts with surface M–O$^-$ species via undissociated carboxyl groups. This view is supported by relative intensity of bands in spectrum included in cited work: peak corresponding to –COO$^-$ groups is more intensive than one associated with –COOH groups.

IEPS values for MgO and ZnO are in similar, alkaline range: ≈ 12. Because pH of impregnation solution used (≈ 6) was far below this value, according to equation (3) the most numerous surface species were M-OH and M–OH$^+_2$ groups. Moreover, if the oxide surface is positively charged it is more likely to happen that EDTA salt will contact with surface via dissociated carboxyl groups, due to electrostatic forces. Higher intensity of the peak at 1626 cm^{-1}, corresponding to asymmetric vibrations of –COO$^-$, in comparison to the peak at 1670 cm^{-1} (–COOH groups) can be explained by dissociation of adsorbed EDTA carboxyl groups. Scheme

(5) describes proposed model of EDTA salt adsorption from weakly acidic solution.

$$
\begin{array}{c}
\left|\begin{array}{ll}
\text{——OH}_2^+ & \text{}^-\text{O-C=O} \\
& | \\
& \text{CH}_2 \\
& | \\
& \text{N-CH}_2\text{-COOH} \\
+ & | \\
& \text{C}_2\text{H}_4 \\
& | \\
& \text{N-CH}_2\text{-COOH} \\
& | \\
& \text{CH}_2 \\
& | \\
\text{——OH}_2^+ & \text{}^-\text{O-C=O}
\end{array}\right.
\quad \longrightarrow \quad
\left|\begin{array}{ll}
\text{——OH}_2\text{---O-C=O} \\
\quad\quad\quad\; | \\
\quad\quad\quad\; \text{CH}_2 \\
\quad\quad\quad\; | \\
\quad\quad\quad\; \text{N-CH}_2\text{-COO}^- + \text{H}^+ \\
\quad\quad\quad\; | \\
\quad\quad\quad\; \text{C}_2\text{H}_4 \\
\quad\quad\quad\; | \\
\quad\quad\quad\; \text{N-CH}_2\text{-COO}^- + \text{H}^+ \\
\quad\quad\quad\; | \\
\quad\quad\quad\; \text{CH}_2 \\
\text{——OH}_2\text{---O-C=O}
\end{array}\right.
\quad (5)
\end{array}
$$
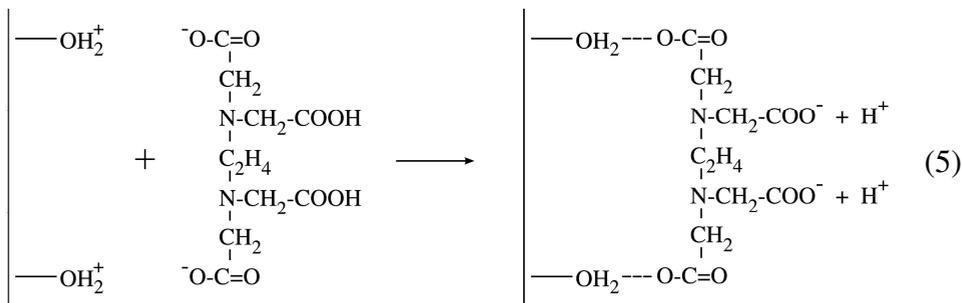
4. CONCLUSIONS

It was demonstrated that EDTA-III is adsorbed on zinc oxide surface and it can be assumed, that application of double impregnation method for preparing catalysts supported on ZnO is possible.

Low pH (c.a. 6) of impregnation solution in combination with high IEPS of ZnO suggest, that during the impregnation $-OH_2^+$ groups were most numerous surface species. This suggestion is supported by relatively high intensity of bands at 1640 cm^{-1} and 1384 cm^{-1}, corresponding to oxide surface hydroxyl groups.

The foregoing statement indicates that EDTA-III adsorbs on surface of zinc oxide mainly via dissociated carboxyl groups. Strong peaks at 1626 cm^{-1} corresponding to assymetric vibrations of $-COO^-$ groups are probably caused by deprotonation of hitherto undissociated EDTA-III carboxyl groups.

REFERENCES

[1] J. Barcicki, D. Nazimek, *React. Kinet. Catal. Lett*., **17**, 169 (1981).
[2] D. Nazimek, J. Ryczkowski, *Appl. Catal*., **26**, 47 (1986).
[3] J. Ryczkowski, T. Borowiecki, *React. Kinet. Catal. Lett*., **49**, 127 (1993).
[4] T. Shimizu, K. Hiroshima, T. Honma, T. Mochizuki, M. Yamada, *Catal. Today*, **45**, 271 (1998).
[5] J. Ryczkowski, *Appl. Surf. Sci*., **252**, 813 (2005).

[6]   F. M. Bautista, J. M. Campelo, A. Garcia, R. Guardeno, D. Luna, J. M. Marina, *J. Catal.*, **125**, 171 (1990).
[7]   C. Qi, T. Bai, L. An, *React. Kinet. Catal. Lett.*, **54**, 131 (1995).
[8]   N. Iwasa, S. Kudo, H. Takahashi, S. Masuda, N. Takezawa, *Catal. Lett.*, **19**, 211 (1993).
[9]   N. Iwasa, S. Masuda, N. Ogawa, N. Takezawa, *Appl. Catal. A*, **125**, 145 (1995).
[10] N. Iwasa, N. Takezawa, *Top. Catal.*, **22**, 215 (2003).
[11] N. Iwasa, H. Suzuki, M. Terashita, M. Arai, N. Takezawa, *Catal. Lett.*, **96**, 75 (2004).
[12] E. B. Borghi, A. E. Regazzoni, A. J. G. Maroto, M. A. Blesa, *J. Colloid Interface Sci.*, **130**, 299 (1989).
[13] J. A. Rumball, G. D. Richmond, *Int. J. Miner. Process*, **48**, 1 (1996).
[14] J. K. Klewicki, J. J. Morgan, *Geochim. Cosmochim. Acta*, **63**, 3017 (1999).
[15] H. Tamura, N. Ito, M. Kitano, S. Takasaki, *Corros. Sci.*, **43**, 1675 (2001).
[16] T. Sawyer, P. J. Paulsen, *Int. J. Chem. Soc.*, **80**, 1597 (1958).
[17] R. E. Sievers, J. C. Bailar Jr., *Inorg. Chem.*, **1**, 174 (1962).
[18] G. Socrates, *Infrared and Raman Characteristic Group Frequencies. Tables and Charts* (Wiley, Chichester 2001) p. 132.
[19] G. A. Parks, *Chem. Rev.*, **65**, 177 (1965).
[20] U. Olsbye, R. Wendelbo, D. Akporiaye, *Appl. Catal. A,* **152**, 127 (1997).
[21] K. M. Hardiman, C. H. Hsu, T. T. Ying, A. A. Adesina, *J. Mol. Catal. A*, **239**, 41 (2005).

CURRICULA VITAE

Marcin Kuśmierz born in Lublin (1971). Graduated from Maria Curie-Skłodowska University in Lublin (1997). Received his Ph. D. degree in physical chemistry (2005) from the Maria Curie-Skłodowska University. His main fields of interest are environmental impacts of biochars use and fate and bioavailability of hydrophobic organic pollutants in environment (especially PAHs and o-PAHs).

Sylwia Pasieczna-Patkowska was born in Lublin, Poland in 1974. She studied chemistry at the Maria Curie-Skłodowska University, graduated in 1998. Received her Ph.D. (2006) in physical chemistry from the UMCS in Lublin. Since 2007 she is an adjunct at UMCS. She is an author and co-author of 73 articles in science-technical press, the author and co-author of 126 papers and posters at domestic and foreign conferences. Scientific interests: infrared spectroscopy, chemical technology. She is member of Polish Chemical Society (1998-) and Polish Catalysis Club (1998-).

Polymer dimensional changes in optical cables

Mateusz Lutomski[a] and Barbara Gawdzik[b]

Department of Polymer Chemistry, Faculty of Chemistry,
Maria Cure-Sklodowska University
Gliniana 33, 20-614 Lublin, Poland,
[a]Mateusz.lutomski@corning.com,
[b]barbara.gawdzik@poczta.umcs.lublin.pl

Optical cables and fibers are extremely sensitive for mechanical, thermal and environmental conditions, which can affect their optical performance. This article describes known reasons and mechanisms responsible for dimensional changes in temperatures cycling, which can influence optical and mechanical performance and properties of the cables, including internal cable components. Understanding all physical and chemical mechanisms which meet different manufacturing parameters, various materials properties and external conditions allows to control and reduction of cable shrinking and as a result, improving mechanical and optical performance of optical cables.

1.INTRODUCTION

All polymers shrink. Depending on the purpose, such phenomena may be an advantage (heat shrinks, etc.), but usually, such effect is unwanted and can cause many problems and failures in various industrial fields. Production of Fiber Optical cables, which are very sensitive to mechanical stresses, forces better understanding of such phenomena. Especially as when the market grows and higher transmission is needed, smaller dimensions of cables and lower prices are required. But still, all cables need to fulfill international standard requirements. Optical

performance is precisely defined, so special mechanical performance should be provided. Indoor cables should retain flame retardant behavior, outdoor, be proofed for environmental and chemical conditions. Also, they should be environmentally friendly and meet RoHS (RoHS stands for Restriction of Hazardous Substances) and REACH (Registration, Evaluation, Authorization, Restriction of Chemicals) requirements. Finally, materials for cable jacket cannot be very expensive but need to perform very steadily during production… and don't shrink too much.

After the rapid technical evolution in the early 80's, attenuation performance was dramatically improved, and the cost of the fiber was significantly reduced. However, shrinking can affect those improvements, causing many issues with cable and fiber performance. Shrinking jacket can increase attenuation. It can also expose ends of fibers (which practically don't shrink) to external humidity and other rough conditions. Different materials, and consequently cable elements, can shrink in a different way. The problem also affects loose tubes and tight buffers, connectors, fanouts and other cable elements. But what is shrinking, shrinkage, shrinkback, and why does it happen? This review will collect information regarding the shrinking phenomena, the nomenclature from optical cables' industry perspective, the reasons which can cause different shrinking, and known methods of controlling and reducing this unwanted behavior on various materials and components. As market started to grow, cable manufacturers increased emphasis on costing and performance optimization. More innovations on polyolefin market was made. Special kind of MDPE (Medium Density Polyethylene) was developed [1], especially for outdoor optical cables, with low temperature modulus properties and a low post extrusion shrinkage, characteristic to minimize the axial compressive stress exerted by the jacketing on the cable core. Also, black version of HDPEs (High Density Polyethylene) [2-6] was used with low compressive stresses for lowest post extrusion shrinkage. Nowadays, most conventional communication cables for outdoor use are made of polyethylene (PE) provided with UV-resistant additive like black carbon. For indoor cables, different kind of materials are used. Flame retardant materials are much more complex, and their shrinking behavior is harder to predict. Also, depending on their composition, production date or even storage conditions, same materials can act differently during manufacturing process. Cables for indoor use had Flame Retardant, PVC (polyvinyl chloride) jackets. PE and PVC materials for jackets of communication cables have now been standardized internationally, (the main standard in Europe is/was EN

50290-2-27). Polyethylene is a very good sheathing material for outdoor use, but it is not flame-retardant. In other words, it does contribute to the spread of fire. In US, PVC is physically an appropriate jacketing material with a high degree of flame-retardancy, but in the event of fire, it generates black smoke, and poisonous and corrosive gas. Such emissions are harmful not only to electrical components, but can also cause death and are prohibited in some European countries. Due to the smoke emission and toxic gas set free when PVC burns, halogen-free (FRNC/LSNH) sheathing compounds have become more and more specified and available *(The definition of FRNC/LSNH is Flame-Retardant, Non Corrosive, Low Smoke, No Halogen).*

FRNC materials usually consist of base polymer like EVA (Ethylene Vinyl Acetate), elastomers, flame retardants ($Al(OH)_3$, ATH, $Mg(OH)_2$, huntite and hydromagnesite, various hydrates, boron compounds and much more). Such complex composition of organic and inorganic compounds affects as well cables performance and shrinking behavior. Another example of cable components which shrinking can reduce cable performance are buffer tubes. Although the buffer tube is within a cable, the shrinkage is limited by the structure of the cable it still can cause some problems during connecting cable to closures or data centers. However the problem might appear just after tube production, or even during manufacturing. Different materials, construction types and tube diameters, requires special conditions, with very narrow temperature ranges and strictly defined production parameters.

Various cable components can shrink in various ways, because of different polymers structure and properties. All plastics parts shrink after processing, as a result of their compressibility and the thermal contraction as they cool from the processing temperature. Because crystallites contain more ordered and better packing of the polymer chains, phase transition increases shrinkage significantly. For amorphous polymers, shrinkage values are not only low, but shrinkage itself is quick to occur. Crystalline polymers are not only affected by compressibility and temperature shrinkage, but also by crystallization shrinkage. As the polymer solidifies, crystals form and the improved packing leads to shrinkage values far greater than those seen in amorphous polymers. For example, typical crystalline polymer such as PP (Polypropylene), shrinkage can be between 5 -10 times the shrinkage of an amorphous polymer [7]. Only about 85% of this higher shrinkage will have taken place in the first 24 hours, about 98-99% will have taken place in the first week and the remaining shrinkage may take up to 3 months to complete. In such cases, annealing for a short

time at the maximum crystallization temperature to force the polymer to equilibrium where full shrinkage can take place within an hour.

2. SHRINKING

Shrinking behavior has been widely described in literature for many years [1-13]. Depending on manufacturing field, country or even company, phenomena is named and understood differently. That is not surprising when such data is compared. Shrinking consists of many mechanisms and appears in different conditions, even when two extrusion lines seems to be copied at the same way. It can change the molecular structure, can be reversible and irreversible, can be partially effect of production parameters, material individual behavior (polymer chains orientation and crystallinity level), temperature, time, external conditions, production line construction and speed, equipment type (and life time) or even individual experience of manufacturing engineer. Because of such complexity of a problem special nomenclature based on world literature will be implemented to easier understanding and distinguish those specific effects.

3. THERMAL EXPANSION AND CONTRACTION

Thermal expansion is the tendency of matter to change in volume in response to a change in temperature [8].

When a substance is heated, its particles begin moving more than usual, maintaining a greater average separation. The degree of expansion divided by the change in temperature is called the material's coefficient of thermal expansion and generally varies with temperature. When heat is added to most materials, the average amplitude of the atoms vibrating within the material increases. Such effect increases the separation between the atoms causing the material to expand. If the material does not go through a phase change, the expansion can be easily related to the temperature change. The linear coefficient of thermal expansion (α) describes the relative change in length of a material per degree temperature change. a is the ratio of change in length (Δl) to the total starting length (l_i) and change in temperature (ΔT).

$$\alpha = \Delta l / \; l_i \cdot \Delta l \qquad\qquad (1)$$

The linear coefficient of thermal expansion [7].

If the linear coefficient of thermal expansion is known, the change in the sample length can be theoretically calculated for each degree of temperature change. This effect also works in reversal. If energy is removed from a material, then the object's temperature will decrease, causing the object to contract. Coefficient of thermal expansion can serve as a material characteristic only where material behavior is reversible. But in world of polymers other mechanisms appears parallel which complicates the topic much more.

4. SHRINKAGE AND SHRINKBACK

The most accurately described effect of shrinking, called shrinkage, consist of a couple other effects, which in combination creates shrinkage. Shrinkage of the cable jacket, commonly referred to as "shrinkback", occurs as this frozen-in polymer orientation relaxes in the solid state [8]. The name shrinkback was firstly used when shrinking behavior of cable jacket was observed, revealing cable ends.

But it would be easier to understand real products' behavior, when we separate those effects theoretically. Going by that way in this review, the whole shrinking effect would be called shrinkage. Technically, shrinkage is temperature dependent volume change. When polymer is slowly cooled down to room temperature, its density changes significantly. Cooling too quickly can prevent the polymer from reaching its final density. Re-heating the cable jacket sometime later may allow plastic to continue its thickening. Two main effects which create shrinkage are shrinkback and aforementioned contraction [2]. The name "shrinkback" appears especially in cables industry publications and literature, as well as in copper transmission cables and in fiber optic cables (FOC). Shrinkback is a kind of response for frozen forces which appeared during extrusion process, while temperature increase and molecules chains have more opportunities to change configuration and come back to a shorter chain [19]. Extrusion process stretched those chains' elongating and orientating them in extrusion direction. High temperature and pressure keep them that away until the temperature is rapidly cooled down. Polymer chains do not have enough time to relax and almost immediately (depending on conditions and dimensions) are frozen in a tensed way. This tension does not disappear and is still trapped in polymer structure, waiting for an opportunity to relax. Such chance appears when cable jacket is heated up and two mechanisms met even

though they might be contrary. Cable jacket during heating grows as a result of reversible thermal expansion until polymer chains have more movement possibilities as polymer is getting more "rubber like" and shrinkback appears. Even though sample is still expanding, opposite force appears, as stretched polymer chains are relaxing. Depending on polymer properties such effect might be correlated with glass transition effect.

If polymer is semi crystalline, during cooling the crystallization also occurs, which also affects shrinking. And at this point, it is necessary to come back to the structure of polymers. Thermoplastic polymers shrinkage also depends on the matrix morphology – amorphous or semi-crystalline. In semi-crystalline polymers, the volumetric shrinkage results from the densification upon crystallization (with crystals being of higher density than the amorphous phase f.e. LDPE vs HDPE, or PP mentioned before), in addition to the shrinkage because of lower temperature. In amorphous polymers, the shrinkage is only due to the latter. The total shrinkage for semi-crystalline matrices can even be ten times higher than for amorphous.

Below Tg (glass transition temperature), there is virtually no molecular motion on a local scale. Polymers have many of the properties associated with ordinary organic glasses, including hardness and stiffness. The crystalline melting point is the temperature at which crystals melt, and a crystalline polymer resembles an amorphous polymer, which has no short-range order. Tm (melting temperature) generally increases as the degree of crystallinity increases. Above Tm, no crystallization exists, and below Tg, no further movement of molecules is possible to nucleate or grow crystals. The fastest rate of crystallization occurs midway between Tg and Tm. The longer a polymer remains between the two, the greater the amount of crystallization [8].

Shrinkback is a permanent effect [13], and is not reversible. The reason of this is that during relaxation, polymer changes the chain configuration. Opposite to shrinkback, contraction is irreversible and chain configuration does not change, only molecules get shorter. Both effects combined together create the shrinkage.

Depending on the temperature range and the time influence, the overall shrinkage process involves a rapid initial stage contraction of the molecular network, associated with disorientation in the amorphous phase, followed by a crystallization stage during which chain folding takes place. Crystallization can occur simultaneously with amorphous disorientation, and once the crystallization starts, further shrinkage is hindered [9].

Changing temperatures increase and speed up this effect. But even in room temperatures, the molecules would like to come back to reduce frozen tension. Of course, because of limited molecule movement in the solid state process is not so fast, and it needs more time to shrink. It can cause problems mentioned before in the longer time period. That is why aging is performed to predict such behavior. To understand it better, the terms from literature can be used as well, like the primary and the secondary shrink [3]. Standard DIN 16901 suggest to take the first length measurement not sooner than 16h after the production. Such long time is needed for strain relaxation, and such shrink is a "primary shrink". Further uncontrolled transformation, which can be couple hundred hours long, is a secondary shrink, where recrystallization, relaxation and participles accumulation take place. As a consequence, energetic equilibration is achieved and strains are relieved. It is believed that sum of those two factors is (approximately) stable, and it is important to achieve highest primary shrink value , which could be controlled during the cooling, to obtain the smallest value of secondary shrink, which is unknown. There is another factor which significantly influences shrinkback – friction between cable elements. Such effect on one hand reduce shrinking of the jacket, but on the other also blocks relaxation in some way and helps creating frozen in stresses.

5. RESIDUAL STRESSES

The strains which can be blocked during polymer cooling can be also separated in respect of transition stage and physical mechanism [2, 3]. Flow Induced Residual Stress takes place, when molted polymer molecules are unstressed, and they tend to an equilibrium, random coil state. During processing, the polymer is sheared and elongated, and the molecules are oriented in the flow direction. If solidification occurs before the polymer molecules are fully relaxed to their state of equilibrium, molecular orientation is locked within the extruded part [17]. Another is the Thermal Induced Residual stress which arises during the cooling stage [2]. During the cooling stage, the polymer cools at different rates. When the polymer starts to cool, the external surface layers start to shrink, while the bulk of polymer is still hot at the core and free to contract. Later, when the internal core cools, it's contraction is constrained by the external layers since they are already rigid.

The problem of thermal residual stresses can be especially found in the extruded polymer products where rapid inhomogeneous cooling is a part of the manufacturing process. For cables, cooling starts at the outer layers of the cable jacket, where the temperature drops almost instantaneously from well above the melting point to room temperature. As a result, the outer layers stiffens, but the inner layers still occupy a larger volume, introducing stresses into the cable jacket or tube. As cooling proceeds radially, solidification produces further thermal stresses. Usually thermal stresses partially persist in the finished product since most polymers are viscoelastic. Furthermore, the stress development is also influenced by the semi-crystalline microstructure of certain polymers like PE. Moreover, high (or "too high") temperature of jacketing process can have an impact on inside cable components like buffer tubes and other materials which could be sensitive for such temperature treatment.

6. ORIENTATION AND CRYSTALLIZATION

Orientation is frozen-in stretching or elongation of the polymer molecules occurring during polymer flowing from the extrusion die to windup area of the extrusion process. On removal of the deforming stresses, the molecules start to coil up again, but the process may not go to equilibrium before the polymer cools to below its glass transition temperature (Tg). This leads to residual orientation (frozen-in strain) and aforementioned corresponding frozen-in stresses. Usually polymers with extensive side branches or bulky side branches along the polymer chain can be more sensible to frozen-in elongation than polymers with smaller side chains. Same result occurs when rubbery and elastic polymers are compared with stiffer ones, which are more susceptible to frozen-in orientation.

Many different factors may affect orientation during the extrusion process [20]. When the extrudate exits the die, the polymer molecules, oriented in the die land area, relax and reentangle, causing die swell. If the extrudate is allowed to droll out the die, the cross section swells, becoming larger than the die opening due to polymer relaxation. Extrudate pulled away from the extruder, orients the polymer molecular chains in the machine direction. The draw depends on the puller speed relative to the extruder output. Draw ratio is directly related to molecular orientation, resulting in higher tensile and flexural properties in the machine direction compared to the transverse position. Process settings

and die should be chosen very carefully. The draw ratio depends on the product size exiting the die versus the required product size [20]. On PBT material example, it has been shown that thermal shrinkage of the tubes with low orientation can be attributed to the rubber-like behavior of a molecular network [9]. The explanation of such phenomena might be that disorientation of the oriented amorphous phase is the predominant mechanism by which shrinkage occurs. Relatively slow crystallization because of low orientation, does not compete with shrinkage. In the highly drawn samples with high orientation, however, crystallization can be extremely rapid, especially at high temperatures, and can impede shrinkage. As mentioned before, shrinkback around glass temperature may be additional force which will oppose thermal expansion during first heating of the tube depending on polymer chains orientation.

But how to measure orientation?

There are many tests which have been devised [20], depending on equipment type, kind of sample material etc. One of the simplest method is called "Chrysler Test" and has a couple of variations. One of them uses measured stripes cut from a sheet (in different directions to determine local orientation!). Then the samples go to the oven at temperature of polymer thermoforming and stripes are measured again. The greater the difference in specified direction, the bigger the orientation in the sample. The other way for transparent polymers is just to observe by passing the sheet between polarized film. The orientation will appear as rainbow patterns across the sheet. One of the more complicated method and much more precise is polarized Raman Spectroscopy [15], which probes information about molecular orientation and symmetry of the bond vibrations, in addition to the general chemical identification which standard Raman provides. *Measurements are made acquiring spectra with polarisation which is either parallel or perpendicular to the inherent polarisation of the excitation laser. Polarisor is inserted in the beam path between the sample and the spectrometer and Raman polarisation is selected by the user [15].* Polarization measurements provide information about molecular shape and the orientation of molecules in ordered materials, such as crystals, polymers and liquid crystals. Other methods which can be also used include Wide Angle X-Ray Diffraction, Linear Dichroism, Sonic Techniques, or Polarised Fluorescence and a described in literature [15, 20].

7. CRYSTALLIZATION

As it was shortly mentioned, when crystalline polymers cool, small areas of short-range order form. These are highly organized and closely packed molecules which can create crystals. There are several models and theories regarding crystal formation, and the most popular is the "fringed micelle" model. It is a two-dimensional representation of molecules in a crystalline polymer according to the fringed micelle theory [16, 18]. It shows the ordered regions or crystallites embedded in an amorphous matrix. A single polymer chain may be present in sections of different crystallites, which can complicate shrinking effects even more. Larger structures, made up of bundles of crystallites, are named "spherulites" and these are formed in the bulk of the material. They behave in a similar manner to the formation and growth of grains in a metal. Those micelles can be observed on Figure 1.
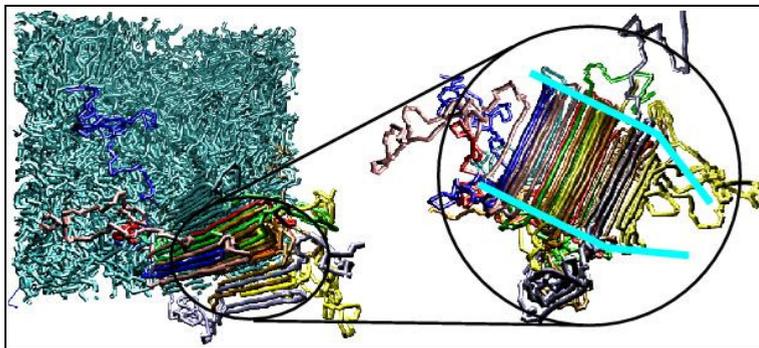
Fig. 1. Formation of a crystal lamella as observed with molecular dynamics. The crystallization domain is observed to extend over several chain diameters [12].

Crystal formation begins at the nucleation points and extends outwards into the bulk of the polymer. The nucleation can be divided into homogenous (small number nucleation sites and a few large crystals) and Heterogeneous, which consists of other elements than the primary polymer. This particles may act as nucleation sites and can form many new crystals. For example, certain coloring agents can act like that and this results in higher shrinkage rates. The type of nucleation process will also affect the properties of crystalline polymers. A product with relatively few large crystals will have different properties than one with more, but smaller crystals.

Not all polymers crystallize to the same degree and in the same way. What is more, different measurement techniques may show different crystallinity level at the same samples. But all of polymers have "s o m e" degree of crystallinity (except for amorphous polymers of course). Crystallinity can vary between 0% (an amorphous polymer) and 80% (a highly crystalline polymer). There are also a number of variables present in polymer structure that affect crystallinity, like length of polymer chain, stereoregularity, number of polar groups and chain branching.
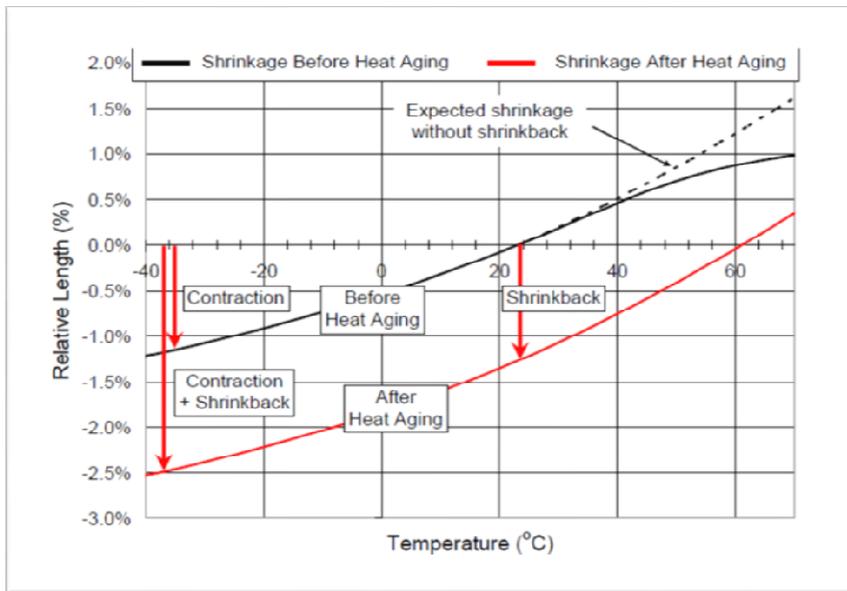
Fig. 2. Bill Hurley Corning – TMA measurement of PE cable jacket [13].

Any of these structures will behave differently in temperature cycling. Most efficient tool for such measurements is **TMA** (Thermo Mechanical Analysis). When measuring program is set for at least two cycles from –40 up to 50°C (depending on polymer type), differences between shrinkage and shrinkback can be easily observed. If production process is controlled, and various structures mentioned before could be obtained, TMA measurement of different crystallinity level and orientation could bring much more interesting conclusion. An example of TMA analysis is showed on Fig. 2.

Some TMA models with modulated measurement system allow to measure total dimensional change and its reversing and non-reversing components. Total signal is identical to standard TMA, but does not uniquely define the *Tg*. Those component signals can clearly separate

actual Tg from the stress relaxation event. Such type of measurement in combination with standard measurement in temperature cycle might give much more information of different shrinking effects.

8. CONTROLLING SHRINKBACK

By modifying processing techniques, crystallinity can be controlled, even in semi-crystalline plastics. It is possible to quench, or rapidly cool, plastic parts to reduce the formation of crystals. However, the success of this depends on the relationship of *Tg* of the polymer and the service temperature. If *Tg* is higher than the service temperature, then the quenching will prevent the formation of crystals during cooling. As a result, they are unlikely to form during the service life of the product. Equally, if the service temperature is approximately the same as or higher than *Tg*, then quenching will only delay the inevitable, and crystallization and shrinkage will eventually occur afterwards, which can cause serious problems after some time [20].

Equally, it is possible to anneal polymers after processing, to ensure that proper crystallization has taken place. Annealing involves holding the polymer above *Tg* but below *Tm* for a specific time to both encourage and control the growth of the crystalline structure. High nucleation and growth rates can also be achieved if heterogeneous nucleation is used. In this case, nucleation is initiated by seeding with a foreign particle, which is typically a polymer similar to the base polymer but with a higher melting point. Some commercial products incorporate special nucleating agents to produce a high degree of crystallization and controlled structures, including coloring agents. It is also possible to induce directional crystallization by stretching polymers below Tm to create crystalline filaments, fibers or sheets with a crystalline structure oriented in the direction of stretching. This cold-drawing technique is used extensively in fiber and film production and in the production of PET bottles.

Another way to control shrinkage is good process controls and understanding of the extrusion process [20]. Many variables have to be controlled and taken into consideration. Even very small changes in the process may change parameters of the product, and affect the behavior of melt material, stress inside and finally, the shrinkage.

Beginning from temperature zone control, the thermocouple must operate properly. Temperature controllers have evolved over the years

with improvements in electronics to provide very accurate control on all extruder zones.

If the actual and set temperatures in a particular zone are significantly different, it may mean i.e., that the temperature is not correctly controlled in that particular zone, or the thermocouple is not operating properly, and may need replacement. Other reason might be that the temperature setting for the material could be wrong or the excess shear heat is being generated in that zone. Also, the polymer melt temperature control is critical to the control and reproducibility of the extrusion process. Melt temperature measurement inside the extruder barrel is not always practical, because the turning screw would shear off a melt probe sticking down in the melt stream.

Melt pressure measurements at the extruder head are also very important. The melt temperature and pressure at the die produce consistent output, resulting in uniform product cross sectional dimension. Like the melt temperature, the melt pressure may show if there are any problems in the extruder and die. The Die pressure fluctuations correspond with the output fluctuations and dimensional changes. Even very small differences in the die shape may result in a bigger shrinking behavior because of the energy dissipation at the probe due to polymer shear heating resulting from the polymer flowing. Also, the usage of a die and shear rate may influence shrinkage.

Another important factor that should be investigated and controlled is rheological behavior [17]. Uncontrolled changes in polymer viscosity may result in product dimensional changes, higher or lower shear heating causing possible res in degradation, or higher motor loads and different melting and metering characteristics. Such behavior may have great importance, especially with flame retardant materials. Other than the equipment problems, viscosity variations are an issue associated with running different regrinds at various levels, flame retardant materials, blends , or coextrusions. Measurement of MFI, or online viscosity measurements could avoid or reduce such problem and detect any sudden viscosity changes. Another, but not so popular method could be online FT-IR measurements which could show any composition and additive levels in a formulation. In-line measurements eliminate the problems associated with sampling methodology, sample preparation, and time delays. In addition, the infrared (IR) crystalline absorption bands are not present, as the polymer is molten and amorphous. In-line systems must be able to handle high temperatures and high melt viscosities, and be able to perform in a manufacturing environment with delicate equipment.

9. SUMMARY

Because of complexity of this phenomena, dimensional change of polymers, is still not 100% understood. The polymers might have the properties of both liquids and solids depending on their properties and conditions. All kind of described mechanisms affect dimensional changing properties of polymers. When cable production factors are added, which additionally affects orientation of polymer chains and sensitivity of optical fibers inside, preparing perfect conditions which prediction of all the consequences in short and long term, might be a real challenge. Especially after realizing how much different kind of polymer materials and components optical cables are made of. Finally – all kind of external conditions, where cables are placed also can be very harmful and can influence shrinking and as a consequence – reduce optical performance. Laboratory tests which can simulate real conditions including thermal cycling, environmental and mechanical influence should not be the only tool for such complex problem. Much more effort should be placed on experiments in real environment, including manufacturing and mounted products in long term behavior.

REFERENCES

[1]   H. De Boer and O. Grosskurth, TKF BV. 7480 AA, Haaksbergen Netherlands; Ann Watson & James Robinson Borealis Polymers NV. B-3583, Beringen Belgium "Low Shrink HDPE for the Sheathing of Fibre Optic Minicable" .

[2]   L. Olasz, Doctoral thesis no. 63 "Residual Stresses and Strains in Cross-linked Polyethylene Power Cable Insulation", TRITA, HFL-0412 KTH Engineering Sciences Stockholm, Sweden

[3]   P. P. Parlevliet, H. E. N. Bersee and Adriaan Beukers "Residual stresses in thermoplastic composites – A study of the literature – Part II: Experimental techniques" Faculty of Aerospace Engineering, Delft University of Technology Delft, The Netherlands, 4 July 2006

[4]   S. T. E. Aldhouse, D. McMahon and J. E. Robinson, "Problems and Opportunities in the Use of Short Relaxation. Linear Polymers in Telecommunication Cable Applications"., Proceedings of Fourth International Conference; Plastics in Telecommunications, 1986, pp. 32.1-32.12.

[5] L. Rogestedt and H. B. Martinsson, "A New Generation Polyethylene Resins For Cable Jacketing Applications", Proceedings of the 47th IWCS, 1999, pp. 126-131.

[6] T. Chen and J. R. Leech, "Design of Polyethylene Cable Jacket Compounds of Superior Jacketing Performance"., Proceedings of the 48th IWCS, 1999, pp. 807-814.

[7] "Crystallinity in Plastics", Zeus Technical Newsletter, Copyright ©2007-2010 Zeus Industrial Products, Inc.

[8] P. P. Parlevliet, H. E. N. Bersee and A. Beukers. "Residual stresses in thermoplastic composites – A study of the literature – Part I: Formation of residual stresses" Faculty of Aerospace Engineering, Delft University of Technology, The Netherlands. 28 December 2005.

[9] V. B. Gupta, J. Radhakrishnan and S. K. Sett, "Interaction between thermal shrinkage and crystallization in axially oriented poly(ethylene terephthalate) fibres and films", Textile Technology Department, Indian Institute of Technology, New Delhi, India 20 January 1993.

[10] M. Trznadel, T. Pakula and M. Kryszewski, Centre of Molecular and Macromolecular Studies, Polish Academy of Science, Łódź, ul. Boczna 5, Poland, 13 February 1984.

[11] M. Trznadel "Naprężenia skurczu termicznego zorientowanych polimerów" PhD thesis Polska Akademia Nauk Łódż 1989.

[12] Polymer crystallization, Équipe "Théorie et Simulation des Polymères" (ETSP),Institut Charles Sadron (ICS), Strasbourg, France.

[13] W. C. Hurley, R. S. Freeland, and M. R. Ellwanger "Shrinkback-Induced Attenuation in Loose Tube" Cables Corning Cable Systems, Hickory, NC.

[14] "Halogen-free Optical Fibre Cables for Outdoor and/or Indoor Use", November 2010, Belden application note.

[15] "What is polarized Raman spectroscopy?" Horriba Scientific Paper and webinar.

[16] S. H. Wasserman and J. LaMonte Adams, Rheology and crystallization in fiber optic cable jacket and conduit extrusion, Union Carbide Corporation, Somerset, NJ

[17] K. Migler, Ch. Liu, and D. J. Pine, "Structure Evolution of a Polymer Solution at High Shear Rates" Exxon Research and Engineering Company, 79 Route 22 East, Annandale, New Jersey 08801Received July 13, 1995; Revised Manuscript Received November 27, 1995X

[18] G. D. Brown, K. P. (Peter) Pang, Ph.D., S. H. Wasserman, Ph.D. "Design of New Easy Processing High Modulus Compounds for Fiber Optic Cable Use".

[19] J. J. Henry, Nafaa "Low Shrinkage in Wire and Cable Extrusion and the Importance of Grade Selection" Mekhilef Arkema Inc. King of Prussia, PA 19406.

[20] H. F. Giles, Jr., J. R.Wagner, Jr. and E. M. Mount, III, "Extrusion: The Definitive Processing Guide and Handbook" 2005.

CURRICULA VITAE

Mateusz Lutomski was born in 1983 in Lublin. After receiving M.Sc. from Maria Curie-Sklodowska (MCS) University in 2007 (Optical Fibers Department) he was hired as a Technical Assistant at Technical University of Lublin. At the end on 2007 he moved to Łódź where he started working for Corning Cable Systems firstly in Research and Development Department, where he prepared his first patent. In the beginning of 2010 he participated in creating Testing and Qualification Laboratory and has been responsible for Materials Laboratory.

Parallel he finished post-graduation studies at Technical University of Łódź – "Innovative materials technologies and measurement-computational systems" (2010) and "Chemical analysis in quality controlling and environmental protection"(2011). He was promoted to Senior Materials Development Engineer in 2012 and joined Global Materials Group. He started PhD studies at MCS University with collaboration with Corning Cable Systems (PL & DE) and Corning Incorporated (US) in 2012, with research area focused on "shrinkback" phenomena and dimensional polymer changes in Optical Cables.

Barbara Gawdzik was born in 1954 in Lublin. After receiving M.Sc. from Maria Curie-Sklodowska (MCS) University in 1978 she was employed at the Department of Polymer Chemistry and Technology in MCS University. She received Ph.D. in 1986 and habilitation in 1993. In 2004 she was appointed by the President of Poland to the post of professor. Since 2006 has also been head of the Department of Polymer Chemistry, MCS University.

She is the author and co-author of 150 original papers in internatio-nal journals, 140 published as conference materials, and 21 patents.

Main areas of her scientific interests include:
- synthesis of new monomers and polymers,
- heterogeneous polymerization techniques,
- investigations of porous structure of polymeric materials,
- preparation of polymeric microspheres for chromatography,
- synthesis and applications of imprinted polymers,
- synthesis and investigations of carbon adsorbents from synthetic precursors.

Synthesis and characterization of activated carbons obtained from nutshells

Diana Mańko[a,c], Mariusz Barczak[b] and Anna Zdziennicka[a]

Faculty of Chemistry, [a]Department of Interfacial Phenomena,
[b]Department of Theoretical Chemistry
Maria Curie-Skłodowska University
M. Curie-Skłodowskiej Sq. 3, 20-031 Lublin, Poland
[c]manko_diana@interia.pl

Walnut and hazelnut shells were used to prepare activated carbons using potassium hydroxide as an activation agent. The obtained activated carbons presented a specific surface areas of 1661 and 1322 m^2/g and pore total volumes of 0.80 and 0.65 cm^3/g, respectively. Moreover, the obtained activated carbons presented high quantity of micropores in their structure and that is why they have a great potential for environmental applications and they could be an alternative to commercially available activated carbons from the viewpoint of adsorption capacity. This paper proves that walnut and hazelnut shells have got a large potential as precursors to obtaining activated carbons and they could be successfully converted into a well-developed porous materials by chemical activation.

1. INTRODUCTION

Activated carbons are popular porous adsorbents with high surface area (more than 500 m^2/g) and turbostratic structure [1]. Crystal structure and the most important properties of activated carbons depend on the type of organic precursor used to produce them and the conditions prevailing during the whole process of preparation of activated carbons. Almost any

carbonaceous source material may be used as a raw material for the preparation of activated carbons. The most commonly used raw materials for the production of commercial activated carbons are wood, charcoal, soft coal, petroleum coke, lignite and peat [2]. The demand for activated carbon is growing and production and regeneration of activated carbons produced from mentioned before raw materials are expensive. Therefore, such agriculture by-products as nutshells, fruit stones, corncobs or spirit leeses are more frequently used as precursors of activated carbons. These materials are usually high in carbon content and low in inorganic matter content [3, 4]. A large number of activated carbons produced from waste materials can replace commercial activated carbons due to their low-cost, well-developed structure, high surface area and high efficiency in adsorption of both gases and solutes from aqueous solutions. Moreover, the production of activated carbons from agriculture waste materials (which are generated in large quantities) allows to dispose them and convert into valuable adsorbents with a reasonable cost [5, 6].

Activated carbons can be obtained by physical or chemical activation of raw material. The physical activation process consists of two stages. The first one is the pyrolysis of raw material in high temperature (500-800°C) without contact with oxygen or other chemical reagent. Thus, this process is called carbonization. After the carbonization, in the second stage, the prepared char is reacting with water steam, carbon dioxide or air, usually at a high temperature (800-1000°C) [7, 8].

In one-step chemical activation the raw material is treated (mixed or impregnated) with a chemical reagent, and then this mixture is pyrolyzed in an inert atmosphere (the activation and the carbonization processes are carried out at the same time) at a lower temperature and a shorter time than those used in the physical activation process [9]. During the chemical activation, the raw material reacts with the chemical agent, which can be: salt ($ZnCl_2$, K_2CO_3), acid (HNO_3, H_2SO_4, H_3PO_4) or hydroxide (NaOH, KOH) [10]. The chemical activation needs a washing step at the end of the whole process because the porosity created in the carbon structure is blocked by the chemical compounds, which have to be removed from the resultant activated carbon to acquire required porosity.

As a result of the activation process, a much richer carbon content material with more ordered and more developed structure than the precursor is obtained [11]. The nature of the precursor, carbonization process conditions (heating rate, time and final temperature of pyrolysis) and activation process conditions (type of activation agent, the chemical

reagent to raw material ratio, heat treatment and washing-step at the end of the process) have an effect on the chemical and properties and the porous structure of the produced activated carbons.

In this paper, a method for preparing activated carbons from the walnut and hazelnut shells by chemical activation using potassium hydroxide as an activation agent has been described. The chemical activation is an effective method to obtain activated carbons with a higher surface area and narrower pore distribution than those prepared in a physical one [12]. Moreover, KOH is a strong base which diffuses into carbon layers, destroys a textural structure of raw material and creates microporosity in the carbon structure (microporosity is a result of a series of chemical reactions and intercalation of alkali metal in the material structure), and it is found to be the most effective alkali hydroxide in the preparation of activated carbons with a well-developed structure [6, 11, 13]. The chemical activation by alkalis involves the hydroxide reduction and carbon oxidation to generate porosity. In such case, KOH is an activation agent which promotes oxidation reactions and catalyzes them [12, 13]. The reactions during KOH activation can take place in the following way [14]:

$$4KOH + C \rightarrow K_2CO_3 + K_2O + 2H_2 \qquad (1)$$
$$K_2CO_3 + 2C \rightarrow 2K + 3CO \qquad (2)$$

and then some surface oxygen complexes can be generated, which are responsible for the continuation of carbon gasification and release of the gaseous substances [11].

The aim of this paper is to investigate the influence of the type of raw material and the selected conditions that prevail during the process of preparation of activated carbons on the pore structure and surface chemistry of obtained adsorbents. The obtained from adsorption isotherms results were also compared with the values of the same textural parameters calculated for the commercially available activated carbon – Norit SX-2.

2. MATERIALS AND METHODS

2. 1. Preparing activated carbons

Two kinds of nutshells were used as precursors to prepare activated carbons: the walnut and hazelnut shells.

Before the carbonization, the nutshells were crushed and weighed. Next, the particulate material was placed in a quartz boat in the heating part of the furnace type PRC 20M and heated up to the carbonization temperature (500°C) under a nitrogen gas flow at 300 cm^3/min with a heating rate of 10°C/min. This temperature was maintained for 2 hours. After this time, the resulting char was cooled down to room temperature, weighed and ground to fine powder in a mortar. The resulting powder was mixed with solid potassium hydroxide (weight ratio of 1:2) and left for 30 minutes at room temperature. After this time, the resulting sample was again placed in the furnace and pyrolyzed under the same nitrogen gas flow and heating rate. The temperature during the process was changed at first from room temperature to 300°C with a residence time of 2 hours and next from 300 to 800°C with the same residence time. After the pyrolysis, the resulting sample was cooled down to room temperature under the nitrogen gas flow, and then it was washed to remove the residual KOH with 0.1 mol/dm^3 hydrochloric acid. After 1 hour, the excess of the acid was leached out by washing with distilled water until the pH of the filtrating solution was neutral (the wash waters were tested with solid AgNO$_3$ for the detection of chloride ions) and finally the cleaned material was dried in an oven for 12 hours at 110°C.

The activated carbons prepared from the walnut and hazelnut shells are designated WS and HS, respectively.

2.2. Characterization of the pore structure

The characteristic of the pore structure of the obtained activated carbons was determined from the nitrogen adsorption/desorption isotherms measured at –196°C on an automatic adsorption apparatus Micrometrics ASAP 2405N. The obtained isotherms were used to calculate the specific surface areas ($S_{Langmuir}$ and S_{BET}) using the Langmuir equation and the BET (Brunauer-Emmet-Teller) one. The *t*-plot and BJH methods were applied to calculate the total pore volumes (V_{Total}), the micropore volumes (V_{micro}) and the pore size distributions. At the end, the average pore diameters ($d_{Average}$) were determined.

The textural parameters of the commercial activated carbon (Norit SX-2) were calculated by the same way for a comparison between the textural properties of widely used commercial carbon and the obtained activated carbons.

2.3. Chemical characterization

The surface chemistry of the obtained activated carbons was studied by means of Fourier transform infrared (FT-IR) spectroscopy. FT-IR spectra were recorded on a 1725X Perkin-Elmer spectrophotometer at room temperature with a resolution of 4 cm^{-1} and KBr discs.

3. RESULTS AND DISCUSSION

Two series of activated carbons were prepared by the chemical activation of walnuts and hazelnuts shells with potassium hydroxide as an activation agent.

Figure 1 shows the nitrogen adsorption/desorption isotherms for the WS, HS and Norit SX-2 activated carbons. The shapes of both obtained for HS and WS adsorption isotherms are Type I in the IUPAC classification. This means that at low values of relative pressure a rapid linear increase in nitrogen adsorption followed by a plateau can be observed. Type I of the isotherm is called the Langmuir isotherm and it indicates that the tested material is mainly microporous [15].
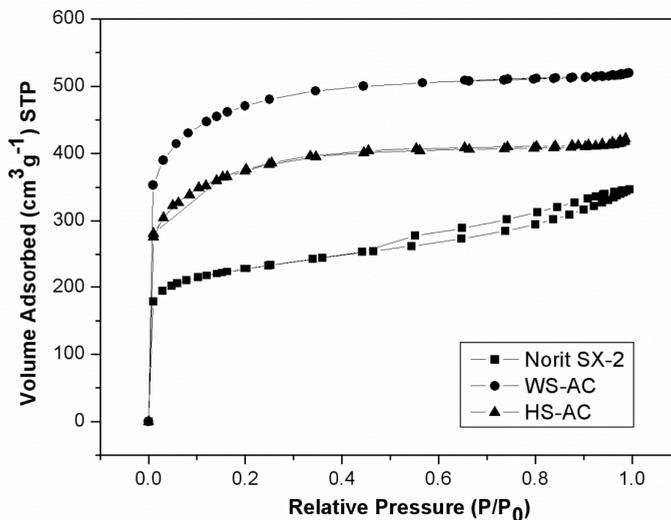
Fig. 1. N$_2$ adsorption/desorption isotherms at 77 K of the WS, HS and Norit SX-2 activated carbons.

The adsorption isotherm for Norit SX-2 is structurally different from those obtained for the WS and HS activated carbons – it rapidly increases at low values of relative pressure but for higher values of relative pressure

it shows no plateau but further gradual increase until it reaches $p/p_0=1$ [13]. Such an increase in the whole range of the relative pressure suggests that Norit SX-2 is a mainly microporous material with a certain mesoporosity development, and the presence of the hysteresis loop (type H4), which occurs at around 0.45 relative pressure, confirms the high content of mesopores in the structure of the adsorbent. The obtained results for the WS and HS activated carbons, for which the major adsorption occurs only below a very low pressure ($p/p_0 = 0.1$), indicates that their pore size distributions are uniform in contrast to the commercial Norit SX-2, for which the pore size distribution is heterogeneous [8, 16].

The obtained from adsorption/desorption isotherms results were also used to calculate the specific surface area of WS, HS and Norit SX-2 activated carbons by means of the BET and the Langmuir equations. The BET equation is commonly used to calculate the specific surface area of porous adsorbents and it can be applied in the range of the relative pressure in which the plot of $1/[V(p_0/p − 1)]$ vs. p/p_0 is linear. It is better to use the Langmuir equation to calculate the specific surface area of microporous adsorbents (for which it is often difficult to establish the relative pressure range in which the BET equation may be applied). The Langmuir method is based on the theory of monomolecular adsorption and this type of adsorption is characteristic of the microporous adsorbents [17, 18].

The values of the specific surface areas calculated from BET and Langmuir isotherms are summarized in Table 1. The values of $S_{Langmuir}$ for all the examined carbons are higher than the values of S_{BET}. The highest values of the specific surface areas are observed for WS activated carbon and at the same time the values of $S_{Langmuir}$ and S_{BET} for both obtained activated carbons are much higher than those for the commercial Norit SX-2.

The values of the total pore and micropore volumes and the average of the pore diameters of examined carbons are also summarized in Table 1.

Table 1. Textural parameters of the WS, HS and Norit SX-2 activated carbons.

Sample code	S_{BET} (m^2g^{-1})	$S_{Langmuir}$ (m^2g^{-1})	V_{Total} (cm^3g^{-1})	V_{micro} (cm^3g^{-1})	$d_{Average}$ (Å)
WS	1661	2098	0.80	0.40	24
HS	1322	1671	0.65	0.28	32
Norit SX-2	804	1011	0.53	0.21	41

The experimental results indicate that the total pore and micropore volumes of WS activated carbon are higher than those of HS one. The inverse relationship is observed for an average pore diameter which is lower for WS than for HS activated carbon. The textural parameters of the obtained activated carbons may be compared to those represented by the commercial activated carbon. Norit SX-2 has got a smaller surface areas, smaller total pore and micropore volumes and higher average pore diameter compared to the obtained activated carbons. The highest ratio of the micropore volume to the total pore volume (0.5) is observed for WS activated carbon. This ratio for HS (0.43) and Norit SX-2 (0.4) is much lower, but still the share of micropores in their structure is significant.

Finally, the pore distribution was also calculated from the nitrogen adsorption data. The porosity and the pore size distribution in the activated carbons depend on the type of raw material and the activation process conditions (including the type of an activation agent). The pore size distributions of both obtained activated carbons are given in Fig. 2 and they characterize the structural heterogeneity of the obtained materials.
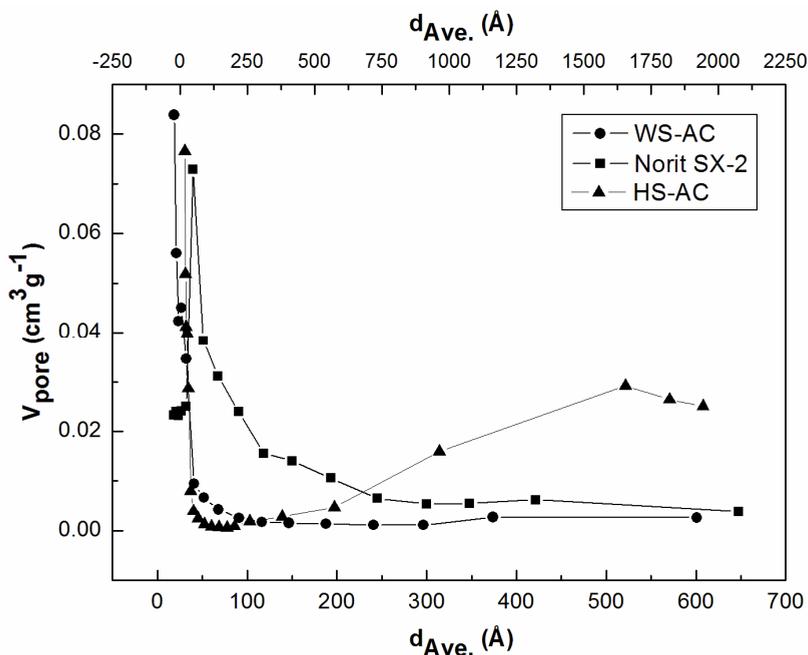
Fig. 2. Pore size distribution of the WS, HS and Norit SX-2 activated carbons.

The walnut shells are more susceptible to develop microporosity on activation with potassium hydroxide than hazelnut shells. For the

commercial Norit SX-2, a wider and more heterogeneous pore size distribution (also shown in Figure 2) is observed. In the structure of the resultant carbons and commercial activated carbon there are micropores (<20Å) located between carbon layers, mesopores (20-500Å) and macropores (>500Å) in different proportions [19]. The pore size distributions indicate that in the structure of the WS activated carbon there are pores with the sizes ranging from 18 to 600Å and most of them are micropores with the sizes smaller than 20Å and small mesopores with the sizes 20-40Å (10% of all the pores are pores with the sizes of 18-20Å). In the structure of the HS activated carbon there are pores with the sizes ranging from 18 to 1950Å, and as in the case of WS activated carbon, there are a lot of micropores and small mesopores (12% of all the pores are pores with the sizes of 18-20Å), but in contrast to the WS activated carbon HS has got a lot of pores with the sizes more than 500Å (macropores). At the same time in the structure of Norit SX-2 there are pores with the sizes ranging from 18 to 650Å and most of them are mesopores with the sizes of 35-50Å (12% for all the pores). It can be seen from the graph presenting the pore size distribution of Norit SX-2 that the porosity of this carbon is very heterogeneous and in its structure there are a lot of pores with different sizes (the pore distributions of the WS and HS activated carbons are narrower).

Essentially microporous WS and HS activated carbons probably have a better adsorption capacity than Norit SX-2 because the adsorption capacity of porous adsorbents largely depends on the amount of micropores that are present in their structure [13].

The chemical characterization of the obtained activated carbons was studied by FT-IR spectroscopy in order to identify what kind of surface functional groups are at their surfaces. Figure 3 shows the FT-IR spectra for the obtained activated carbons.

Both samples show the broadband adsorption spectra around 3700-3000 cm^{-1} typical for O–H stretching vibrations in hydroxyl groups associated with the surface, or for O–H–O stretching vibrations in water molecules which could be adsorbed on the surface. Higher intensity of this band for the WS than HS activated carbon indicates its more hydrophilic character. Moreover, all the samples exhibit two weak peaks around 2850 and 2900 cm^{-1} which can be attributed to C–H stretching vibrations in the methyl group [20].
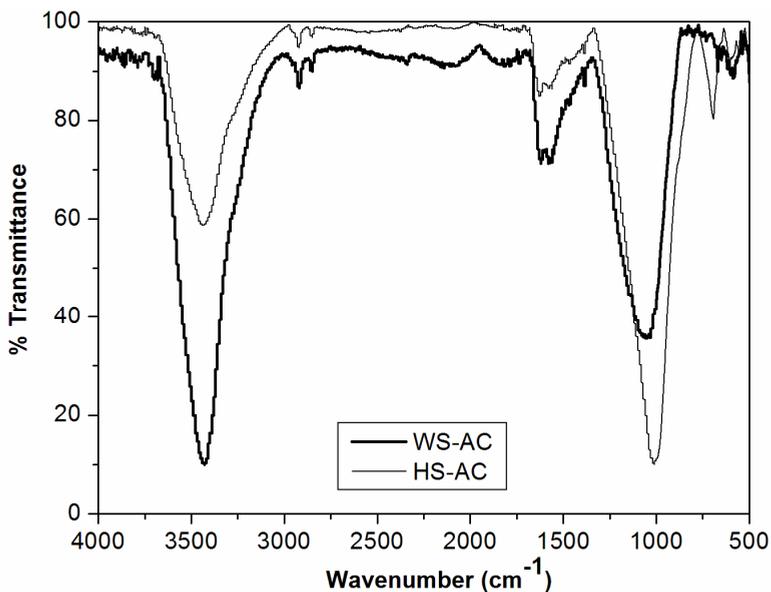
Fig. 3. FT-IR spectra of the WS and HS activated carbons.

The peaks around 1700-1350 cm^{-1}, visible for both activated carbons, are probably the result of a combination of several bands characteristic for different types of vibrations: C=O stretching vibrations in the carbonyl or lactonic groups (1650-1700 cm^{-1}) [14], C=C aromatic ring stretching vibrations (~1600 cm^{-1}), –(C=C)$_n$– bonds stretching vibrations in polienes (1590 cm^{-1}), C–H stretching alkane (1350-1400 cm^{-1}), and also vibrations typical for the carboxyl-carbonate structures near the wavenumber of 1400 cm^{-1} [20, 21].

Strong and broad band for both activated carbons is observed around 1350-800 cm^{-1}, and it can be attributed to C–O stretching vibrations in phenolic, carboxylic or ether groups which are dominant in the HS activated carbons (higher intensity of the band).

Moreover, for the HS activated carbon, the weak peak around 700 cm^{-1} is observed. It probably correspond with –COH deformation vibrations or it could be related to the cyclic aromatic structures [20].

Probably at the surface of the resultant carbons there are oxygen groups like carbonyl, ether, alcohol, carboxyl and phenolic groups [22].

4. CONCLUSIONS

Highly microporous activated carbons with the presence of oxygenated functional groups at their surfaces were prepared from the walnut and hazelnut shells by the chemical activation with solid potassium hydroxide. The resultant activated carbons attained high values of the specific surface areas and micropore volumes up to 2.5 cm^3/g. The obtained results indicated that the walnut and hazelnut shells could be great raw materials for the preparation of activated carbons with the large surface area and well-developed porosity.

It was also found that the obtained activated carbons had higher surface areas, narrower pore size distributions and more developed structures than commercial Norit SX-2. Therefore, they have also better adsorption properties and could be used in numerous fields which require the higher surface areas carbons, e.g. for gas storages or as an electrode materials for electric double layer capacitors and supercapacitors [7, 23].

REFERENCES

[1]   F. H. Stoeckli, *Carbon*, **28**, 1-6, (1990).
[2]   A. Dąbrowski, P. Podkościelny, Z. Hubicki and M. Barczak, *Chemosphere*, **58**, 1049-1070, (2005).
[3]   C. Pechyen, D. Aht-Ong, V. Sricharoenchaikul and D. Atong, *Mater. Sci. Forum*, **658**, 113-116, (2010).
[4]   L. Z. Chen, D. X. Miao, X. J. Feng and J. Z. Xu, *Adv. Mat. Res.*, **881-883**, 579-583, (2014).
[5]   R. M. Suzuki, A. D. Andrade, J. C. Sousa and M. C. Rollemberg, *Bioresource Technol.*, **98**, 1985-1991, (2007).
[6]   N. Ferrera-Lorenzo, E. Fuente, I. Suárez-Ruiz and B. Ruiz, *Fuel Process. Technol.*, **121**, 25-31, (2014).
[7]   A. Klijanienko, E. Lorenc-Grabowska and G. Gryglewicz, *Bioresource Technol.*, **99**, 7208-7214, (2008).
[8]   Z. Sarbak, *Adsorpcja i adsorbenty. Teoria i zastosowanie* (in Polish), Wydawnictwo Naukowe UAM, Poznań, (2000).
[9]   J. Hayashi, T. Horikawa, I. Takeda, K. Muroyama and F. N. Ani, *Carbon*, **40**, 2381-2386, (2002).
[10] H. Treviño-Cordero, L. G. Juárez-Aguilar, D. I. Mendoza-Castillo, V. Hernández-Montoya, A. Bonilla-Petriciolet and M. A. Montes-Morán, *Ind. Crop. Prod.*, **42**, 315-323, (2013)

[11] D. Lozano-Castelló, M. A. Lillo-Ródenas, D. Cazorla-Amorós and A. Linares-Solano, *Carbon*, **39**, 741-749, (2001).

[12] D. Adinata, W. M. A. Wan Daud and M. K. Aroua, *Bioresource Technol.*, **98**, 145-149, (2007).

[13] A. Ahmadpour and D. D. Do, *Carbon*, **35**, 1723-1732, (1997).

[14] Y. Ji, T. Li, L. Zhu, X. Wang and Q. Lin, *Appl. Surf. Sci.*, **254**, 506-512, (2007).

[15] T. J. Barton, L. M. Bull, W. G. Klemperer, D. A. Loy, B. McEnaney, M. Misono, P. A. Monson, G. Pez, G. W. Scherer, J. C. Vartuli and O. M. Yaghi, *Chem. Mater.*, **11**, 2633-656, (1999).

[16] R. Ch. Bansal and M. Goyal, *Adsorpcja na węglu aktywnym* (in Polish), Wydawnictwo Naukowo – Techniczne, Warszawa, (2009).

[17] V. Gómez-Serrano, E. M. Cuerda-Correa, M. C. Fernández-González, M. F. Alexandre-Franco and A. Macías-García, *Smart Mater. Struct.*, **14**, 363-368, (2005).

[18] M. L. Paderewski, *Procesy adsorpcyjne w inżynierii chemicznej* (in Polish), Wydawnictwo Naukowo-Techniczne, Warszawa, (1999).

[19] Wan Mohd Ashri Wan Daud and A. H. Houshmand, *J. Nat. Gas Chem.*, **19**, 267-279, (2010).

[20] O. F. Olorundare, T. A. M. Msagati, R. W. M. Krause, J. O. Okonkwo and B. B. Mamba, *Water Air Soil Poll.*, 225, 1876, (2014).

[21] S. Román, J. M. Valente Nabais, B. Ledesma, J. F. González, C. Laginhas and M. M. Titirici, *Micropor. Mesopor. Mater.*, **165**, 127-133, (2013).

[22] S. Z. Mohammadi, M. A. Karimi, D. Afzali and F. Mansouri, *Cent. Eur. J. Chem.*, **8(6)**, 1273-1280, (2010).

[23] J. Hayashi, M. Uchibayashi, T. Horikawa, K. Muroyama and V. G. Gomes, *Carbon*, **40**, 2747-2752, (2002).

CURRICULA VITAE

Diana Mańko. Born in Radzyń Podlaski (Poland) in 1988. Graduated from Maria Curie-Sklodowska University in Lublin (2012, Department of Theoretical Chemistry). Since 2012 she has been a Ph.D. student in the Department of Interfacial Phenomena at UMCS. Currently she is carrying out research on physicochemical properties of water solutions of sugar-based surfactants, biosurfactants and their mixtures with different additives.

Mariusz Barczak. Born in Swidnik in Poland in 1978. Received his Ph.D. degree in 2007. Since 2007 he has been held a position of adjunct in the Department of Theoretical Chemistry of UMCS. He is a co-author of over 40 papers. Main fields of his interest are: synthesis, functionalization and investigation of porous silica, carbon and hybrid nanomaterials and their application as sorbents of heavy metal ions, phenols and biomolecules.

Anna Zdziennicka. Graduated from Maria Curie-Sklodowska University in Lublin (1988, Faculty of Mathematics, Physics and Chemistry). Received her Ph.D. degree in 1996 in physical chemistry from UMCS. She works in the Department of Interfacial Phenomena in the Faculty of UMCS. Her research work is largely concentrated on physicochemistry of the surface and interface phenomena. She is a co-author of 63 publications.

Statistical analysis of adsorption experimental data – the influence of the selection of error function on optimized isotherm parameters

Dawid Myśliwiec[a] and Stanisław Chibowski[b]

Department of Radiochemistry and Colloid Chemistry, Faculty of Chemistry,
Maria Curie-Skłodowska University
Pl. Marii Curie-Skłodowskiej 3, 20-031 Lublin, Poland
[a]d.k.mysliwiec@gmail.com
[b]stanislaw.chibowski@umcs.lublin.pl

Experimental adsorption data were analysed by fitting them to nonlinear forms of Langmuir and Freundlich isotherms. Optimization of the parameters was performed by nonlinear least square regression with different forms of error function, namely: vertical, horizontal, orthogonal, normal and squared normal. The results showed, that isotherm parameters may be affected by the selection of error function and that they are more sensitive to its' form in case of Langmuir equation. We did not find any correlation between a type of the function and performance of the regression – procedure requires optimization for every experimental dataset and every model being fitted.

1. INTRODUCTION

One of the processes that is most commonly applied in the industry, *e.g.* a wastewater treatment, is adsorption [1-4]. Hence, much effort is put into quantitative and qualitative description of this process. One of the models that is most widely used is a Langmuir model [5], which can be denoted in a form of the following isotherm:

$$a = a_m \frac{Kc}{1 + Kc} \tag{1}$$

where a stands for adsorbed amount, a_m monolayer capacity, K and c for adsorption constant and equilibrium concentration of the adsorbate, respectively. This model has strong theoretical foundations – it assumes that adsorption is localised, surface is energetically homogenous and there is no interaction between adsorbed particles. The constant K may describe thermodynamics of the studied system. The other commonly used isotherm is Freundlich isotherm [6]:

$$a = kc^{1/n} \tag{2}$$

where: k and n are empirical constants.

For many years parameters of mentioned equations were estimated after linearization. After data were transformed simple linear least squares could have been applied. However, one must note, that such transformation increases error of the estimates and may result in biased parameters [1, 7-9]. Therefore, applying nonlinear regression (NLR) directly to (1) and (2) is welcomed. Typically this procedure requires defining some measure of the distance from the experimental point to a model function [7-9]. In general we can write down that:

$$a_i^{\exp}(c_i) = a_i^{pred}(\beta, c_i) + \varepsilon_i\left(c_i, a_i^{\exp}(c_i)\right) \tag{3}$$

where: β and ε stand for the set of the parameters and error function respectively; superscript *exp* means that values were measured experimental, while *pred* means that they are predicted by a model. The optimum estimation of the parameters is achieved when the sum of squares of all error functions is minimized – in other words, the model is closest to experimental points. Figure 1. presents geometrical interpretation of some possible error functions.

Vertical distance is used as an error function the most commonly, mainly due to the fact, that it can be easily computed:

$$a_i^{\exp}(c_i) = a_i^{pred}(\beta, c_i) + \varepsilon_i^{vert} \tag{4}$$

However, estimates calculated using vertical distance as an error function are biased towards the steepest region of the estimated function – in case of adsorption isotherm: towards low concentrations [1, 7, 10]. The opposite situation occurs in case of vertical distance – it usually results in

estimates strongly biased towards points located in a high concentration region. Thus, this approach should better predict monolayer capacity.

$$a_i^{\exp}(c_i) = a_i^{pred}(\beta, c_i - \varepsilon_i^{hor}) \qquad (5)$$
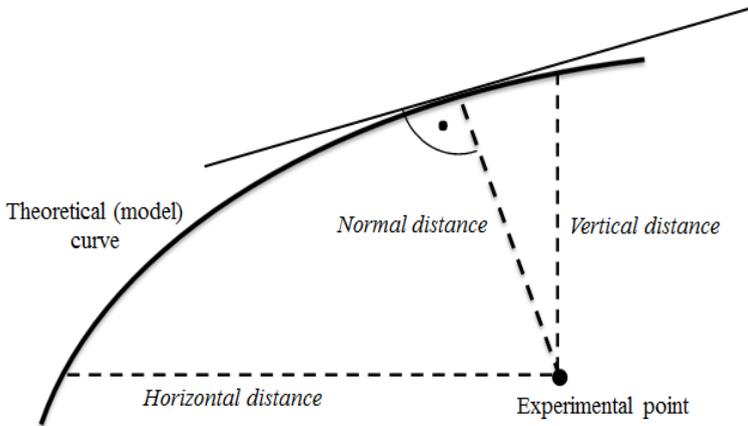

Fig.1. Geometrical representations of some error functions.

To avoid any bias at all (theoretically) one can use orthogonal distance as an error function according to [1]:

$$\varepsilon_i^{ort} = \frac{1}{2}\left[\left(\varepsilon_i^{ver}\right)^2 + \left(\varepsilon_i^{ort}\right)^2\right] \qquad (6)$$

Some comment is needed at this point. In mathematical formalism equation above does not describe orthogonal distance, but it approximates square of orthogonal distance. To avoid confusion between following paper and [1] it will be still called orthogonal. The true orthogonal distance (distance from the experimental points to a closest point of the model isotherm) and its' square are called normal and squared normal, respectively. Normal error is given by:

$$\varepsilon_i^{norm} = \min\left\{d\left((a_i^{\exp}, c_i), (x, y) \in \text{izotherm}\right)\right\} \qquad (7)$$

The goal of this work is examine which of the proposed measures of an error is the most efficient for fitting data to Langmuir and Freundlich model. One must have in mind that nonlinear regression is most credible when following assumptions are justified:

- expected value of errors is zero (verified via t-Student test) [11];
- errors are homoscedastic, which means that they have constant variance (verified via error vs. score plot);
- errors are normally distributed (verified via Shapiro-Wilk test) [11] and uncorrelated.

Violation of these assumptions may potentially lead to misleading results.

2. EXPERIMENTAL

Data sets were experimental adsorption isotherms of L-phenylalanine (>99.9%, SigmaAldrich) on graphite (SigmaAldrich). Each isotherm consists of at least 20 experimental points (each obtained from 3 to 6 replicates). Concentration of all solutions (before and after adsorption) were measured with Carry 100 UV-Vis spectrometer by Varian at wavelength 206 nm.

Single replicate was done according to a following procedure. 10mL of a solution of L-phenylalanine in a borate buffer was added to 0.20g of graphite in an Erlenmeyer flask. The suspension was shaken (120 osc./min) for 30 minutes to equilibrate and after that the solid was filtrated on a cellulose filter. Postadsorption concentration was measured via UV-Vis spectroscopy. A pH was equal to 6.1, 8.1 and 10.0; in all cases concentration of the buffer was constant and equal to 0.075 mol/dm^3. The ionic strength was also kept constant and was equal to 0.1 mol/dm^3 in all experiments.

Optimization procedure was performed with Newton-Raphson algorithm with multistart (1000 different initial points in a range ± 50 % of optimal parameters). We did not weight experimental points with their uncertainties despite the fact that they have been precisely calculated.

Due to the experimental method adsorption and concentration errors are not independent. However, most of the adsorption experiments are performed in a similar way, therefore, we believe that our results might be helpful for some researchers.

3. RESULTS AND DISCUSSION

In Table 1. we have presented best estimates of the parameters of equations (1) and (2) depending on the type of error function. First thing to notice is a fact, that in case of Langmuir isotherm vertical error

function always gives the smallest monolayer capacity a_m. At the same time the biggest values of this parameter are obtained when error function is defined as horizontal distance from point to isotherm. A relative standard deviation (RSD) was calculated for each parameter to evaluate its' sensitivity to type of error function. In all 3 Langmuir isotherms higher variability was observed for K than a_m, therefore we postulate, that thermodynamic constant is a parameter more sensitive to the choice of error function. In case of Freundlich equation there is almost no sensitivity of k on the type of error function applied in optimization. It is interesting to notice, that orthogonal and squared normal error function leads to almost exactly the same results in both Langmuir and Freundlich equation.

Table 1. Best estimates of the parameters of the isotherm.

	vertical	horizontal	orthogonal	normal	squared normal	RSD
Langmuir, pH = 6.1						
a_m	9.612	10.22	9.691	10.13	10.22	0.032
K	2.477	2.106	2.504	2.136	2.105	0.091
Langmuir, pH = 8.1						
a_m	9.989	11.14	10.06	11.05	11.13	0.056
K	2.268	1.735	2.299	1.809	1.725	0.148
Langmuir, pH = 10.0						
a_m	5.143	5.643	5.396	5.470	5.581	0.036
K	2.626	2.232	2.497	2.232	2.235	0.079
Freundlich, pH = 6.1						
k	6.810	6.858	6.903	6.829	6.858	0.005
n	2.045	2.211	2.060	2.197	2.203	0.039
Freundlich, pH = 8.1						
k	6.846	6.883	6.853	6.973	6.884	0.007
n	1.982	2.143	1.985	2.062	2.148	0.039

cont. Table 1.

	Freundlich, pH = 10.0					
k	3.799	3.865	3.898	3.839	3.861	0.009
n	1.951	2.000	1.937	2.000	1.989	0.015

Despite the fact, that some parameters may differ by as much as 12 % depending on the error function, plots of model isotherms are very similar to each other (see Figure 2 and Figure 3).
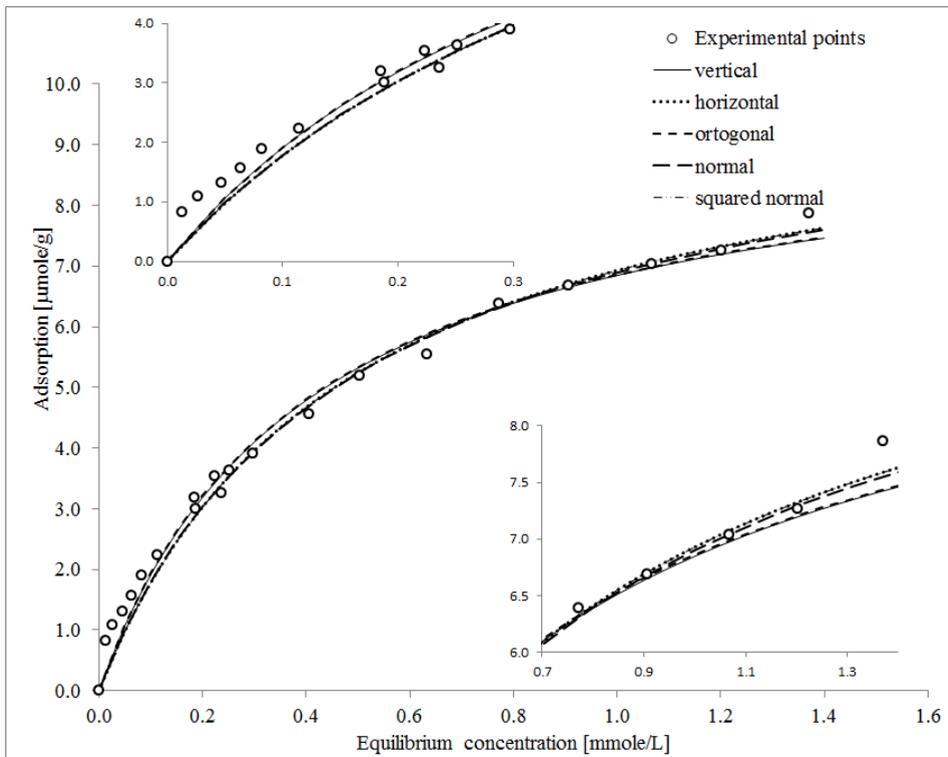
Fig. 2. Plots of optimized Langmuir isotherms for different error functions (pH = 6.1).

In all cases t-Student test confirmed that mean value of the error is equal to zero (at 95 % confidence interval). The homoscedasticy of the residuals is discussed on the basis of plots similar to Figure 4. and Figure 5. The errors are homoscedastic when there are neither patterns on the plot (residuals are not grouped) neither outliers. In case of Langmuir model in the pH = 6.1, see Figure 4., one can see a possible outlier (observation number 17) on all plots and a possible pattern (observations

1-8 have same sign), which makes a homoscedastic assumption speculative. For Freundlich isotherm in pH = 6.1 we did not observe such obvious outliers and the pattern is less significant, especially when we apply orthogonal error function. This suggested that in this case we were dealing with a homoscedastic error.
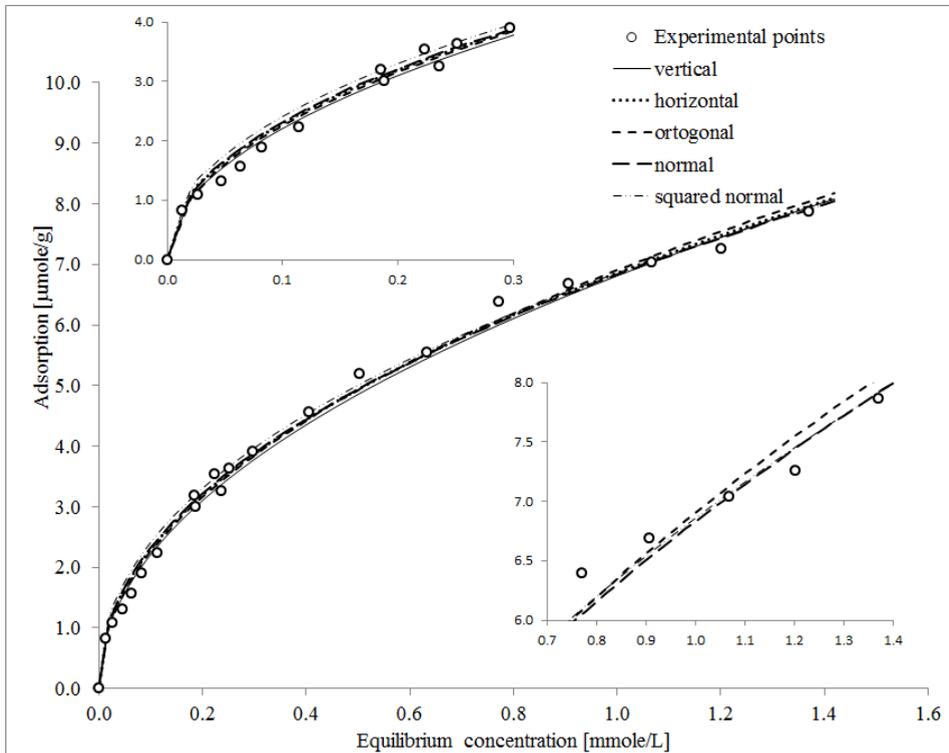
Fig. 3. Plots of optimized Freundlich isotherms for different error functions (pH = 6.1).

A Figure 6. presents a bar plot of p-values of Shapiro-Wilk test for normality of the distribution of an error. In general we can say, that the lower the p-value the less Gaussian is the distribution. It is clear that in this example change of the error function from vertical to orthogonal 'improved normality' in case of Freundlich isotherm but totally 'destroyed' it in case of Langmuir model.
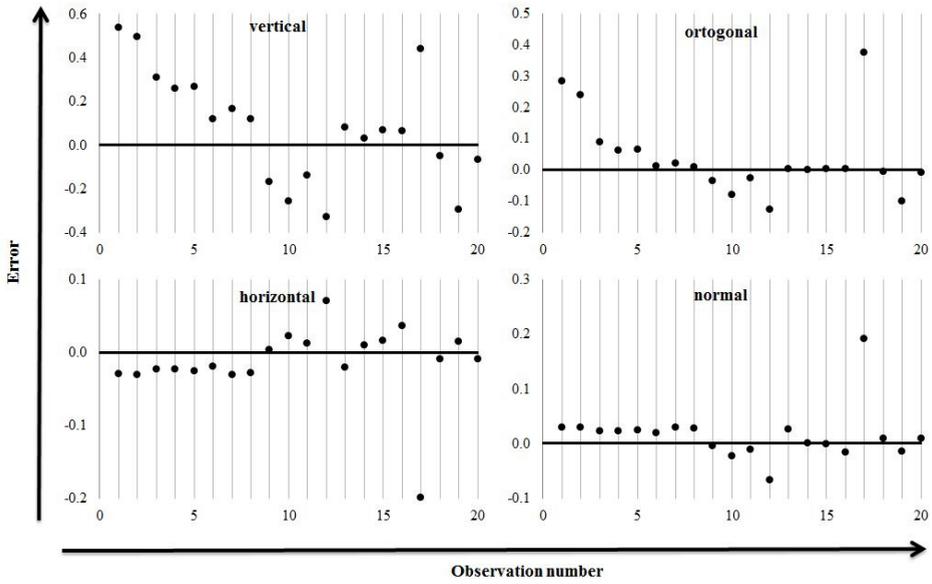
Fig.4. Residuals (errors) of the best estimate Langmuir model (pH = 6.1).
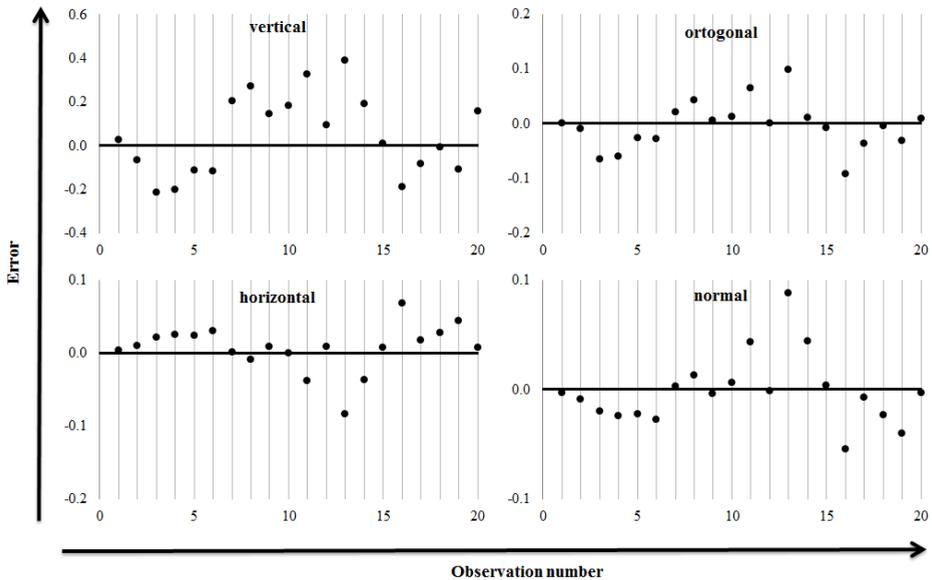
Fig. 5. Residuals (errors) of the best estimate Freundlich isotherm (pH = 6.1).
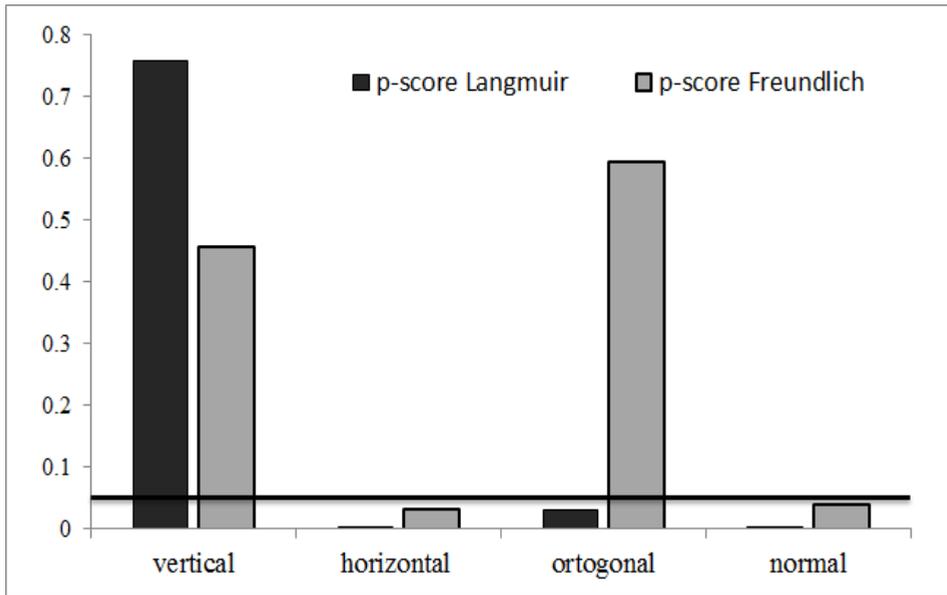
Fig. 6. p-scores of Shapiro-Wilk test for normality of the residuals (errors); (pH = 6.1).

Summing up the all results mentioned, the most reliable isotherm to describe experimental data of adsorption of L-phenylalanine on graphite in pH=6.1 seems to be Freundlich isotherm with the orthogonal error function. It is so because for this choice errors are normally distributed, homoscedastic and their expected value is equal to 0 at 95% confidence interval.

It has to be said, that this choice is not universal not only for studied system but even for different model applied to the same experimental data. However, we have showed that changing the error function might be a very useful tool in analysis of experimental data. It allows to change properties of the regression analysis without changing the studied model, and therefore increase data reliability.

In case of 'permanent' heteroscedasticy of the residuals very efficient is so-called 'robust regression' [7-8]. It can be easily implemented to an algorithm and its' application will be discussed in our future papers.

Presented approach is only a small piece of a complex data analysis proecdure. The following steps should include confidence interval parameters estimation for fitted parameters and calculating goodness of fit coefficients [9, 12-15]. Moreover, various procedures of optimization

may be examined, bias should be discussed as well as robustness should be introduced. This topics will be discussed in subsequent articles.

4. CONCLUSIONS

We have studied the effect of the form of error functions on the properties of the regression analysis of a set of experimental data. The conclusions are following:

1. Results confirm that vertical error function is biased towards region of low equilibrium concentrations, opposite to horizontal error function;
2. Langmuir isotherm seems to be more sensitive to the error function type;
3. There are no universal correlations between form of error function and general properties of regression – optimization is a necessity for every data set;
4. Changing an error function may be a very useful tool allowing one to increase data analysis reliability.

REFERENCES

[1]   M. I. El-Khaiary, *Journal of Hazardous Materials*, **158**, 73, (2008).
[2]   T. Robinson et al., *Bioresource Technology*, **77**, 247, (2001).
[3]   Y. S. Ho et al., *Process Biochemistry*, **40**, 119, (2005).
[4]   G. McKay et al., *Water Air Soil Pollution*, **114**, 423, (1999).
[5]   I. Langmuir, *Journal of the American Chemical Society*, **38**, 2221, (1916).
[6]   H. M. F. Freundlich, *Zeitschrift für Physikalische Chemie*, **57**, 385, (1906).
[7]   S. Chatterjee and J. S. Simonoff, "*Handbook of Regression Analysis*", John Wiley and Sons, New Jersey, 2013.
[8]   N. R. Draper and H. Smith, "*Applied Regression Analysis*", John Wiley and Sons, New York, 1998.
[9]   "*Measurement Error in Nonlinear Models. A Modern Perspective*", Monographs on Statistics and Applied Probability, **105**, Taylor and Francis Group, Boca Raton, 2006.
[10] M. Hadi et al., *Chemical Engineering Journal*, **160**, 408, (2010).

[11] M. Walesiuk and E. Gantar, "*Statystyczna analiza danych z wykorzystaniem programu R*", Wydawnictwo Naukowe PWN, Warszawa, 2012.

[12] H.-T. Thai et al., *Journal of Pharmacokinetics and Pharmaco-dynamics*, **41**, 15, (2014).

[13] A. Spiess and N. Neumayer, *BioMed Central Pharmacology*, **10**, 6, (2010)

[14] W. C. Rooney and L. T. Biegler, *Process Systems Engineering*, **47**, 1794, (2001).

CURRICULA VITAE

Dawid Myśliwiec was born in Lublin in 1988. He studied Basic and Applied Chemistry at Maria Curie-Skłodowska University in Lublin. In 2012 he obtained M.Sc. degree based on master thesis entitled: "A research on the influence of magnetic field on adsorptive properties of the system: hematite – aqueous solution of polyrthyleneimine", supervised by prof. Stanisław Chibowski. Since 2012 he is a Ph.D. Chemistry student at Maria Curie-Skłodowska University in Lublin.

Stanisław Chibowski was born in Przegaliny in 1946. He studied Chemistry at at Maria Curie-Skłodowska University in Lublin. After graduation in 1971 he worked in Institute of Agrophysics of Polish Science Academy. Since 1972 he works in Department of Radiochemistry an Colloid Chemistry at Maria Curie-Skłodowska University in Lublin. He recived his Ph.D. in 1980. Since 2002 he is a Professor. His main field of interest is adsorption of macromolecules on solid surfaces.

ANNALES
UNIVERSITATIS MARIAE CURIE-SKŁODOWSKA
LUBLIN – POLONIA

Influence of the electrolyte type on the adsorption and electrokinetic properties of the ionic polyamino acids – Cr$_2$O$_3$ system

Iwona Ostolska[a] and Małgorzata Wiśniewska

Maria Curie-Sklodowska University, Faculty of Chemistry,
Department of Radiochemistry and Colloids Chemistry,
M. Curie-Sklodowska Sq. 3, 20-031 Lublin, Poland,
[a]*i_ostolska@wp.pl*

The influence of a kind of support electrolyte on the ionic polyamino acids adsorption at the chromium (III) oxide – polymer solution interface was investigated. The NaCl and CaCl$_2$ were used as the background electrolytes. In order to determine the effect of the electrolyte, the same value of ionic strength of the test solutions were taken. It was proved that formation of intermolecular and intramolecular complexes in the presence of divalent calcium ions is responsible for essential changes in polymer adsorption.

Related to the ionic character of polyamino acid two different adsorption behaviours can be observed. The increase of the ASP adsorption amount in the presence of calcium ions may be explained by formation of complexes between the dissociated carboxylic groups and Ca^{2+} ions. The opposite situation takes place in the case of polylysine – the application of CaCl$_2$ results in the dramatic decrease in the polymer adsorption caused by blocking the active sites available for LYS macromolecules. In order to make a comprehensive analysis, the zeta potential and surface charge density measurements were performed taking into account the kind of the background electrolyte. The above-mentioned tests were carried out in the absence and presence of the polyamino acid at two different concentrations – 10 and 100 ppm respectively.

Key words: Polyamino acid, polyaspartic acid, polylysine, chromium (III) oxide, polymer adsorption, potentiometric titration, zeta potential.

1. INTRODUCTION

Polymer adsorption on the solid surface is a very complicated process, determined by many different factors. One of them is the presence of inorganic impurities. They can influence the polymer behaviour at the solid–liquid interface by changing the macromolecules conformation. Moreover, they may modify the surface properties as a consequence of blocking active centers accessible for polymer macromolecules. Explanation of such a phenomena is essential to many areas of human activity, in which adsorption of both natural and synthetic polymers is applied [1-6].

Chromium (III) oxide (Cr_2O_3) was applied as the adsorbent. It is a green, amorphous solid. Cr_2O_3 is used as a stable, non-toxic dye in the paint and ceramic industries as well as for glass production. A broad application of this oxide causes that Cr_2O_3 is a common pollutant in sewages. Because of its intense colour, it is particularly undesirable in an aqueous medium [7, 8].

In the studies two polymers from the polyamino acid group were used: anionic polyamino acid (ASP) and cationic polylysine (LYS). These synthetic macromolecular compounds contain in their structure appropriate amino acids linked by a covalent bond. Due to their structure, these compounds combine the characteristic features of both synthetic (excellent water solubility, stability in a wide pH range) and natural origin polymers (complete biodegradability, a lack of the toxicity). Studies of the adsorption properties of the above mentioned polymers can contribute to a wider use of this class of compounds. Due to the complete biodegradability and nontoxicity of used polymers, the studied systems can find an application mainly in the sewage treatment and water purification processes. Formation of the stable Cr_2O_3 suspensions in the presence of the polyelectrolytes is also important in ceramics.

The aim of this paper was to determine the influence of a background electrolyte type and solution pH on the adsorption properties of two polyamino acids of different ionic nature of functional groups. In order to make a comprehensive analysis of the interactions present in the studied systems, the adsorption amount of the macromolecular compounds on the surface of colloidal chromium (III) oxide was measured. Additionally, the surface charge density measurements as well as the zeta potential tests in the absence and presence of the polymers (in a suitable background electrolyte) were performed. These studies allow to determine the

influence of the earlier mentioned factors on the adsorption and electrokinetic properties of the polyamino acid solution/ Cr_2O_3 systems.

2. MATERIAL AND METHODS

Chromium (III) oxide (Cr_2O_3) produced by POCh Gliwice (Poland) was used as an adsorbent in the experiments. The specific surface area of Cr_2O_3 determined by the BET method (analysis of nitrogen adsorption-desorption isotherms; Micromeritics ASAP 2405 analyzer) was found to be 7.12 m^2/g. The solid was washed with doubly distilled water to remove the impurities until the conductivity of the supernatant was smaller than 2 µS/cm. The point of charge (pH_{pzc}) of chromium (III) oxide was 7.6 (obtained from the potentiometric titration) and its isoelectric point (pH_{iep}) was about 6 (zeta potential measurements; Zetasizer 3000, Malvern Instruments) [9]. Despite the small surface area, chromium (III) oxide was applied as the adsorbent. It was the consequence of the fact that in the studied pH range on the Cr_2O_3 surface can exist surface active groups of different charge (positively charged in acidic pH and negatively charged at higher pH values). Although γ-Al_2O_3 exhibits considerably higher surface area, the pH_{pzc} point of this material is equal to 8-9. It denotes that the alumina particles become negatively charged above pH 9. The presence of positive charge on the adsorbent surface lead to the situation in which the cationic polylysine do not undergo adsorption at the solid-liquid interface.

Polyamino acids: sodium salt of polyaspartic acid (ASP) and poly(lysine hydrochloride) – LYS were produced by Alamanda-Polymers (USA). The average molecular weights of the polymers in question were: 27.000 for ASP and 33.000 for LYS. The polyamino acids exhibit ionic character (anionic and cationic for ASP and LYS respectively) These polymers contain one type of functional groups in their macromolecule chains which is able to dissociate in the aqueous solution. The structures of polymeric substances are shown in Fig. 1.The polydispersity index data (obtained from the producer) were in the range from 1.02 to 1.05. As a supporting electrolyte sodium chloride or calcium chloride (Fluka) were used. The concentration of NaCl was 0.01 mole/dm^3 whereas the concentration of $CaCl_2$ was equal to 0.003 mole/dm^3. Such concentrations of the salts give demanded ionic strength of the solutions ($I = 0.01$) for both electrolytes. The experiments were carried out in doubly-distilled water at room temperature ($\approx 25°C$).
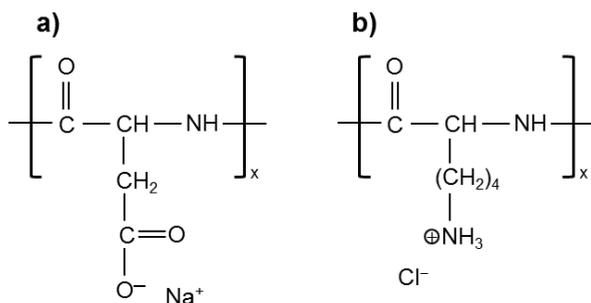
Fig. 1. Structures of used polymers: a) ASP, b) LYS.

2.1. Adsorption measurements

Adsorbed amount (Γ, mg/m^2) of the applied polyamino acids was measured by the spectrophotometric method with a UV-Vis Spectro-photometer Carry 100 (Varian) connected to the computer with the use of ASP and LYS absorption spectra. Experiments were carried out for the two different pH values for each polymer: 3 and 10 for ASP as well as 7.6 and 10 for LYS. Previous studies shown that LYS does not adsorb on the Cr_2O_3 surface at $pH = 3$. The concentrations of both polymers ranged from 10 to 120 ppm. All samples were prepared by diluting the stock solution of macromolecular compounds whose concentrations were determined by the gravimetric method. The concentration of the supporting electrolyte (NaCl or $CaCl_2$) was constant.

To determine the adsorption amount of polyamino acids, the following procedure was applied. 0.1 g of chromium (III) oxide was added to 10 cm^3 of polymer solution in the supporting electrolyte with suitable concentration. Next pH was adjusted to the desired value using HCl and NaOH at a concentration of 0.1 mole/dm^3. To achieve adsorption – desorption equilibrium, the suspension was shaken for 20 hours in a thermostated stirrer (25°C). Then, the suspension was centrifuged twice for 10 minutes and 5 ml of clear solution was taken for further analysis. The absorbance of ASP and LYS was measured at a wavelength 210 nm. The extent of polymer adsorption was calculated from the calibration curves measured in solutions of different pH values. The measurement uncertainty in the analysis was up to 3%.

2.2. Potentiometric titration

The surface charge on the metal oxide is formed as a result of reactions between the surface hydroxyl groups and electrolyte ions. The

most important factor in the surface charge formation process is the concentration of hydrogen and hydroxide ions as well as ions of background electrolyte. Hydrogen ions influence the surface charge density through the reactions of surface hydroxyl groups:

$$\equiv SOH_2^+ \quad \leftrightarrow \quad \equiv SOH + H^+ \tag{1}$$

$$\equiv SOH \quad \leftrightarrow \quad \equiv SO^- + H^+ \tag{2}$$
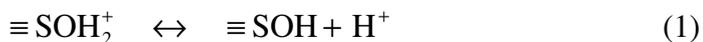
Depending on the considered theory of the electric double layer, supporting electrolyte ions could undergo specific adsorption as well as bind to the surface through non-specific interactions. Ions become specifically adsorbed as a result of short-range interactions. It is assumed that non-specifically adsorbed ions can be in contact with the metal oxide surface due to long-range coulombic interactions (repulsion or attraction).

Surface charge density of chromium (III) oxide was determined by potentiometric titration. The surface charge density was calculated from the dependence between the volume of base added to the suspension in order to obtain desired pH value:

$$\sigma_0 = \frac{\Delta V c F}{mS} \tag{3}$$

where: ΔV – the difference between volume of acid/base added to the suspension to obtain the desired pH of the solution, c – the molar concentration of acid/base, F – the Faraday constant ($9.648 \cdot 10^4$ C/mole), m – the mass of the metal oxide, S – the specific surface area of applied metal oxide.

Chromium (III) oxide surface charge density in the presence and absence of polyamino acid (ASP and LYS) in a suitable supporting electrolyte was measured. The influence of the polymers concentration on the surface charge was investigated. The polymer concentrations were 10 and 100 ppm. 1.5 g of Cr_2O_3 was added to a thermostated Teflon vessel containing 50 cm^3 of supporting electrolyte solution or polymer solution with a fixed concentration. The suspensions were titrated with the NaOH solution with a concentration of 0.1 mole/dm^3. A thermostated Teflon vessel with a stirrer, an automatic burette (Dosimat 765, Methrom), glass and calomel electrodes (Beckman Instruments), the pH meter PHM 240 (Radiometer) were the parts of the measurements set. The process was controlled by a computer. The surface charge density was calculated using the "Titr_v3" program written by Władysław Janusz.

2.3. Zeta potential measurements

The zeta potential measurements were carried out in the absence and presence of polyamino acids in the pH value range of 3 – 10 (Zetasizer 3000, Malvern Instruments). In this case, a suspension of 500 cm^3 containing 0.03g of Cr_2O_3 in the supporting electrolyte solution with suitable concentration was prepared. After the suspension was sonicated for 3 minutes (Ultrasonic Processor XL, Misonix) and the required pH value in the samples was adjusted by adding an appropriate amount of 0.1M HCl or 0.1M NaOH. In order to study polymer adsorption influence on the zeta potential of the chromium (III) oxide colloidal particles, 0.03 g of the solid was added to the NaCl solution with a fixed polymer concentration (ranging from 0.01 to 1 ppm). The electrokinetic potential was measured with the zeta meter connected with the computer. Each average zeta value is the result of eight repetitions. The measurement error did not exceed 3 %.

3. RESULTS AND DISCUSSION

3.1. Adsorption measurements

As it can be seen from the analysis of Figs. 2 and 3, a kind of the supported electrolyte has a great influence on the ionic polyamino acids adsorption process. Concentrations of the applied electrolytes were chosen to provide the constant ionic strength (I) equal to 0.01. In the presence of $CaCl_2$, the increase in the adsorption amount of the anionic polymer both at pH 3 and 10 is observed. The opposite situation takes place in the case of the cationic polylysine, where in the studied pH range the addition of the calcium chloride leads to reduction of the polyamino acid adsorption amount. The reason for such polymers behaviour at the Cr_2O_3 – aqueous solution interface are the coordination complexes formed between the macromolecules and calcium ions, which affect changes of the interactions present in the system. Moreover, Ca^{2+} ions can undergo adsorption on the Cr_2O_3 surface and block the active sites which become inaccessible to the polymer macromolecules.

The adsorption measurement results indicate that in the presence of $CaCl_2$, the amount of ASP adsorbed on the Cr_2O_3 surface rises compared to the values obtained for NaCl (Fig. 2). The reason for such a behaviour is the appearance of the complexes between the calcium ions and the dissociated carboxylic groups present in the polymer chain. The above

mentioned complexes can be created between the $-COO^-$ groups belonging to the same or different macromolecules (Fig. 4). The formation of a given type of connections results in the significant macromolecules conformation changes on the solid surface [10]. The previous studies of ASP in the presence of NaCl as the support electrolyte proved that adsorption of the polymer at pH 3 is mainly driven by electrostatic attraction forces and hydrogen bonds [11].

Table 1. Degree of dissociation of studied polyamino acids [11].

pH	ASP dissociation degree	LYS dissociation degree
3.0	0.157	1.00
6.0	0.995	0.998
7.6	0.999	0.997
10.0	1.00	0.780

What is more, ASP shows the tendency to formation of the associated macromolecular pairs due to the interactions between the undissociated carboxylic groups of the adjacent chains [12]. In turn, with the increasing solution pH, the decrease in the ASP adsorption amount is significant. It follows from the repulsion forces occurring between the strongly ionized polyamino acid chains and the negatively charged surface active groups. Under these conditions, the polymer adsorption can be explained mainly by the hydrogen bridges formation. The use of $CaCl_2$ as the background electrolyte increases the magnitude of the ASP adsorption in both studied pH values. This fact is a consequence of probable formation of the complexes between the functional groups belonging to two different ASP macromolecules and Ca^{2+} ions.

Due to the strong adsorption of the anionic polymer at pH 3 and the repulsion forces occurring between the positively charged adsorbent surface and Ca^{2+} ions ($pH_{pzc} = 7.6$ in NaCl), one of the macromolecules undergoes binding to the solid surface, while the other one must be directed toward the bulk solution. Moreover, formation of the complexes between the dissociated carboxylic groups placed to the same polymer chain and the calcium ions (intramolecular complexes) in the solution is also possible. As a result, the polymer macromolecules exhibit the conformation of the more densely packed coil [13]. In both cases the obtained polymer conformation allows to adsorb a larger number of ASP macromolecules per unit of the adsorbent surface area, which explains the

increase in the adsorption in the higher polymer concentrations range. In the acidic solutions, the differences in the amount of the polymer bounded to the metal oxide surface are negligible (in comparison to NaCl). It is obvious that the increase in the polymer concentration accompanies the rise in the –COO⁻ groups and the probability of the formation of the complexes between the groups belonging to the same chain is also larger. At low ASP levels, the number of polymer–Ca^{2+} ions complexes is small due to a lack of a sufficient number of carboxylic groups capable of creating this type of connections (ASP dissociation degree at pH 3 is equal to 16%, see Table 1). The proposed ASP adsorption mechanism in the $CaCl_2$ environment is presented in Fig. 5.
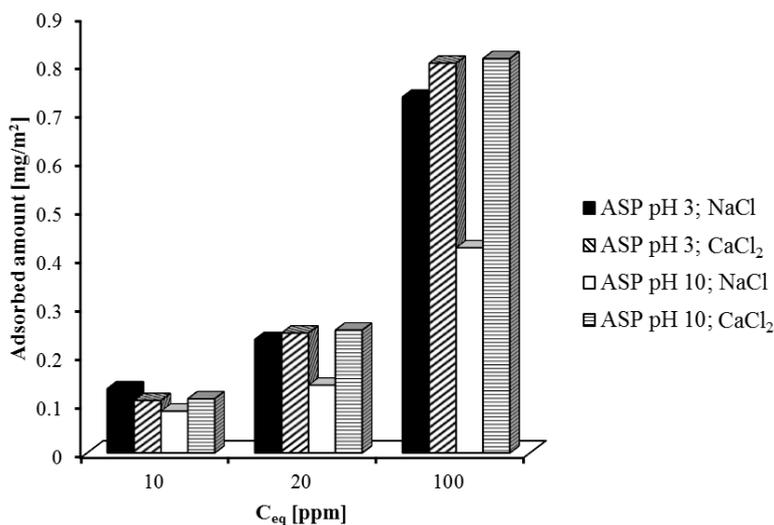
Fig. 2. Adsorption of ASP 27 000 on the Cr_2O_3 surface as a function of solution pH in the presence of various background electrolytes.

The influence of $CaCl_2$ as the background electrolyte on the ASP adsorption is more clearly visible at pH = 10. The divalent calcium ions attendance leads to the considerable growth of the ASP adsorbed amount throughout the measured concentrations range. This allows to draw a conclusion, that under these conditions the polymer adsorption is likely driven by formation of intramolecular complexes. As a result, the highly ionized ASP macromolecule ($\alpha = 100\%$) become more neutralized causing the reduction of the polymer coil dimensions. Decrease in the amount of the negatively charged functional groups placed in the polymer chains reduces the repulsion forces occurring between the polymer coil and the solid surface. In addition, divalent Ca^{2+} cations more effectively

screen the repulsive forces between the polymer chains and the Cr_2O_3 surface. Specific adsorption of the calcium ions does not inhibit the polymer binding since the remaining carboxylic groups can still create the intermolecular connections. It favours formation of the adsorption layer rich in the loops and tails, which is responsible for the meaningful increase of the ASP adsorption amount compared to the analogous pH value when NaCl is used as the support electrolyte.
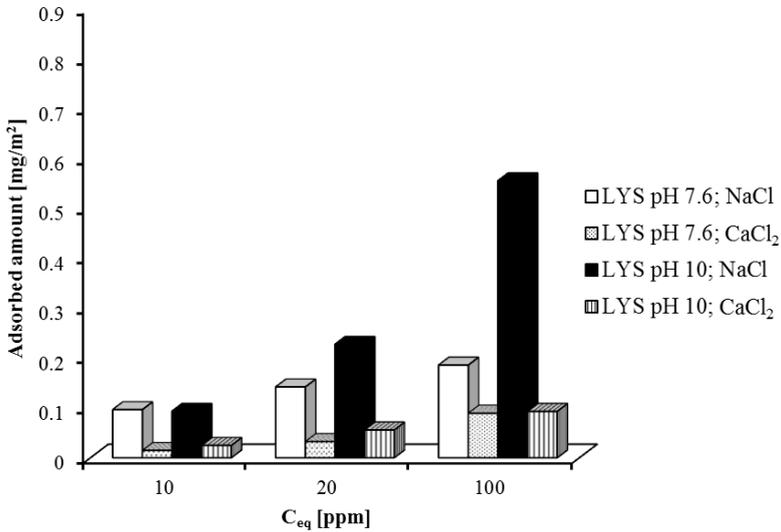

Fig. 3. Adsorption of LYS 33 000 on the Cr_2O_3 surface as a function of solution pH in the presence of various background electrolytes.

The comparison between the polylysine adsorption data as a function of the studied background electrolytes (Fig. 3.) indicates that in the presence of calcium chloride, the adsorption amount of the cationic polymer is significantly decreased both at pH = 7.6 and 10. The earlier research proved that electrostatic attraction between the ionized amino groups and the negatively charged Cr_2O_3 surface as well as the hydrogen bonds formation are responsible for LYS adsorption under these conditions [11]. Reduction of the polymer adsorption after the addition of $CaCl_2$ (Fig. 6) can be explained by strong tendency of Ca^{2+} ions to undergo a specific adsorption on the Cr_2O_3 surface resulting in a block of the adsorbent active sites accessible to the macromolecules. Another fact that must be taken into consideration during the discussion is the attendance of the quaternary amino groups in the LYS structure, which do not participate in the formation of complexes with the calcium ions. These connections can arise only as a result of the Ca^{2+} ions coordination

by the lone electron pairs of nitrogen and oxygen atoms originating from the peptide bond.
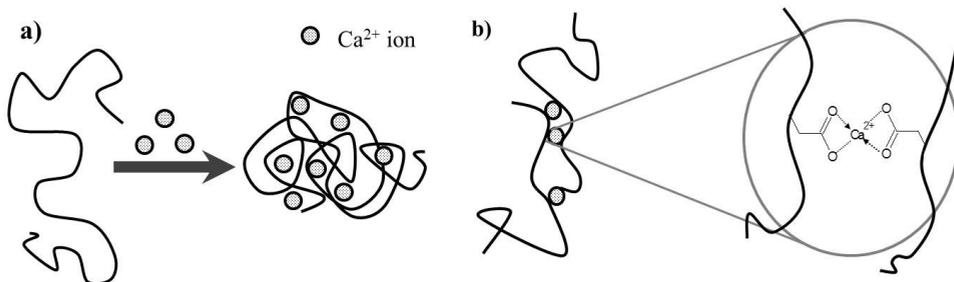
Fig. 4. Interactions between the polymer and Ca^{2+} ions: a) intramolecular complexes, b) intermolecular complexes.
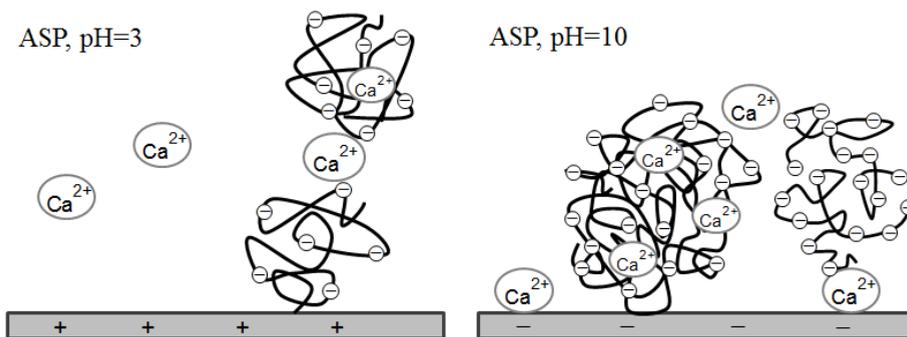
Fig. 5. A proposed mechanism of ASP adsorption on the Cr$_2$O$_3$ surface in the presence of CaCl$_2$ as a function of studied solution pH values.
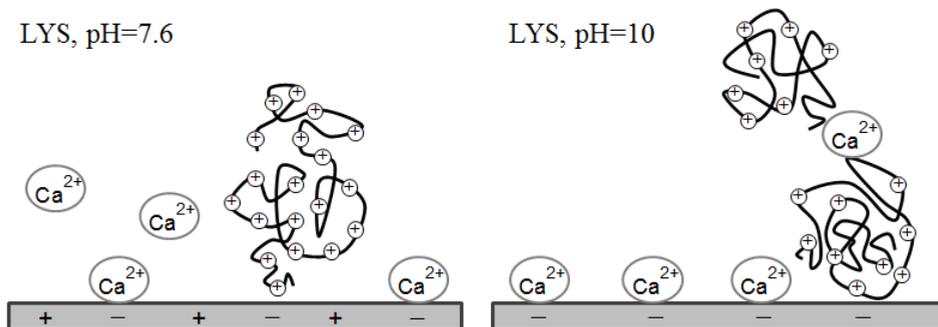
Fig. 6. A proposed mechanism of LYS adsorption on the Cr$_2$O$_3$ surface in the presence of CaCl$_2$ as a function of studied solution pH values.

Moreover, the calcium ions bring about the growth of the electrostatic repulsion between the LYS chains and the positively charged surface active groups. A slight increase in LYS adsorption at pH 10 (in comparison to pH = 7.6) is a consequence of a number of the intermolecular and intramolecular complexes appearance resulting from the interactions between Ca^{2+} ions and a lone electron pair of nitrogen atoms present in the undissociated amino group (the increase of solution pH accompanies the reduction of the LYS dissociation degree, Table 1).

3.2. Potentiometric titration

The analysis of the data obtained from the potentiometric measurements points out that the presence of the divalent cations has great influence on the surface charge density of chromium (III) oxide. As follows from the run of these dependencies, changes in the surface charge of the Cr_2O_3 particles, when $CaCl_2$ is used as the background electrolyte, are more visible in comparison to the values obtained in the presence of NaCl. The specific adsorption of Ca^{2+} cations induces the surface negative charges formation and therefore it is a cause of the surface charge density reduction in the whole measured solution pH range. These results are in good agreement with the theoretical predictions. In order to investigate the influence of the ionic polyamino acids attendance, the potentiometric measurements at the polymer concentrations of 10 and 100 ppm were conducted. The distinct changes in the σ_0 were noted only for the concentration at the level of 100 ppm. The reason for such a behaviour can be found in the insignificant adsorption of the macromolecules in the low polymer concentration system.

It is clearly seen from Fig. 7 that the addition of ASP leads to the decrease of the surface charge density when $CaCl_2$ or NaCl is used as the background electrolyte. As a result of the anionic polymer adsorption, near the solid surface there is formed a negatively charged adsorption layer containing numerous loops and tails. The observed changes come from the simultaneous occurrence of two effects. The adsorbed negatively charged polymer segments contribute to the induction of the positive charges on the Cr_2O_3 surface. However, the dominant number of the dissociated carboxylic groups is located in the metal oxide by-surface layer (in the form of loops and tails) and it is responsible for the total reduction of the Cr_2O_3 surface charge density values. The considerable decrease in the σ_0 values when $CaCl_2$ is used as the background electrolyte comes from ASP – Ca^{2+} ions complexes formation and their adsorption on the solid surface. On account of the interactions between

the calcium ions and the carboxylic groups belonging to one or more polymeric chains, the densely packed adsorption layer is created. The presence of a larger number of the negatively charged carboxylic groups in the by-surface part of solid reduces the surface charge density. In addition, the increase of solution pH accompanies the growth of ASP dissociation degree, which favours the formation of a larger number of the complexes. Increase in the number of the $-COO^-$ groups placed near the Cr_2O_3 surface due to $CaCl_2$ attendance results from the more effective screening of the negative polymer charge by the divalent calcium ions compared to the monovalent sodium ions.
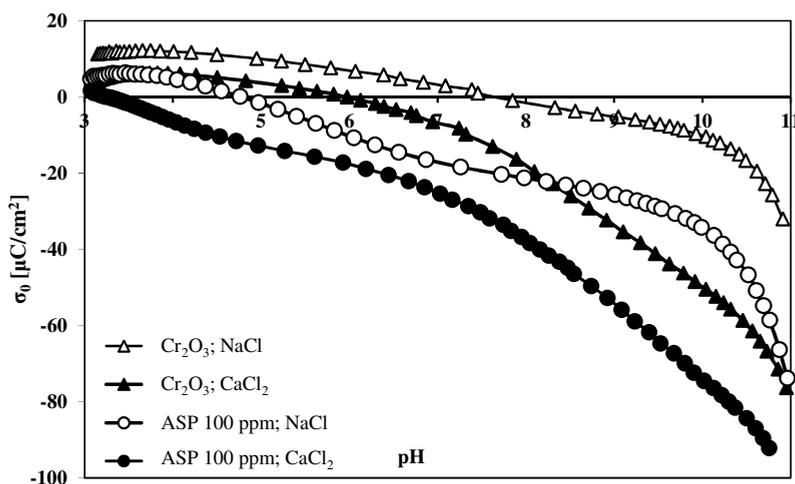

Fig. 7. Chromium (III) oxide surface charge density as a function of pH in the presence of different electrolytes ($I = 0.01$) and ASP 27 000.

The course of the surface charge density curves in the presence of LYS as a function of the solution pH is presented in Fig. 8. The collected potentiometric data point out that the distinct reduction of the Cr_2O_3 surface charge density is observed when NaCl is used as the electrolyte, whereas in the system containing $CaCl_2$, the influence of the polymer can be seen only in the pH range from 8 to 11 (compared to the values obtained without LYS). This is likely to come from the competitive calcium ions adsorption on the adsorbed active sites. It leads to the situation in which the majority of the cationic polyamino acid macromolecules occur in the bulk solution. Moreover, the attendance of the divalent calcium ions is responsible for the growth of the repulsion forces between the positively charged LYS macromolecules and the Cr_2O_3 surface.

The reduction of σ_0 values in the presence of Ca^{2+} ions observed for the high solution pH can be caused by the formation of the a number of the coordination complexes between the amino groups originating from the adsorbed LYS chains and the background electrolyte cations (Fig. 8). This is possible as a result of the decrease in the polymer dissociation degree with the increasing solution pH values. Under these conditions, the polymer adsorption layer composed of a definite number of positively charged amino groups is formed. These groups can interact with the adsorbent surface groups leading to reduction of the solid particles surface charge [14]. The comparison between the potentiometric curves obtained for both electrolytes indicates that in the presence of $CaCl_2$, the less compact LYS adsorption layer with fewer loops and tails in the structure is formed resulting in the slight surface charge density decrease.
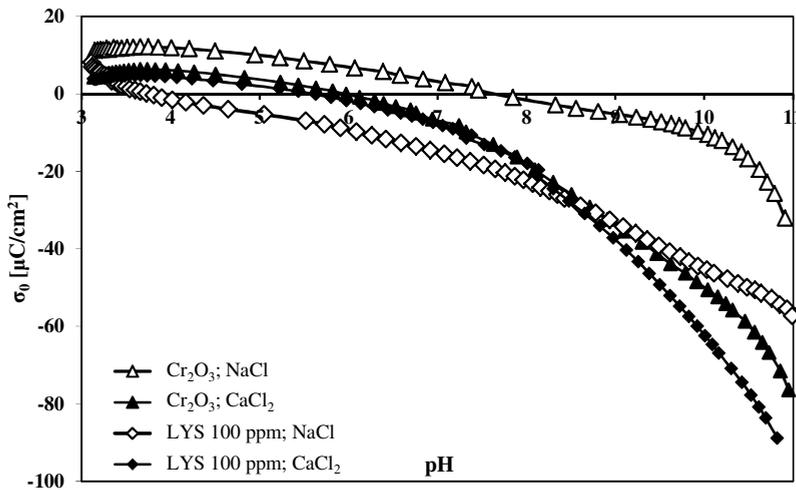
Fig. 8. Chromium (III) oxide surface charge density as a function of pH in the presence of different electrolytes (I=0.01) and LYS 33 000.

3.3. Zeta potential measurements

The effect of the supporting electrolyte type on the zeta potential of the colloidal Cr_2O_3 particles in the absence and presence of the ionic polyamino acids is presented in Figs. 10 and 11. As follows from the run of the curves, the Cr_2O_3 zeta potential reaches the lowest values in all measured pH range when NaCl is applied as the background electrolyte. This phenomenon can be explained on the basis of the specific calcium ions adsorption on the Cr_2O_3 surface. At the acidic pH values, the number

of negatively charged surface active sites is low and Ca^{2+} ions can undergo an ion exchange according to the equations 4-6 [17].

$$\equiv SOH + Ca^{2+} \leftrightarrow \; \equiv SO^- Ca^{2+} + H^+ \tag{4}$$

$$2 \equiv SOH + Ca^{2+} \leftrightarrow \left(\equiv SO^-\right)_2 Ca^{2+} + 2H^+ \tag{5}$$

$$\equiv SOH + Ca^{2+} + H_2O \; \leftrightarrow \; \equiv SO^- CaOH^+ + 2H^+ \tag{6}$$
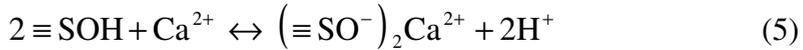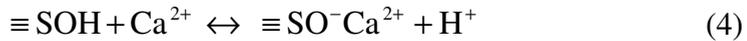
At pH about 6.5, the zeta potential increase follows from the adsorption of the $CaOH^+$ ions appearing in the test system. These cations exhibit large affinity for the negative metal oxide surface (Fig. 9). Strong divalent ions binding is responsible for the double electrical layer thickness reduction. As a consequence, the contribution of the slipping plane shift effect is reduced and the zeta potential value rises [15, 16]. Moreover, Ca^{2+} ions possess greater charge compared to sodium cations, hence in a consequence of their adsorption on the Cr_2O_3 particles leads to acquisition of the positive charge. As follows from the ionic equilibria graph presented in Fig. 9 the calcium hydroxide precipitation do not occur (in the opposite situation, the zeta potential of Cr_2O_3 should be observed).
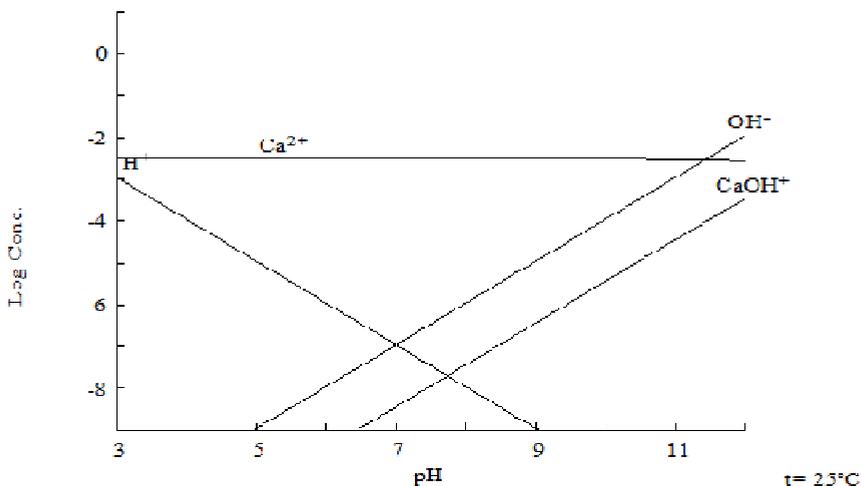

Fig. 9. Type of calcium ions present in the solution as a function of pH [the values were calculated by using the MEDUSA program written by Ignasi Puigdomenech].

Some interesting conclusions on the effect of the background electrolyte type on the zeta potential can be drawn from Fig. 10.

Analyzing the presented data it was found that regardless of the applied electrolyte, ASP reduces the Cr_2O_3 zeta potential throughout the measured pH range. However, the observed changes are more visible for NaCl containing systems. Moreover, in the presence of sodium chloride the increase in the ASP concentration contributes to the further zeta decrease, whereas after the addition of $CaCl_2$ the ASP concentration change does not affect the ζ potential values. The zeta reduction with the rising of the ASP concentration in the Cr_2O_3/NaCl system comes from the presence of a larger number of negatively charged functional groups in the diffusion part of the solid particles. In addition, the polymer chains adsorbed on the Cr_2O_3 surface are responsible for the increase in the slipping plane shift effect. When $CaCl_2$ is used as the background electrolyte, the magnitude of the zeta lowering is smaller. As it was mentioned before, the interactions between the ASP segments and Ca^{2+} ions conduct to decrease in the ionization degree of the adsorbed macromolecules through formation of the intramolecular complexes (R-COO-Ca-COO-R). As a result, a smaller number of the $-COO^-$ groups is located in the diffusion part of the metal oxide electrical double layer. The reduction of the polymer coil dimensions favours formation of the more densely packed polymer adsorption layer, which shifts the slipping plane less effectively. The above mentioned phenomena are the reason for the notable Cr_2O_3 zeta decrease.

Fig. 11 presents the ζ potential dependencies obtained for the Cr_2O_3 particles with and without LYS as a function of the solution pH. In the NaCl containing systems, the presence of the cationic polymer causes a marked increase in the zeta potential in all measured pH (compared to the values drawn in the polymer absence). This is a consequence of numerous positively charged amino groups attendance in the Cr_2O_3 diffusion layer. The decrease of the zeta potential at pH > 7 is related to the slipping plane shift by the adsorbed LYS macromolecules. When $CaCl_2$ is applied, the addition of polylysine contributes to less visible growth of the ζ potential. It is a clear evidence for the competitive adsorption between the LYS macromolecules and the calcium ions which results in lowering of the polymer binding. Another fact that can be taken into consideration is the occurrence of strong repulsion forces between the LYS adsorbed chains. As can be noticed by analyzing Fig. 11, the lower LYS concentration (0.1 ppm) causes the higher increase of the zeta potential in comparison to the system containing 1 ppm of the polymer. It comes from the appearance of two competitive effects influencing the zeta potential. At the concentration of 0.1 ppm the effect of the positively charged amino groups

presence in the diffusion layer of Cr_2O_3 particles predominates. With the increasing LYS concentration a larger number of LYS-Ca^{2+} ions complexes is formed and shifting the slipping plane becomes the dominant effect.
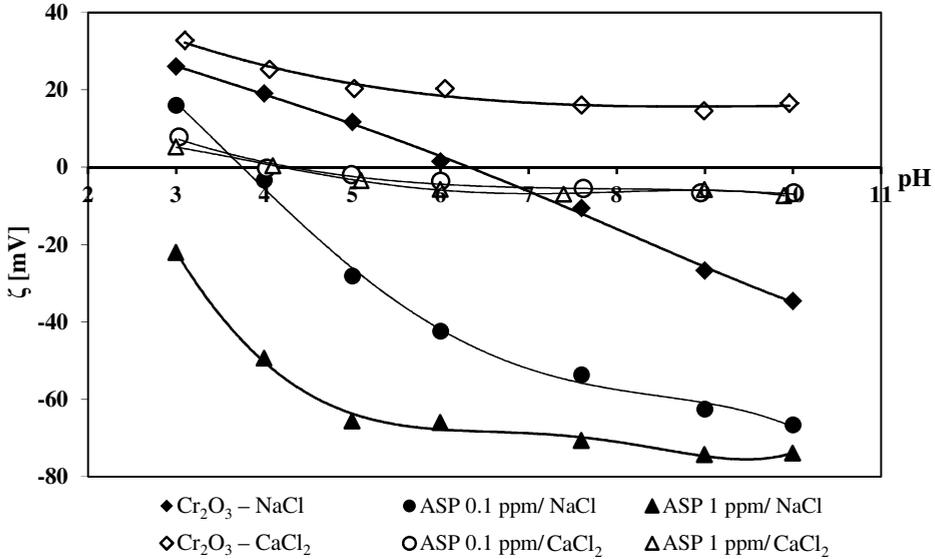

Fig. 10. Influence of the background electrolyte type on the zeta potential of Cr_2O_3 particles in the presence and absence of ASP at the concentration of 0.1 and 1 ppm.
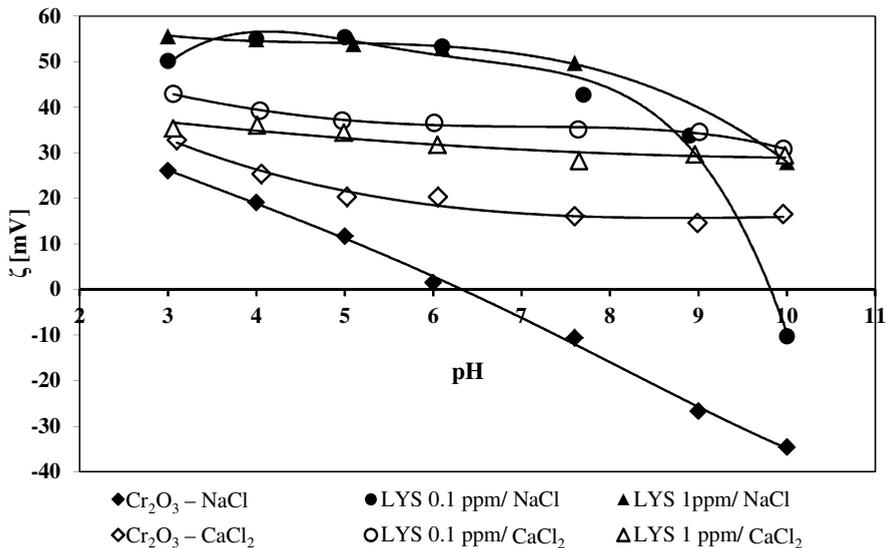

Fig. 11. Influence of the background electrolyte type on the zeta potential of Cr_2O_3 particles in the presence and absence of LYS at the concentrations of 0.1 and 1 ppm.

4. CONCLUSIONS

The influence of the type of the background electrolyte on the adsorption and electrokinetic properties of the Cr_2O_3/ ionic polyamino acid solution system was investigated. It was pointed out that the adsorption of the studied polymers at the solid – liquid interface depends not only on the presence of Ca^{2+} ions. The obtained results showed that both the solution pH and the polymer functional groups type have the essential contribution to the interfacial behaviour of the system. It can be clearly visible that for the anionic polymer (ASP), the use of $CaCl_2$ as the supporting electrolyte increases the amount of adsorbed macromolecules irrespective of the solution pH values. This is a consequence of the formation of complexes between the calcium ions and the carboxyl groups belonging to the same or different polymer chains. In turn, the opposite situation takes place in the case of polylysine (LYS), whose the magnitude of adsorption clearly decreases in the presence of $CaCl_2$. It comes from the specific adsorption of the supporting electrolyte ions on the Cr_2O_3 surface and growth of the electrostatic repulsion forces between the components of the system.

The potentiometric titration data proved that there is strong influence of the background electrolyte type on the electrokinetic properties of the studied system. The formation of the complexes between the calcium ions and the carboxylic groups of the anionic polyamino acid results in the marked reduction of the surface charge density compared to the values obtained for chromium (III) oxide in the presence of a suitable supporting electrolyte. In the polylysine containing system, $CaCl_2$ attendance induces small changes in the Cr_2O_3 particles surface charge density as a consequence of the small adsorbed amount of the cationic polymer macromolecules under the alkaline pH conditions.

The type of the electrolyte cation has the essential influence on the metal oxide zeta potential value, but it is can also affect the magnitude of changes obtained in the presence of polyamino acid. It was also found that the addition of anionic ASP causes the zeta potential reduction throughout the measured pH range. The increase in the polymer concentration promotes the further decrease in the electrokinetic potential. The comparison of the data obtained for the studied electrolytes leads to the conclusion that in the presence of NaCl these changes are distinct, whereas in the $CaCl_2$ environment the zeta potential reduction is not clearly shown. The reason for such a behaviour is the formation of closely packed adsorption layer due to the predominating effect of the slipping

plane shift by the adsorbed polymer macromolecules. The cationic character of LYS functional groups is a main reason responsible for the Cr_2O_3 particles zeta potential growth regardless of the background electrolyte used in the studies. In the presence of NaCl, large zeta changes are observed. Application of $CaCl_2$ leads to the insignificant zeta increase in comparison to the values obtained for Cr_2O_3 without the polymer under the same conditions. Such a behaviour can be explained by the considerable reduction of the polylysine adsorption in the presence of Ca^{2+} ions and as a consequence of a small number of created complexes.

REFERENCES

[1] S. Liufu, X. Xiao, Y. Li, *Journal of Colloid and Interface Science*, **281**, 155, (2005).

[2] F. Shahidi, J. K. V. Arachchi, Y. J. Yeon, *Trends in Food Science & Technology*, **10**, 37, (1999).

[3] C. K. S. Pillai, C. P. Sharma, *Journal of Biomaterials Application*, **25**, 291, (2010).

[4] M. Silvander, *Progress in Colloid and Polymer Science*, **120**, 35, (2002).

[5] S. Farrokhpay, *Advances in Colloid and Interface Science*, **151**, 24, (2009).

[6] E. Grządka, *Materials Chemistry and Physics*, **126**, 488, (2011).

[7] R. J. Gettens, G. L. Stout, *Painting materials: a short encyclopedia*, Dover Publications, 2012.

[8] U. Filipkowska, W. Janczukowicz, J. Rodziewicz, E. Jopp, *Journal of Environmental Engeeniring*, **24**, 243, (2011).

[9] M. Wiśniewska, K. Szewczuk-Karpisz, *Environmental Science and Pollution Research*, **20**, 3657, (2013).

[10] K. Wermöhlen, H. Lewandowski, H. D. Narres, M. J. Schwuger, *Colloids and Surfaces A*, **163**, 45, (2000).

[11] I. Ostolska, M. Wiśniewska, *Central European Journal of Chemistry*, in press.

[12] V. M. Gun'ko, V. I. Zarko, E. F. Voronin, E. V. Goncharuk, L. S. Andriyko, N. V. Guzenko, L. V. Nosach, W. Janusz, *Journal of Colloid and Interface Science*, **300**, 20, (2006).

[13] S. Chibowski, E. Grządka, J. Patkowski, *Croatica Chemica Acta*, **82**, 623, (2009).

[14] S. Chibowski, J. Patkowski, E. Grządka, *Journal of Colloid and Interface Science*, **329**, 1, (2009).
[15] J. K. Mitchell, *Fundamentals of Soil Behaviour*, 2nd edition, John Viley & Sons Inc., 1993.
[16] Y. Yukselen, A. Kaya, *Water, Air, and Soil Pollution*, **145**, 155, (2003).
[17] W. Janusz, J. Patkowski, S. Chibowski, *Journal of Colloid and Interface Science*, **266**, 259, (2003).

CURRICULA VITAE

Iwona Ostolska was born in 1988, Garwolin, Poland. Graduated from Maria Curie-Sklodowska University in Lublin in 2012 receiving an M. Sc. Degree in chemistry. Since 2012 on Ph. D. studies in Department of Radiochemistry and Colloid Chemistry, UMCS. Her research area is adsorption of homopoly-mers and copolymers at the metal oxide – polymer solution interface and the influence of this process on the suspension stability.

Małgorzata Wiśniewska studied chemistry at Maria Curie-Sklodowska University in Lublin and was graduated in 1998 receiving M.Sc. In 1999 she was employed at the Department of Radiochemistry and Colloid Chemistry, Faculty of Chemistry. She received Ph.D. in 2002. In 2011 she achieved postdoctoral degree. Main field of her interest is adsorption mechanism of polymer chains at the solid-liquid interface. She published 56 papers.

Analysis of cosmetic products using different IR spectroscopy techniques

Sylwia Pasieczna-Patkowska[a] and Tomasz Olejnik

Department of Chemical Technology, Faculty of Chemistry,
Maria Curie-Sklodowska University,
pl. M. Curie-Skłodowskiej 3, 20-031 Lublin, Poland
[a]*sylwia.pasieczna@poczta.umcs.lublin.pl*

This article describes the application of IR spectroscopic methods in the study of the composition of finished cosmetic products. Four spectroscopic techniques: TS (transmission spectroscopy), PAS (photoacoustic spectroscopy), ATR (attenuated total reflectance) and DRS (diffuse reflectance spectroscopy) were used for this purpose. Tested cosmetic products were of different consistency and application. The choice of spectroscopic techniques was dictated by the physical state and consistency of the sample.

1. INTRODUCTION

The cosmetic is any substance intended for external contact with the human body (skin, lips, nails, hair, teeth and mucous membranes of the mouth and external genital organs), whose aim is to keep it clean, to protect, nurture, beautify or perfume [1]. A cosmetic product put on the market can not endanger human health. In the cosmetics Act [1] there was defined the list of prohibited substances (420 substances), substances allowed in limited quantities (67 substances) and substances allowed for use in cosmetics. Among the substances permitted for the use in cosmetic formulations are dyes, preservative agents or UV protection substances. The Act also determines what information should appear on the

packaging of cosmetics (trade name, manufacturer's data, ingredients, durability term, special warnings when applying, data allowing to determine the series of cosmetics). The list of cosmetic ingredients, appearing on the packaging, is written by contractual systems. INCI (*International Nomenclature of Cosmetic Ingredients*) is a naming system designed to standardize the nomenclature of ingredients.

In order to ensure the safety of their use, cosmetics are subjected to numerous tests. Research on cosmetics are divided into two groups – obligatory and additional. Clinical tests, sensory and instrumental tests belong to additional tests. Among the obligatory tests there are application tests, dermatological tests, recipe's stability tests or the safety assessment of cosmetic products. Cosmetic product safety assessment is intended to primarily assess its composition in terms of quantity and quality [2].

In the legislation and other legal documents there have been developed a number of procedures for quantitative and qualitative analysis of finished cosmetic products and raw materials for cosmetics production. The example of such procedure may be the identification and determination of benzyl alcohol, silver nitrate or selenium disulphide in anti-dandruff shampoos. These procedures are very laborious, and their repeatability is often low, due to mistakes made during the measurements. When analyzing cosmetics and their raw materials different methods are used: chromatographic (liquid, gas and thin layer chromatography), calorimetric, acid-base titration, UV-VIS spectrophotometric, refractometric methods or mass spectrometry. These methods are associated with a specific, often laborious, sample preparation and usage of numerous measuring equipment. The analysis of the cosmetic products is difficult due to their complex composition and, as it was mentioned above, often involves variety of methods, what can increase the possibility of making mistakes and increases the time of analysis.

The solution to this problem may be the application of IR spectroscopic techniques. This is due to the fact that minimal cosmetic sample preparation is required, so that its composition is not significantly changed. The time of analysis is short and the results of such analysis are highly reproducible. Another advantage of IR spectroscopy is the ability to simultaneously obtain information about several of its components. During the analysis of cosmetic with infrared spectroscopy techniques *fingerprint* method is used, so that IR spectroscopy can be used as an analytical sifting technique. Fingerprint region (1300-700 cm^{-1}) has the characteristic arrangement of the molecules bands. This range is used to

identify tested substance by comparing its spectrum with the spectrum of a model substance. The identity of both spectra in the fingerprint region is a confirmation of the identity of the tested compound with the standard one. Infrared spectroscopy methods allow not only for determination of the composition of the cosmetic product in quantitative or qualitative terms, but can also be used in assessing the effectiveness of their components [3].

Minimal sample preparation when performing measurements using IR spectroscopy techniques is very important because many times during the preparation of the sample, the composition of cosmetic products may be irreversible modified, and then the results are not reliable. However, IR spectroscopy techniques are more appropriate to determine qualitative cosmetics composition than the quantitative one. For example, the ATR technique is restricted to examine a layer of cosmetic sample what, in the case of inhomogeneity of the cosmetic formulation, does not reflect its actual quantitative composition. IR spectroscopy is a very good technique for the analysis of mineral pigments used in cosmetic products [4].

A non-destructive infrared spectroscopy has been used in the analysis of archaeological finds, including cosmetics used in prehistoric times. Using IR spectroscopy it is possible to determine the composition of cosmetics from before hundreds of years. However, it is very difficult or even impossible to determine the presence of trace amounts of the sample's components and then the application of the additional methods is advisable (chromatography, Raman spectroscopy). Usually the combination of two methods (e.g. FT-IR and Raman spectroscopy) gives more complete and more explicit knowledge about the composition of the sample [5]. Infrared spectroscopy was used to determine the presence of surfactants [6,7], emulsifiers [8] and alcohols [6].

2. MATERIALS AND METHODS

The aim of this study was to analyze the finished cosmetic products using various IR spectroscopic techniques: TS (T*ransmission Spectroscopy*), PAS (P*hotoacoustic Spectroscopy*), ATR (A*ttenuated Total Reflectance*) and DRS (D*iffuse Reflectance Spectroscopy*) and then evaluation the usefulness of those techniques in the analysis of selected cosmetics. Tested cosmetic products were of different consistency and application. The choice of spectroscopic technique was dictated by the physical state and consistency of the sample. Eye shadow, red lipstick,

black eye pencil and depigmentant cream were analyzed. In the last case (depigmentant cream) photoacoustic spectroscopy could not be used because of the fact that humidity in such liquid formulation could damage the sensitive microphone in the photoacoustic cell.

TS spectra were recorded by means of Bio-Rad Excalibur FT-IR spectrometer over the 4000-600 cm^{-1} range at room temperature, resolution 4 cm^{-1} and maximum source aperture. Preparation of materials for spectroscopic measurement was based on (1) application of a small amount of the greasy sample (red lipstick, black eye pencil, depigmentant cream) on the compressed KBr pellet or, in the case of powdery materials (eye shadow), (2) the sample (~5 mg) was mixed and ground in an agate mortar with 400 mg of spectroscopically pure dry potassium bromide to a fine powder and then it was pressed to form a disk less than 1 mm thick. Data were collected in the transmission mode at room temperature under air. Interferograms of 64 scans were average for each spectrum.

FT-IR/ATR spectra were recorded at room temperature using a Nicolet 6700 spectrometer equipped with ATR detector with the diamond crystal. A sample of the tested material was mechanically pressed onto the diamond crystal. Interferograms of 64 scans were average for each spectrum.

FT-IR/DRS spectra were obtained by placing the sample mixed with a small amount of KBr in a metal container. Spectra were recorded using Nicolet 6700 spectrometer equipped with a DRS detector at room temperature, in the 4000-600cm^{-1} range. Interferograms of 256 scans were average for each spectrum. Normalization of the spectra was made by comparing the obtained spectra to the background spectrum (KBr).

FT-IR/PAS studies were performed by means of Bio-Rad spectrometer and helium purged MTEC300 photoacoustic detector, over the 4000-600 cm^{-1}. Spectra were measured at room temperature at 4 cm^{-1} resolution. The spectra were normalized by computing the ratio of a sample spectrum to the spectrum of a MTEC carbon black standard. A stainless steel cup (diameter 10 mm) was filled with a sample (thickness <6 mm). Before each data collection, the PA cell was purged with dry helium for 5 minutes. Interferograms of 1024 scans were average for each spectrum.

For a better comparison of individual bands on the IR spectra obtained for particular cosmetic products, TS, ATR, DRS and PAS spectra were normalized with respect to –CH band (2920 cm^{-1}).

3. RESULTS AND DISCUSSION

Interpretation of the IR spectra of cosmetic products is complicated due to the fact that each of the functional groups visible on the IR spectrum may be responsible for the appearance of multiple bands in a wide range of wavenumbers, so that each band may have a contribution of many functional groups. Additionally, the presence of substances such as water or paraffin compounds may are also impede the analysis. These paraffin substances are visible in the IR spectrum in the range of 3000-2800 cm^{-1} (–CH bands) and 1500-1100 cm^{-1}. Water reveals bands within 3600-2800 cm^{-1} and 1700-1300 cm^{-1} range, and those bands may overlap with the bands of tested cosmetics and hinder the interpretation of the spectra. As it was mentioned, photoacoustic spectroscopy is not an appropriate technique for the analysis of liquid cosmetics. Such samples contain in its composition a significant amount of water. The incident beam of infrared radiation could cause the evaporation of water from the sample and damage the microphone in photoacoustic detector.

For the purpose of better visibility, FT-IR spectra presented further in this work were divided into two ranges: 4000–2000 cm^{-1} (where mainly –OH and –CH groups vibrations are visible) and 2000–600 cm^{-1} (fingerprint region).

3.1. Eye shadow

Figure 1 shows the FT-IR spectra of analyzed eye shadow. In all IR spectra (PAS, TS, ATR, DRS) there are bands indicating the presence of compounds containing –CH groups: 2978, 2955, 2925, 2852, 1456, 1376 cm^{-1}. The sharp band of -OH at 3676 cm^{-1} and a broad band of SiO in the range of 1270-850 cm^{-1} indicates the presence of silica. The broad band within 3600-3000 cm^{-1} indicates the presence of intramolecular hydrogen bonding. The presence of the band with maximum at ~3070, 1560 and 670 cm^{-1} may indicate the presence of aromatic compounds in the tested cosmetic product. These bands are most apparent in the TS, PAS and DRS spectra and practically absent in the ATR spectrum. In the case of the DRS spectrum (Fig. 1b) the latter band at ~670 cm^{-1} (out-of-plane deformation vibration of aromatic rings) is slightly shifted towards higher wavenumbers (~700 cm^{-1}). This band (670 cm^{-1}) and the band at 986 cm^{-1} may also indicate the presence of talc or mica (2925, 1017 and 700 cm^{-1}) [9]. The amino group bands are visible at about 3309 and 1610 cm^{-1}, although the latter may also indicate the presence of C=O groups (ketones, esthers) [10]. The presence of ester bonds in the

cosmetic can be also confirmed by the appearance of 1735 and 1715 cm^{-1} bands. These bands are absent in the ATR spectrum. Moreover, the ATR spectrum does not allow for any profound analysis. The most intense band in the ATR spectrum is the band of silica groups within 1270-900 cm^{-1} range. Although the –CH, C=O and amine groups bands have the same position in the TS, PAS and DRS spectra, large differences appear in the range of SiO groups (1270-850 cm^{-1}).
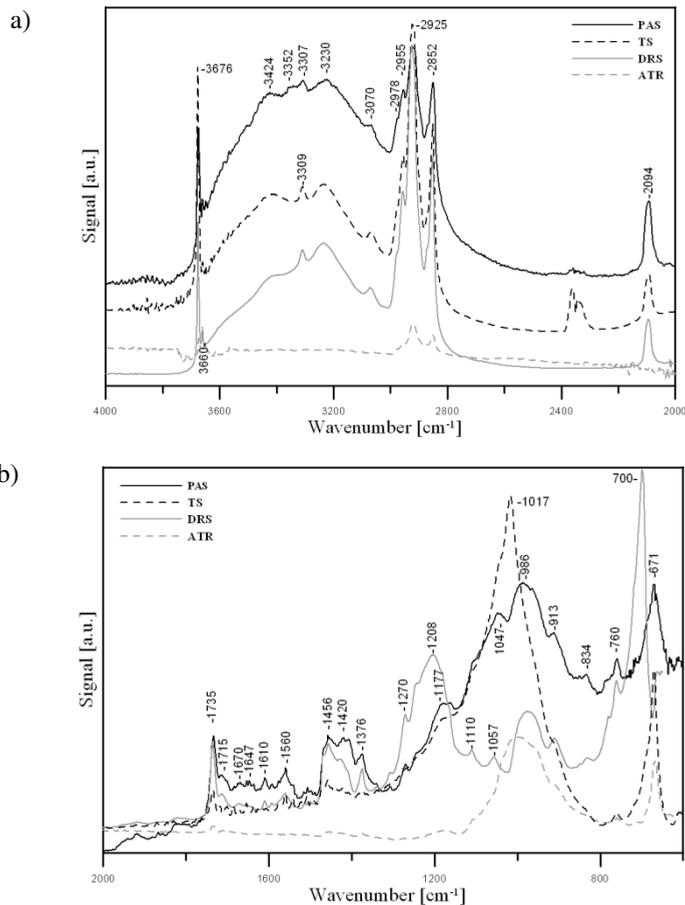

Fig. 1. FT-IR spectra of eye shadow: a) 4000-2000 cm^{-1} range, b) 2000-600 cm^{-1} range.

3.2. Red lipstick

Figure 2 shows the FT-IR spectra of analyzed red lipstick. In all IR spectra of tested lipstick the absorption bands have the same position, but the greatest similarity can be observed in the photoacoustic and transmission

spectra. Although, there are bands in the 1650-1500 cm^{-1} range, which are not visible on ATR or DRS spectra. Additionally, the bands at 3212 and 825 cm^{-1} are present only in the photoacoustic spectrum (Fig. 2a, 2b).

Broad band in the range of 3600-3000 cm^{-1} indicates the presence of intramolecular hydrogen bonds. The bands in 3000-2800 cm^{-1} (2957, 2924, 2852 cm^{-1}) indicate the presence of aliphatic hydrocarbons in the tested cosmetic. The latter may be confirmed analyzing the spectra in the 1460-1379 cm^{-1} range (aliphatic –CH groups). The bands at ~1560 and ~1370 cm^{-1} indicate the presence of aromatic compounds. The wide band of SiO in the 1270-850 cm^{-1} range indicates the presence of silicates in considered cosmetic product. Obtained IR spectra display multiple bands which correspond to the wavenumbers characteristic for propyl ester of hexanoic acid (1743, 1460, 1418, 1379, 1363, 1163, 1109, 1040, 723 cm^{-1}) [11].
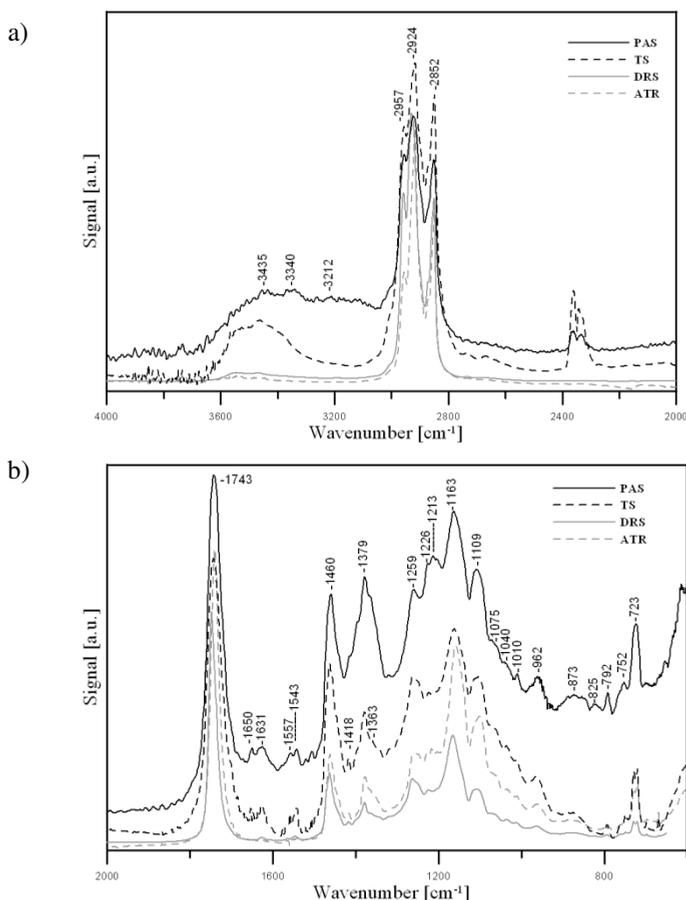

Fig. 2. FT-IR spectra of red lipsticks: a) 4000-2000 cm^{-1} range, b) 2000-600 cm^{-1} range.

3.3. Black eye pencil

While interpreting the IR spectra of black eye pencil (Fig. 3) one can observe that aromatic compounds (3026, 1750, 1450, 730 cm^{-1}), esters (1744 cm^{-1}) and amino compounds (3300, 1637 cm^{-1}) are present in the examined cosmetic. These bands are the most visible in the photoacoustic spectrum. The bands at 2953, 2921, 2851, 1456 and 1376 cm^{-1} indicate the presence of aliphatic compounds and the bands in the 1100-700 cm^{-1} range indicate the presence of silica compounds in the tested sample.
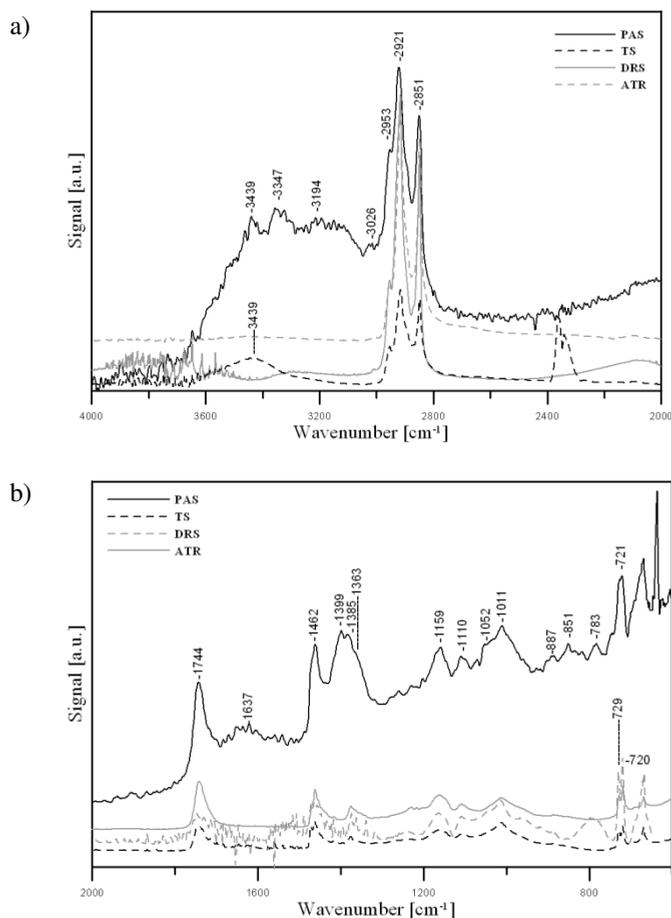
Fig. 3. FT-IR spectra of black eye pencils: a) 4000-2000 cm^{-1} range, b) 2000-600 cm^{-1} range.

The bands at 2920, 2850, 1462, 1363, 1159 and 720 cm^{-1} indicate the presence of paraffin compounds. Another compound whose presence can be confirmed when analyzing the obtained IR spectra is polyethylene

glycol [11]. The bands characteristic for that compound are visible at 3347, 1637, 1462, 1159, 1110 and 887 cm^{-1}. There are also bands corresponding to the presence of mica (1390, 1011 or 720 cm^{-1}) [9].

The most information about the composition of the black eye pencil can be obtained by analyzing the photoacoustic spectrum. This fact indicates that photoacoustic technique is the best IR technique for the analysis of such cosmetic product.

3.4. Depigmentant cream

Interpretation of TS and ATR spectra of depigmentant cream (Fig. 4a) and confirming the presence of water (broad and intense band in the 3700-3000 cm^{-1} range) excludes IR analysis using photoacoustic technique.
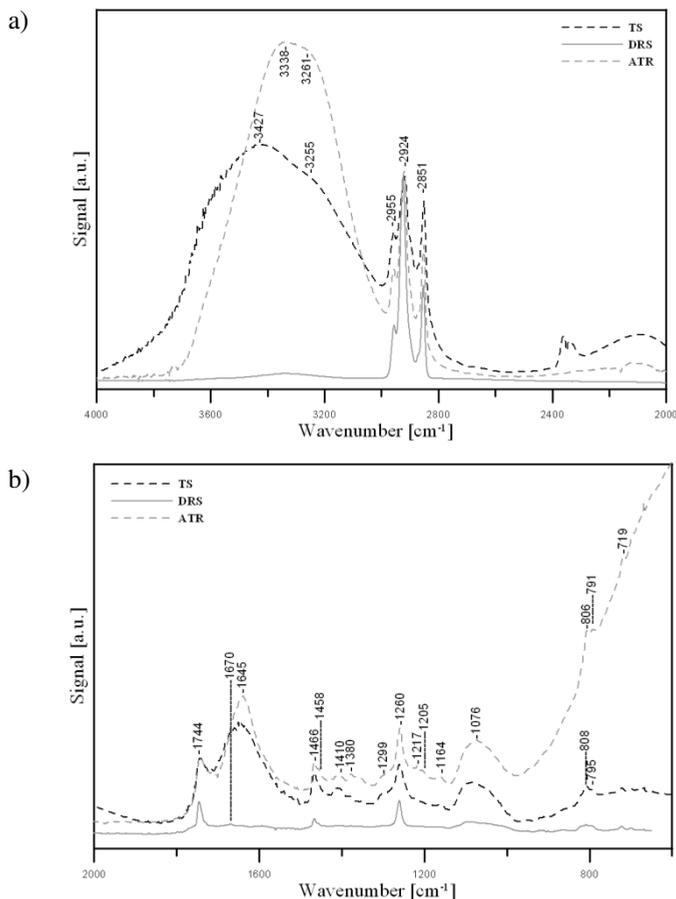
Fig. 4. FT-IR spectra of depigmentant cream: a) 4000-2000 cm^{-1} range, b) 2000-600 cm^{-1} range.

The bands appearing at ~1744 and 1645 cm^{-1} (Fig. 4b) may indicate the presence of C=O groups in carboxylic acids and aromatic ketones, respectively [10]. Another group identified on the basis of IR spectra is aliphatic –CH (2955, 2924, 2851 and 1380 cm^{-1}). The IR spectra of the tested cream have a number of bands located at wavenumbers similar to cetyl alcohol (e.g. 2955, 2851, 1466 or 719 cm^{-1}) and cyclopentasiloxane (1645, 1410, 1260, 1076 and 806 cm^{-1}) [11]. Obtained DRS spectrum is of poor quality (Fig. 4a, 4b).

4. CONCLUSION

An unambiguous analysis of the IR spectra of cosmetics is difficult due to the presence of many ingredients. The signals coming from one compound can be masked by other or may even overlap. It is hard to distinctly confirm the presence of the compound in the cosmetic, but one can confirm the presence of specific functional groups.

Based on the results presented in this paper for various types of cosmetic, the following conclusions can be made:

– similar information can be obtained by analyzing the TS and ATR spectra, the bands have similar intensity at similar wavenumbers;

– DRS spectra usually differ significantly from the TS, ATR and PAS spectra;

– DRS technique is not suitable for the analysis of liquid samples;

– in the case of liquid samples the ATR technique was the best choice, while PAS could not be used at all;

– transmission technique have to be modified in some cases (greasy samples have to be applied on the compressed KBr pellet) and the measurement had to be made relatively quickly, to avoid the destruction of KBr pellet;

– in the case of powdery samples with low water content (i.e. eye shadow) PAS and TS techniques have proved to be the best;

– the best analysis of solid samples with oil consistency (lipsticks, eyeliners) can be performed using the TS and PAS technique;

Not all techniques are suitable for the analysis of various types of cosmetics which was confirmed by research done in this work. Selection

of the appropriate technique must be dictated by the physical state, the content of water, consistency and homogeneity of the cosmetic sample.

REFERENCES

[1]   Ustawa o kosmetykach z dnia 30 marca 2001 (Dz. U. nr. 42, poz. 473 z późniejszymi zmianami) (in Polish).

[2]   P. Pietruszka, *Wiadomości kosmetyczne*, **3**, 21, (2008) (in polish).

[3]   W. Zieliński, *Metody spektroskopowe i ich zastosowanie do identyfikacji związków organicznych*, Wydawnictwo Naukowo-Techniczne, Warszawa, (1995) (in Polish).

[4]   E. Ribechini, F. Modugno, J. Pérez-Arantegui, M. P. Colombini, *Discovering the composition of ancient cosmetics and remedies: analytical techniques and materials*, Springer-Verlag, (2011).

[5]   M. C. Gamberini, C. Baraldi , F. Palazzoli, E. Ribechini, P. Baraldi, *Vibrational Spectroscopy*, **47,** 82, (2008).

[6]   N. A. Puttnam, B. H. Baxter, S. Lee, P. L Stott, *J. Soc. Cosmetic Chemists*, **17**, 9, (1966).

[7]   J.C. Bowman, *Qualitative Analysis and Structural Confirmation of Several Surfactants by FT-Raman and FT-IR Spectroscopies*, Nicolet Application Note , Madison, (1993).

[8]   A. Rohman, Y. B. Che Man, *Middle-East Journal of Scientific Research*, **5**, 7, (2011).

[9]   N. V. Chukanov, *Infrared spectra of mineral species,* Extended library, Vol. 1, Springer (2014).

[10] G. Socrates, *Infrared and Raman Characteristic Group Frequencies. Tables and Charts,* John Wiley&Sons Ltd. (2001).

[11] OMNIC^{TM} Specta Software, *database of spectral data*

CURRICULA VITAE
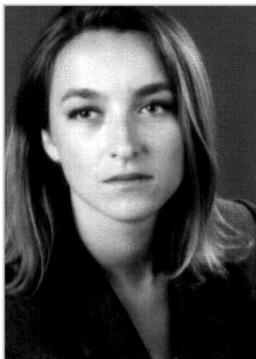
Sylwia Pasieczna-Patkowska was born in Lublin, Poland in 1974. She studied chemistry at the Maria Curie-Skłodowska University, graduated in 1998. Received her Ph.D. (2006) in physical chemistry from the UMCS in Lublin. Since 2007 she is an adjunct at UMCS. She is an author and co-author of 73 articles in science-technical press, the author and co-author of 126 papers and posters at domestic and foreign conferences. Scientific interests: infrared spectroscopy, chemical technology. She is member of Polish Chemical Society (1998-) and Polish Catalysis Club (1998-).

Tomasz Olejnik was born in Radom in Poland in 1988. He studied Basic and Applied Chemistry at Maria Curie-Skłodowska University in Lublin. In 2012 he obtained M.Sc. degree based on master thesis entitled: "The ordered mesoporous silica materials – influence of modification on the physicochemical properties of silica". His master thesis was awarded by the Polish Chemical Society. After graduation from the Faculty of Chemistry, Maria Curie-Skłodowska University in August 2012, he started Ph.D. studies in Department of Chemical Technology, M.C.S. University in Lublin. He is member of Polish Chemical Society (2010-) and Polish Catalysis Club (2012-).

An application of microemulsion method for synthesis of copper-zinc materials

Justyna Pawlonka[a], Grzegorz Słowik[b], Wojciech Gac[c]
and Tadeusz Borowiecki[d]

Faculty of Chemistry, Department of Chemical Technology,
Maria Curie-Sklodowska University
3 M. Curie-Skłodowskiej Square, 20-031 Lublin, Poland
[a]*justyna.pawlonka@gmail.com*
[b]*grzesiek.slowik@gmail.com*
[c]*wojtek.gac@poczta.umcs.lublin.pl*
[d]*tadeusz.borowiecki@umcs.lublin.pl*

Microemulsion method was used for preparation of copper-zinc mixed oxides. Samples were prepared from the solutions containing zinc and copper nitrates. Sodium carbonate was used as a precipitant and hydrazine as reducing agent. Water-in-oil (W/O) microemulsions were formed by the application of cyclohexane, isopropyl alcohol, and hexadecyltrimethylammonium bromide (CTAB) as surfactant. The aim of the studies was determination of the influence of the sequence of synthesis stages on the formation of materials, their surface and structural properties. Thermal decomposition studies of materials were carried out by infrared spectroscopy. The physicochemical properties were characterized by nitrogen adsorption-desorption method, X-ray diffraction (XRD) and temperature-programmed reduction (TPR).

1. INTRODUCTION

Nanotechnology gained a huge increase of interest in the recent years. New nanomaterials may find wide application in many fields in the

near future, ranging from common goods to advanced technologies. Much attention has been paid to new synthesis methods, which allow better control of the size or shape of nanoparticles. For this reason it is understandable why the development of microemulsion method for new nanomaterials synthesis enjoys great interest.

This method enables in easy way to control the size of reversed micelles, and thereby the particle size, by changing water-to-surfactant molar ratio (W_0). Not only the particle size, but also their shape or composition of materials can be readily modified. Various intermetallic nanoparticles can be obtained just by changing the composition of water cores of micelles. Microemulsion method has been used for the synthesis of many types of materials, including metals, alloys, metal oxides, sulfides and selenides, metal borides, halides, carbonates and hydroxides of metals. The microemulsion method might be used for preparation of oxide materials of suitable chemical composition on nanometer level, porosity and specific surface area [1]. Usually such colloidal templates give smaller particles than those produced by precipitation method in aqueous system. It has been observed that the type and concentration of surfactant, the nature of oil phase and alcohol, the reaction temperature and rate of microemulsion mixing strongly influenced particle size, shape and growth rate, however the mechanism of the control of the size and shape of formed particles is still under debate [2]. Moreover the sequence of precipitation or reduction stages in complex microemulsion systems has not been well documented.

Zinc oxide is a very interesting material. It is widely used in the ceramic industry, the manufacture of tires, cement, pigments, and cosmetics. It shows unique optical, electronic and photo-catalytic properties, such as those connected with high energy band gap. ZnO is also a component of many adsorption and catalytic systems, including low-temperature CO conversion catalyst, methanol synthesis, steam reforming of methanol [3-4]. Mechanical, optical, sensory, catalytic, electrical and thermal conductivity of ZnO depends on the size, shape and even nanomaterials morphology. Additionally ZnO holds the possibility of dilute magnetic semiconductor with a Curie temperature above room temperature. It has been predicted that Cu-ZnO is a ferromagnetic and shown signs of magnetic behavior. Because of that, various chemical and physical methods have been used for preparation of copper-zinc oxide systems and nowadays its examination enjoys huge interest [5].

Microemulsions are normally transparent, isotropic solutions, and are divided into two types, oil-in-water (O/W) and water-in-oil (W/O). The

reverse microemulsion – W/O type, consists of at least three components: the continuous phase – an organic solvent, dispersed phase – water and surfactants (ionic or nonionic), accumulated at the interface which stabilize the system. The resulting micelles create specific microenvironment for chemical reactions, where precipitation or reduction can occur. As a result, the nanoparticles could be formed inside small confinements. Micelles during synthesis play complex role, both they serve as nano-reactors, and also they control the growth of formed nanoparticles. When the dimensions of the crystallite approaches the size of entire micelles, surfactant molecules are adsorbed on its surface, preventing agglomeration. This result in the formation of very small crystallites of similar size [6-7]. The synthesis of nanomaterials often refers to the combination of two microemulsions containing the appropriate reagents, e.g., metal salts and reducing substances or precipitants. After mixing, micelles collision occurs, which results in the exchange of content and percolation [7]. The size and shape of the micelles can be controlled in several ways. The most common way is changing of the ingredients proportions of the mixture or introducing various external factors (such as temperature or electric field).

The aim of the studies was to determine the influence of the sequence of synthesis stages on the formation of copper-zinc mixed oxides by water-in-oil (W/O) microemulsion method, and the surface and structural properties of obtained materials.

2. MATERIALS AND METHODS

Copper-zinc oxides, have been prepared by reverse microemulsion method. The assumed copper content was 30 wt. %. Different sequence of particular stages of synthesis was applied. The scheme is shown on Fig. 1. The microemulsion systems was consisted of cyclohexane (44 wt. %) as continuous oil phase, aqueous solution as dispersed phase (36 wt. %), hexadecyltrimethylammonium bromide (CTAB) as surfactant (10 wt. %) and isopropanol (10 wt. %) as cosurfactant.

The CuO-ZnO-1 sample was obtained by co-precipitation method in microemulsion. The aqueous phase of first microemulsion was a 0.01 M of copper nitrate and 1.25 M of zinc nitrate solution. The microemulsion was then mixed with another microemulsion containing precipitation agent (sodium carbonate 1.25 M solution).

Preparation of CuO-ZnO-2 sample was preceded by reduction of copper using ten-fold excess of hydrazine prior mixing with microemulsions containing zinc and carbonate ions. CuO-ZnO-4 was prepared by the same way, while using double amount of surfactant.
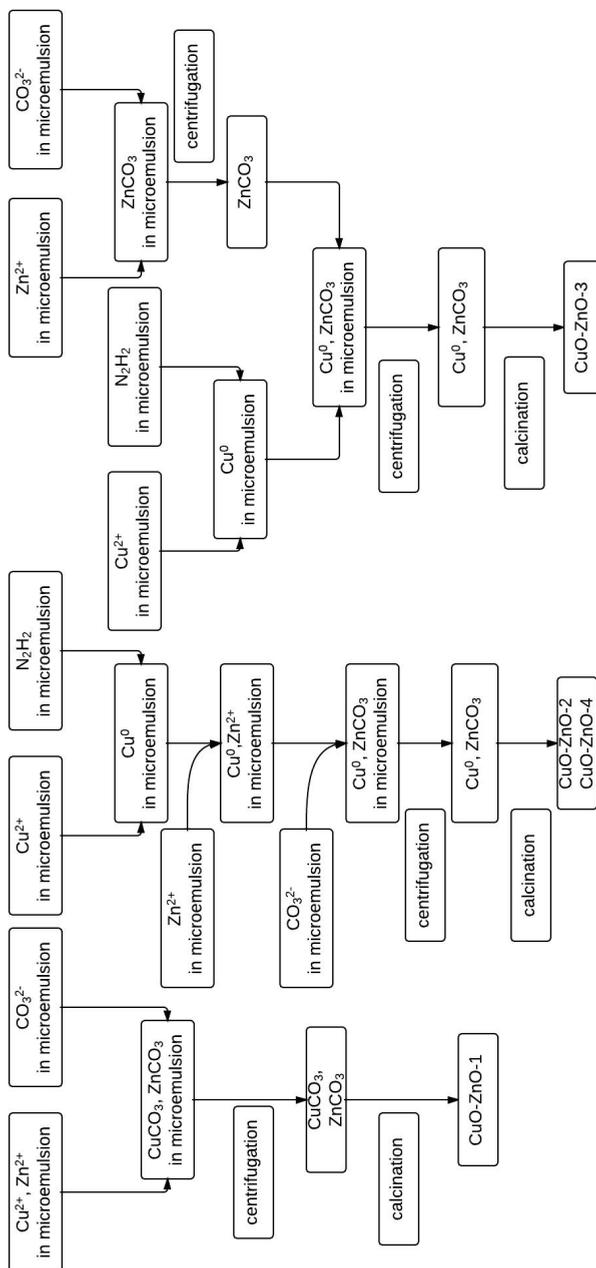
Fig. 1. Schema of the samples preparation.

During the synthesis of CuO-ZnO-3 sample, the reduced copper nanoparticles obtained by microemulsion method with application of hydrazine were deposited on the precipitate, formed from microemulsions containing $Zn(NO_3)_2$ and Na_2CO_3.

The synthesis was carried out at room temperature for 3 h under vigorous stirring. The microemulsions were destabilized with a few ml of tetrahydrofuran (THF). The precipitates were as separated by centrifugation and were washed with chloroform, water and methanol-water mixture. Samples were dried at room temperature overnight, and then calcined in air at 350°C for 1h.

Diffuse Reflectance Infrared Fourier Transform Spectroscopy (DRIFTS) studies were performed using Nicolet 6700 (Thermo Scientific) spectrometer equipped with high-temperature reaction chamber (Harrick). FT-IR spectra were recorded in the mid-IR region (400 – 4000 cm^{-1}) with resolution of 4 cm^{-1}. Samples were heated in the flow of ~8% of oxygen in argon with the rate 30 cm^3/min. The spectra were recorded every 50°C from room temperature to 450°C.

The specific surface area and porosity were calculated from nitrogen adsorption-desorption isotherms gained on a Micromeritics ASAP 2405 instrument after outgassing of the samples at 200°C. The BET method was used to calculate the specific surface areas. The adsorption branch of isotherms was used to obtain BJH pore size distribution.

Microscopic images were obtained using Scanning Electron Microscope Phenom FEI Company with magnification range from 120x to 24,000x and 5kV accelerating voltage.

Powder X-ray diffraction (XRD) studies were carried out in an Empyrean (PANalytical) diffractometer, using CuK_α radiation.

Temperature-programmed reduction (TPR) with hydrogen was carried out on the Autochem II Micromeritics instrument. About 50 mg of sample was introduced into the quartz U-tube microreactor. Sample was heated in the flow of H_2(5 vol.%)/Ar mixture with the rate 10°C/min from –30°C to 600°C.

1. RESULTS AND DISCUSSION

The DRIFTS spectra (Fig. 2) of the samples, before calcination, were collected during heating from 25°C to 450°C. Wide band at about 3400 cm^{-1} can be seen for all samples, which is characteristic of the stretching vibrations of O-H groups, coming from surface hydroxyl

groups and water adsorbed. Small differences in the number and band position within this region in the spectra of dried samples recorded at 25°C indicate on the different chemical nature of CuO-ZnO precursor phases. Samples prepared by different methods show also different thermal stability.
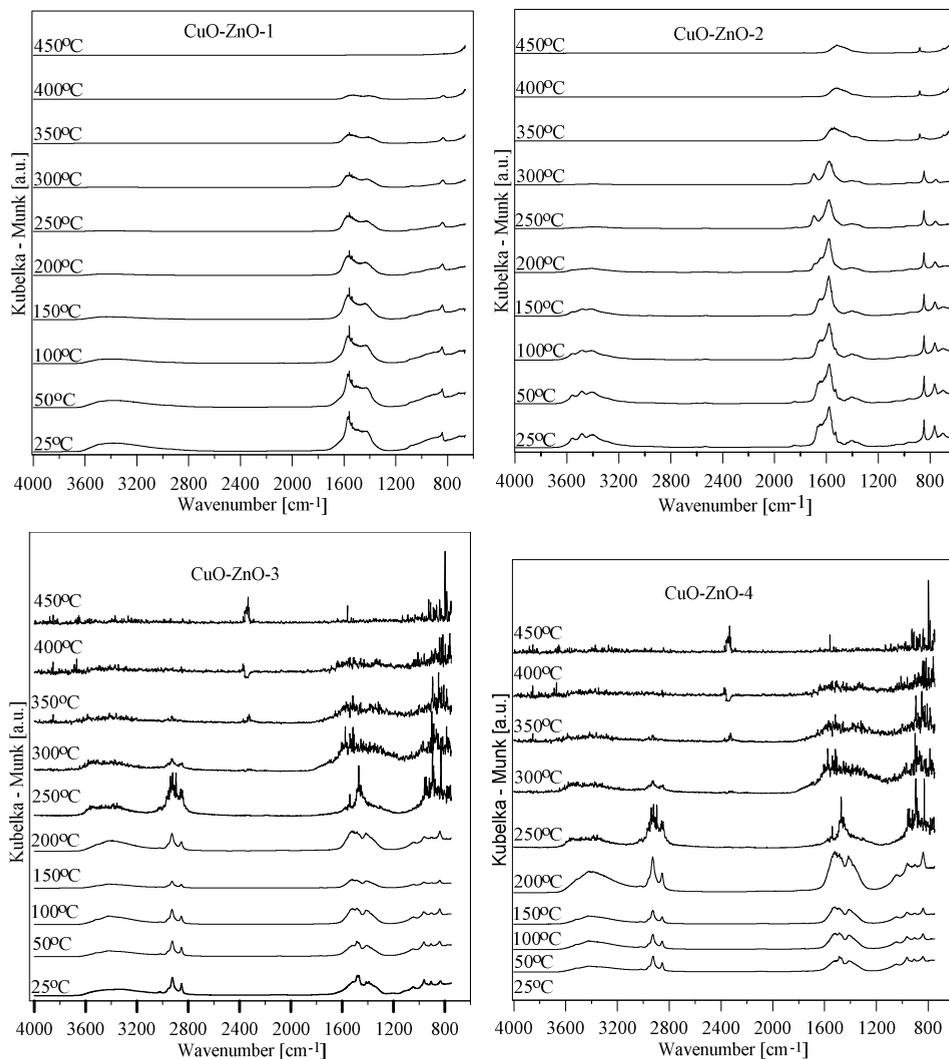

Fig. 2. DRIFTS spectra of CuO-ZnO (dried) samples, recorded during thermal decomposition in the flow of oxygen/argon mixture from 25 to 450°C.

The transformation of the species can be observed by comparison of the intensity of hydroxyl group vibration. The large disappearance of hydroxyl groups vibrations takes place in the case of CuO-ZnO-1 sample

between 150°C and 200°C, while this effect in the case of Cu-ZnO-2 is observed between 200-250°C. The samples CuO-ZnO-3 and CuO-ZnO-4 show higher stability, and disappearance of pronounced amounts of hydroxyl groups is observed above 350°C.

The two bands at 2950 cm^{-1} and 2850 cm^{-1} on the spectra of CuO-ZnO-3 and CuO-ZnO-4 result from stretching vibrations of C-H hydrocarbon groups, which decline at temperature around 350°C for both samples. Their presence is connected with the traces of surfactant molecules left on the surface after washing.

The bands at 1550 cm^{-1} and 1400 cm^{-1}, which are present on the spectra of all samples before thermal treatment, come mostly from C=O stretching vibrations. Small differences indicate different chemical bonding. The shape of the spectra is changing during thermal treatment. However these vibration bands do not completely disappear at 350°C (at applied calcination temperature). Large interferences in two last samples are caused by high gas evolution during samples decompositions [8].

The sequence of preparation stages influences structural and surface properties of materials. The BET specific surface areas of the samples after calcination, pore volume and mean pore diameter are presented in the Table 1. The largest specific surface area is observed for the sCuO-ZnO-1 sample, which was obtained by the co-precipitation in microemulsion of Zn^{2+} and Cu^{2+} by sodium carbonate (in microemulsion). Similar values were observed by Hingorani and coworkers [9]. This sample shows also relatively small mean pore diameter. Similar surface area is observed for the CuO-ZnO-2 sample, obtained by precipitation of Zn^{2+} with Na_2CO_3, with deposited Cu nanoparticle formed in a separate microemulsion. This sample shows also relatively large pore volume and large mean pore diameter.

Table 1. Physicochemical properties of prepared samples.

Sample	Specific surface area [m^2/g]	Total pore volume [cm^3/g]	Mean pore diameter [nm]
CuO-ZnO-1	27.3	0.08	14.3
CuO-ZnO-2	23.3	0.13	26.0
CuO-ZnO-3	13.3	0.05	16.8
CuO-ZnO-4	8.0	0.03	21.0

It is interesting that CuO-ZnO-3 sample, which was prepared by deposition of copper nanoparticles on the surface of isolated zinc containing solid shows much lower specific surface area and smaller pore volume. The influence of surfactant concentration is well reflected in the changes of the surface and structural properties of CuO-ZnO-2 and CuO-ZnO-4 samples. The latter one shows smaller surface area and pore volume.
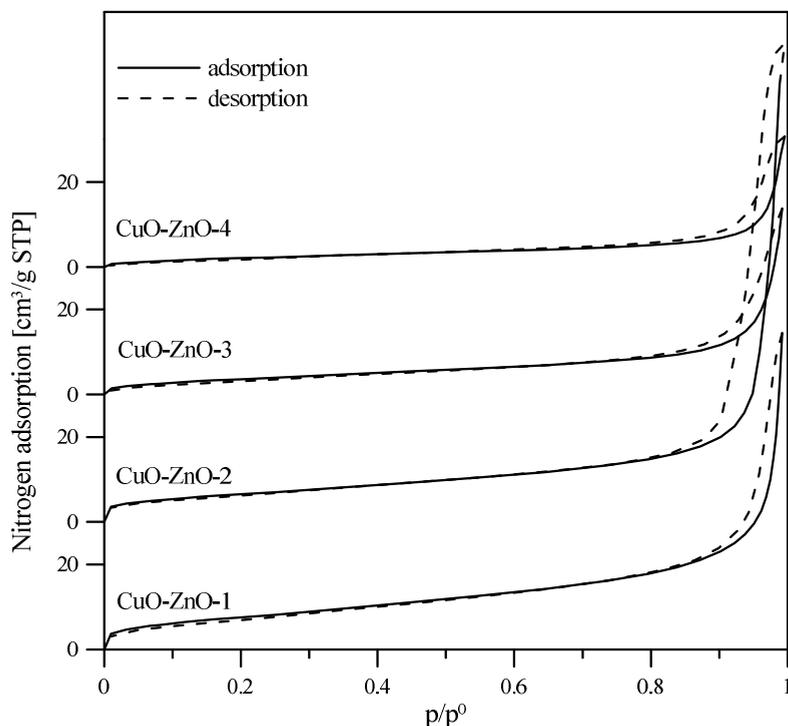

Fig. 3. Low temperature adsorption-desorption of nitrogen.

The shape of isotherm (Fig. 3.) indicates on the presence of slit-shaped pores formed by regular interconnected species.

The CuO-ZnO-4 sample shows different morphology from that observed for remaining samples. The changes are evidenced on SEM images (Fig. 4). The samples prepared in the presence of the smaller amount of surfactant show sponge-like morphology. Small species are connected together in rather random way, forming empty voids. In the case of CuO-ZnO-4 these species are linked into thin regular belts, which are deposited on more amorphous part of material.

CuO-ZnO-1

CuO-ZnO-2
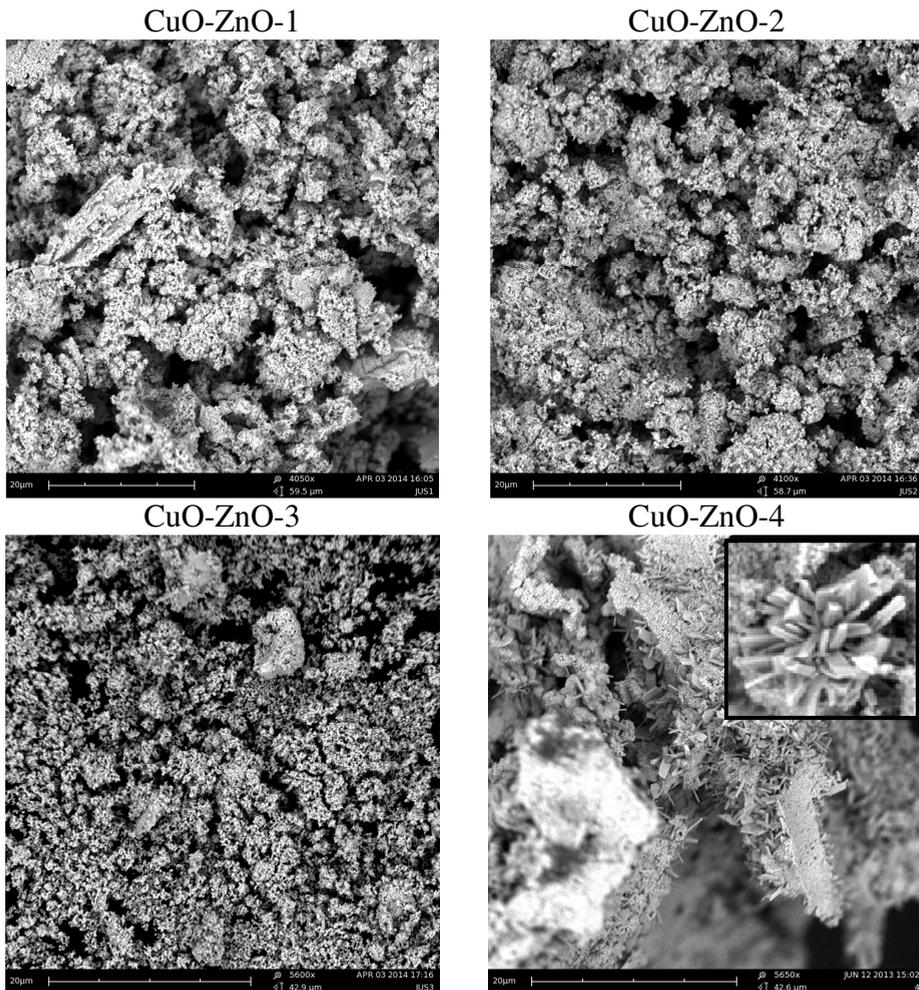
CuO-ZnO-3

CuO-ZnO-4

Fig. 4. SEM images of CuO-ZnO samples. Scale bars: 20 µm.

The XRD pattern for CuO-ZnO-1 sample (Fig. 5) shows diffraction peaks, located at 2θ = 31.8, 34.5, 36.3, 47.6, 56.6, 62.9, 66.4, 67.9, 69.0 and 72.6, which correspond to ZnO hexagonal P63mc phase (PDF # 80-0074). The main CuO reflection peaks, which are located at 2θ = 32.5, 35.5, 38.7, 48.8, 58.2, 59.0, 61.6, 65.7 and 66.4 well correspond to the phase of PDF# 04-0836. Similar phases are identified for all samples. One can observe reflection lines on the spectra of CuO-ZnO-2 and CuO-ZnO-4 samples coming from residual carbon, left on the surface after surfactant decomposition.

The size of ZnO and CuO crystallites was estimated by the application of Scherrer equation (Table 2). The reflections used for

calculations were $2\theta = 36.3$ for ZnO and $2\theta = 38.7$ for CuO. The smallest CuO and ZnO particles are observed for CuO-ZnO-2 sample. The size of ZnO is changed from 13.9 to 35.4 nm as the surfactant concentration is increased. The more pronounced effect is visible for copper oxide crystallites, which size is increased from 11.4 to 20.1 nm.
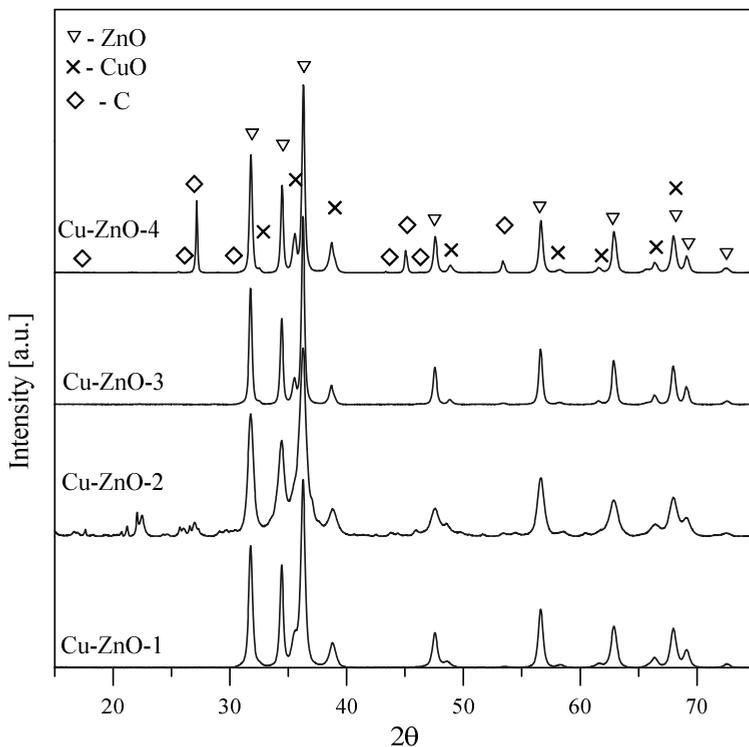

Fig. 5. XRD patterns of the samples after calcination.

Table 2. The size of crystallites of CuO and ZnO calculated from XRD studies.

Sample	CuO [nm]	ZnO [nm]
CuO-ZnO-1	17.6	21.6
CuO-ZnO-2	11.4	13.9
CuO-ZnO-3	19.1	33.1
CuO-ZnO-4	20.1	35.4

Fig. 6 shows temperature-programmed reduction profiles of CuO-ZnO samples. The main peak in CuO-ZnO-1 profile is placed

between 150 and 350°C. Low temperature peaks are usually ascribed to the reduction of copper oxide accordingly to the reaction:

$$CuO + H_2 \rightarrow Cu + H_2O$$
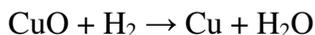
However the reduction temperatures may change due to different chemical environment of copper oxides and their different size. According to Fierro and coworkers the reduction temperature of copper-zinc mixed oxides containing 30% CuO ranges from 150 to 200°C [10]. However pure copper oxide, as well as copper-zinc oxide systems of much lower reducibility were also widely described in the literature [11-13]. Agrell and coworkers prepared copper supported zinc oxide catalysts using microemulsion method, which have similar composition. Reduction peak for similar catalysts was placed between 180-240°C and reducibility decreased after reoxidation to temperatures ranging from 220 to 250°C. High temperature reduction maxima were explained by strong interaction between ZnO and CuO [14]. High temperature peaks on the TPR curves of Cu/ZnO catalysts have been also ascribed to the reduction of ZnO in the vicinity of copper metallic species.

The TPR profile for CuO-ZnO-2 sample is more complex. One can observe several overlapped peaks, which suggest the presence of various copper oxide species. It is visible low-temperature peak located between 150 and 250°C, the peak with similar position as in the CuO-ZnO-1 sample, and sharp peak with maximum at around 350°C. There is also observed high temperature broad peak. Low temperature peak may result from reduction of CuO of different environment, especially located in the vicinity of very small copper metallic species or Cu_2O surface phases, which may remain in the samples after reduction with hydrazine and encapsulation with some oxide or carbonate species. While high intermediate peaks, with maximum at 350°C could be related to the reduction of small crystallites located in the pores of materials or strongly interacted CuO-ZnO mixed oxide phases or zinc oxide layers inhibiting CuO reduction [13]. An increase of surfactant concentration used in the synthesis condition caused the decrease of reducibility of CuO. The stronger decrease of reducibility is observed for CuO-ZnO-3 sample obtained by deposition of copper nanoparticles on the surface of as prepared ZnO-based support. The almost symmetrical and the narrowest reduction peak one can observe for first sample, which indicates a homogenous material and narrow particle size distribution [14].
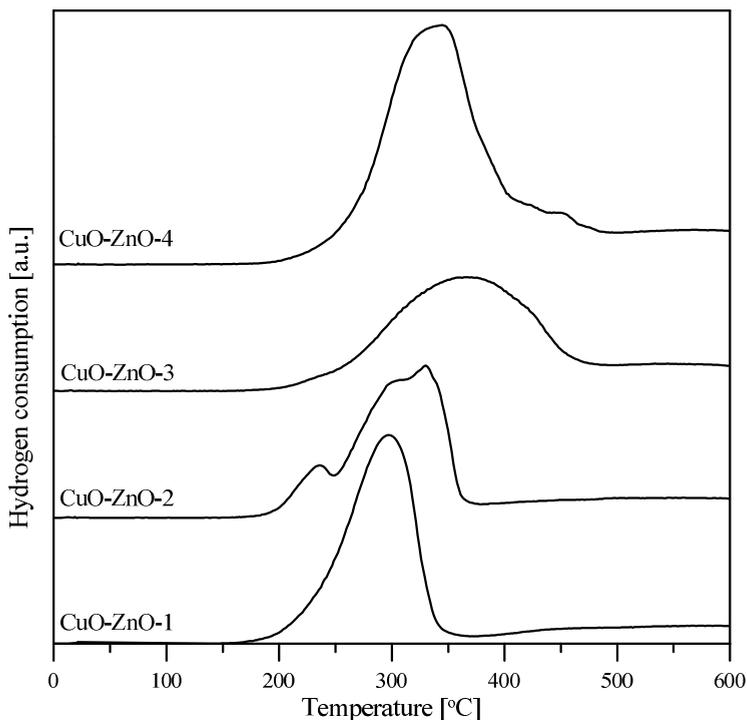
Fig. 6. Temperature-programmed reduction (TPR) of the samples.

4. CONCLUSIONS

Copper-zinc oxides were synthesized by microemulsion method. The sequence of particular stages of preparation have the influence on structural and surface properties of obtained materials. The CuO-ZnO-1 sample, prepared by co-precipitation in microemulsion exhibited the highest specific surface area. The smallest crystals size of both oxides was observed for CuO-ZnO-2 sample. SEM and XRD measurements confirmed formation of CuO and ZnO crystallites of different morphology and size in the samples. DRIFTS and temperature programmed reduction studies shed more light on the formation of and mutual interaction between oxide phases in the samples.

5. ACKNOWLEDGMENTS

REFERENCES

[1] M. Boutonnet, S. Lögdberg and E.E. Svensson, *Current Opinion in Colloid & Interface Science,* **13**, 270, (2008).

[2] A. Bumajdad, J. Eastoe, M. I. Zaki, R. K. Heenan and L. Pasupulety, *Journal of Colloid and Interface Science*, **312,** 68, (2007).

[3] A. Moezzi, A. M. McDonagh and M. B. Cortie, *Chem. Eng. J.*, **185–186**, 1, (2012).

[4] H. Lu, X. Yu, Z. Zeng, D. Chen, K. Bao, L. Zhang, H. Wang, H. Xu and R. Zhang, *Ceramics International*, **37**, 287, (2011).

[5] N. L. Tarwal, K. V. Gurav, S. H. Mujawar, S. B. Sadale, K. W. Nam, W. R. Bae, A. V. Moholkar, J. H. Kim, P. S. Patil and J. H. Jang, *Ceramics International,* **40**, 7669, (2014).

[6] C. Wang, D. Chen and T. Huang, *Colloids and Surfaces A:Physicochem. Eng. Aspects*, **189**, 145, (2001).

[7] I. Capek, *Emulsion Science and Technology*, WILEY-VCH, Weinheim 2009.

[8] G. Xiong, L. Luo, C. Li and X. Yang, *Energy & Fuels*, **23***, 1342, (2009).

[9] S. Hingorani, V. Pillai, P. Kumar, M. S. Multani and D. O. Shah, *Mat. Res. Bull.*, **28**, 1303, (1993).

[10] G. Fierro, M. L. Jacono, M. Inversi, P. Porta, F. Cioci and R. Lavecchia, *Applied Catalysis: General*, **137**, 327, (1996).

[11] S. H. Taylor, G. J. Hutchings, A. A. Mirzaei, *Catalysis Today*, **84**, 113. (2003).

[12] W. Tong, A. West, K. Cheung, K. Yu and S. C. E. Tsang, *ACS Catal.*, **3**, 1231, (2013).

[13] P. Pfeifer, K. Schubert and G. Emig, *Applied Catalysis A: General*, **286**, 175, (2003).

[14] J. Agrell, M. Boutonnet, I. Melián-Cabrera and J. L. G. Fierro, *Applied Catalysis A: General*, **253**, 201, (2003).

CURRICULA VITAE

Justyna Pawlonka was born in Pulawy in 1988. She studied Basic and Applied Chemistry on Maria Curie-Sklodowska University, where she obtained the M. Sc. degree in 2012. Her master thesis entitled: "Decomposition of biodegradable polymers in natural conditions" (supervisors: Prof. dr hab. Janusz Ryczkowski and dr Sylwia Pasieczna-Patkowska) was awarded by the Polish Chemical Society. In 2012 she started her Ph. D. studies in Department of Chemical Technology, on Maria Curie-Sklodowska University in Lublin.

Grzegorz Słowik was born in Włodawa in 1986. He studied Basic and Applied Chemistry on Maria Curie-Sklodowska University, where he obtained the M. Sc. degree in 2010. His master thesis entitled: "Fractionation of selected elements in fly ashes and spend nickel catalyst" (supervisors: dr hab. Ryszard Dobrowolski) was awarded by the Polish Chemical Society. In 2008 he began second studies on Faculty of Mathematics, Physics and Computer Science on Maria Curie-Sklodowska University, where in 2011 received a bachelor's degree from physics. From 2011 he works in the Department of Chemical Technology, on Maria Curie-Sklodowska University in Lublin.

Wojciech Gac was born in Poland in 1967. He was graduated from Maria Curie-Sklodowska University in Lublin in 1992. He received his Ph.D. in chemistry (1996) from the UMCS. He works in the Department of Chemical Technology, Faculty of Chemistry Maria Curie-Sklodowska University in Lublin. His activity is focused on the preparation and characterisation of catalysts and nanostructured materials for production and utilisation of hydrogen and CO oxidation. Scientific coordinator and participant of national and international research projects.

Tadeusz Borowiecki was born in Lublin in 1945. In 1968 he graduated from the Faculty of Mathematics, Physics and Chemistry, Maria Curie-Skłodowska University (MCSU) of Lublin. He received his Ph.D. degree in 1977 and full professor title in 2002. In the period 1996-99 and 1999-2002 he was a Dean of the Faculty of Chemistry. Moreover, from 2005 to 2008 he was a Vice-Rector of MCSU. He is the author of above 150 original papers and 13 patents. His research areas are: heterogeneous catalysis and chemical technology. The studies are focused on: physicochemical properties of catalysts, temperature-programming techniques in catalysts characterization, catalysts deactivation process, processes for obtaining synthesis gas and hydrogen.

ANNALES
UNIVERSITATIS MARIAE CURIE-SKŁODOWSKA
LUBLIN – POLONIA

Influence of volume drop on surface free energy of glass

Diana Rymuszka[a], Konrad Terpiłowski and Lucyna Hołysz

Department of Interfacial Phenomena, Faculty of Chemistry,
Maria Curie-Skłodowska University, Lublin, Poland
[a]*d_rymuszka@vp.pl*

The aim of the research was to determine how the drop size affects the contact angle values and determine its optimal size for further contact angle measurements and comparison of the contact angle values measured for three probe liquids (water, formamide, diiodomethane) on the glass surface using the: sessile drop and tilting plate methods. Next, using the measured contact angles, the total surface free energy and its components were determined from the van Oss et al. (Lifshitz-van der Waals acid- base component, LWAB), Owens-Wendt, Neumann and contact angle hysteresis (CAH) approaches. The studies showed, that drop size is very important for contact angle measurements and consequently, for surface free energy estimation.

Keywords: contact angle, surface free energy.

1. INTRODUCTION

Solid surface properties play a crucial role in many processes in nature, everyday life, agriculture and industry. One of the important properties is wettability, which depends on the surface hydrophilic-hydrophobic nature. The measure of solid surface wettability is the contact angle θ, the one between the solid surface plane and the tangent to the drop settled on this solid surface in the three-phase contact point. Another very important parameter is the solid surface free energy which

provides much valuable information about the surface properties of the examined material. There are many surface free energy approaches but in these studies only four of them will be discussed.

1.1. Owens-Wendt approach

Owens-Wendt [1] assumed that if the interface polar interactions (non-dispersive) appear, then based on Young equation [2] dispersive γ_s^d and polar γ_s^p components can be determined as a geometric function of these components:

$$\gamma_l(1+\cos\theta) = 2(\gamma_s^d \gamma_l^d)^{1/2} + 2(\gamma_s^p \gamma_l^p)^{1/2} - \pi_e \tag{1}$$

Assuming that $\pi_e \cong 0$ and based on the average contact angle values measured for two liquids (apolar and polar), the γ_s^d and γ_s^p components of solid can be calculated. This method is commonly used for surface free energy determination especially for polymers.

1.2. van Oss, Good, Chaudhury approach

Van Oss et al. expressed the surface free energy as a sum of two components: the Lifshitz van der Waals (γ_i^{LW}) component and the acid-basic component of Lewis (γ_i^{AB}) [3]:

$$\gamma_i^{LW} = \gamma^d + \gamma^p + \gamma^i \tag{2}$$

$$\gamma_i = \gamma_i^{LW} + \gamma_i^{AB} \tag{3}$$

According to these authors [4], the acid-basic interactions component (γ_i^{AB}) can be also expressed using the geometric average:

$$\gamma_i = \gamma_i^{LW} + \gamma_i^{AB} = 2\left(\gamma_i^+ \cdot \gamma_i^-\right)^{\frac{1}{2}} \tag{4}$$

Based on this model, adhesion work can be expressed with the components:

$$W_A = \gamma_l(1+\cos\theta) = 2\sqrt{\gamma_s^{LW}\gamma_l^{LW}} + 2\sqrt{\gamma_s^+\gamma_l^-} + 2\sqrt{\gamma_s^-\gamma_l^+} \tag{5}$$

The γ_s^{LW} component and γ_s^+, γ_s^- parameters of the surface free energy can be determined from equation (5) by measuring the contact

angles of three different polarity liquids whose surface tension components are known: γ_l^{LW}, γ_l^+ and γ_l^-. Solving three equations with three unknowns (γ_s^{LW}, γ_s^+, γ_s^-) allows determination of the surface free energy components (γ^{LW}, γ^{AB}) and finally the total surface free energy value.

2.3. Neumann approach

In contrast to the surface free energy estimation methods based on its separation into the independent components, where using two or three different liquids is required, in the Neumann approach only one liquid is desirable [5]:

$$(\gamma_s/\gamma_l)^{0.5} \exp[-\beta_1(\gamma_l - \gamma_s)^2] = 0.5(1 + cos\theta) \tag{6}$$

2.4. Contact angle hysteresis

Chibowski proposed a quantitative interpretation of the contact angle hysteresis (CAH) [6, 7]. He related the total surface free energy of solid (γ_s^{tot}) with the three measurable parameters: advancing (θ_a) and receding (θ_r) contact angles and liquid surface tension (γ_L) used during measurements. The surface free energy estimated in this way depends on the interaction type and its size occurring at the interface.

$$\gamma_s^{tot} = \frac{\gamma_1(1 + \cos\theta_a)^2}{(2 + \cos\theta_r + \cos\theta_a)} \tag{7}$$

3. MATERIALS AND METHODS

3.1. Materials

20 mm x 30 mm glass plates (Comex, Wrocław, Poland) which were cut from microscope slides were used during the studies. Before measurements the plates were washed with water containing detergent, and then rinsed with the Milli-Q 185 system water several times. The next step included plates washing in methanol and doubly-distilled water in the ultrasonic for 15 minutes and then dried in a dryer. Before contact angle measurements all plates were stored in a desiccator.

The liquids used during the contact angle measurements: diiodomethane (99%, Aldrich, Germany), formamide, (98%, Aldrich, Germany, deionizated water Milli-Q 185 (pH ≈ 6.5).

The liquids used during the glass plates preparation: methanol, (POCH S.A, Poland), redestillated water.

3.2. Methods

Contact angle measurements using the sessile drop method

Digidrop GBX Contact Angle Meter (France) equipped with the video-camera system and computer software was used for the contact angle measurements by the sessile drop and tilting plate methods. In the sessile drop method, the advancing contact angles of water and two other probe liquids, diiodomethane and formamide of 1, 2, 3, 4, 5, 6, 7, 8 μl volume were measured after settling droplets with appropriate drop volume on the glass surface. Then after sucking of 1/3 from the droplet into the syringe, the receding contact angle was measured. The contact angles of probe liquids were measured at $20 \pm 1°C$ in a closed chamber.

Contact angle measurements using the tilting plate method

Using the tilting plate method the contact angles were measured on the glass surface which is inclined relative to the optical axis and in that position liquid gathered on one side of the droplet and retracted on the other one. The droplet was set in the chamber in front of the Contact Angle Apparatus camera and then using a small table, droplet was tilted at the appropriate angle. The whole process was filmed. Then the frame of a movie piece in which the droplet was the most deformed but did not slide from the surface was chosen and the advancing (in front of droplet) and receding (rear drops) contact angle were measured using the "Manual mode 1" method.

Surface free energy estimation

The total surface free energy and its components were determined based on the measured contact angles for three probe liquids (water, formamide, diiodomethane) from van Oss et al. (Lifshitz-van der Waals acid- base component, LWAB), Owens-Wendt, Neumann and contact angle hysteresis (CAH) approaches.

Surface roughness

The surface mapping studies was carried out by AFM method using a standard silicon tip in the "contact mode", at room temperature in an open system. The results were processed with the program WSxM 4.0, Develop 8.0.

4. RESULTS AND DISCUSSION
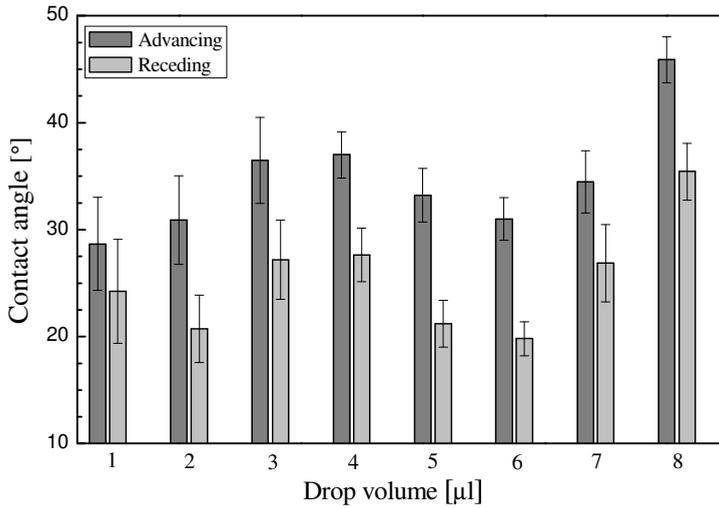
Fig. 1. Values of advancing and receding contact angles measured for water on the glass surface.

As is it shown in Fig. 1 in a range of values, the water contact angles depend on the droplet volume used for measurements. The contact angle of $1 \, cm^3$ droplet was the smallest volume with the biggest standard deviation. The surface covered with the drop during measurements was about $0.6 \, mm^2$. However, the average roughness on the glass surface determined by the AFM technique was 2.6 nm (Fig. 3). Large deviation shows that the droplets with that volume are very sensitive to the local surface irregularities. Therefore using such small droplets is not appropriate because they are not representative even with such small surface roughness. It seems that the larger volume of droplets ($2 – 4 \, cm^3$) is not so sensitive to the glass surface irregularities but the standard deviation is still about twice larger than that for droplets with a slightly larger volume. The water contact angles measured on the glass surface in the range of $5 – 7 \, cm^3$ are much more representative because the surface

area occupied by the droplets is larger. They are not so sensitive to the local surface irregularities, as indicated by the standard deviation. However, for 7 cm^3 drop volume and larger, gravity has much bigger influence on the contact angle measurements (Fig. 2). The standard deviation of droplets volume from 2 to 8 cm^3 does not exceed 1.4°.
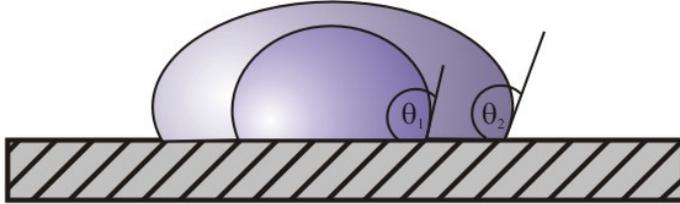

Fig. 2. Liquid droplets behaviour on the solid surface depending on the droplet volume.

As shown in Fig. 2, the contact angle θ_2 is a little larger than θ_1. Although, using droplets with much larger volume causes that they occupy much bigger surface and are less sensitive to the local heterogeneity which leads to the gravity influence exposure. Based on the obtained results (Fig. 1) 6 cm^3 droplets seem to be optimal for the contact angle measurements.

Very similar studies were carried out by Good and Koo [8]. They investigated the droplet volume influence on the advancing and receding contact angles. As the experimental materials teflon and poly(methyl methacrylate) were used and as the tested liquids: water, ethyl glycol and decane. The contact angles were measured for a different droplet diameters 0.1 – 1.2 cm. The studies show that the contact angle can increase with diameter droplet increasing to reach a certain threshold value typical of the solid-liquid system. This increase is particularly pronounced in the case of water droplets deposited on the teflon. The contact angle rises by 15° when the droplet diameter increases in the 0.1 – 0.4 cm range. The authors explained this effect with as due to the existence hydrophobic areas on the teflon surface.

In the process of his studies including the effect of droplet size on the contact angle and using various solid surfaces Drelich [9], found that advancing contact angles in many real systems, namely smooth homogeneous, heterogeneous, slightly heterogeneous and other surfaces, were practically constant until the 7 mm water droplets diameter was achieved.

During the studies of solid surfaces covered with a wax layerobserved contact angle changes with the droplet volume changes [10]. The contact angles changed from 50° to 90° if the droplet volume was $0.4 – 3.65$ cm^3. For small droplet (0.1 cm^3 – 0.4 cm^3) the contact angle was almost constant at 88° – 90°. Mack, like other researchers, attributed this relationship to the result of the gravity presence. In light of the above studies it is difficult to agree with the results of the research presented by Mack. In order to eliminate the gravity effect, the droplets volume should not exceed 0.5 cm^3. As was it shown earlier, the droplets are very sensitive to the local surface heterogeneity.

He, Neelesh and Patankar studied out the drop volume influence on the contact angle on rough surfaces [11]. Water contact angles were measured on the rough polydimethylsiloxane surface modified with plasma. The water droplets volume on the surface changed from 1 to 8 cm^3. The aim of the study was to compare the droplets volume effect on the measured contact angle in two states: when the liquid wets the surface completely (Wenzel state) and when the ruggedness does not allow for the complete surface wetting (Cassie-Baxter state). In all described cases the contact angle increases with the increasing drop volume. This is much clearer for the droplets whose behaviour on the surface can be explained by the mechanism proposed by Wenzel. Confirmation of the hypothesis that gravity does not affect smaller droplets can be found by computer simulations carried out by Vafei and Podowski [12].

Considering the theoretical issue of the droplet size effect on the contact angle Iwamatsu [13] modified the Cassie equation [14]. He assumed the cylindricity droplet shape and considered chemically heterogeneous smooth solid surface. He concluded that the contact angle is a linear volume function. The line slope is different and depends on the surface hydrophobicity on which the contact angle was measured. In the light of the research carried out in this paper, the calculations presented by Iwamatsu only for the $1 – 3$ μm volume range can be confirmed.

a)

b)

R_{rms}= 0.94 nm, Av. Heigh = 2.6 nm

c)
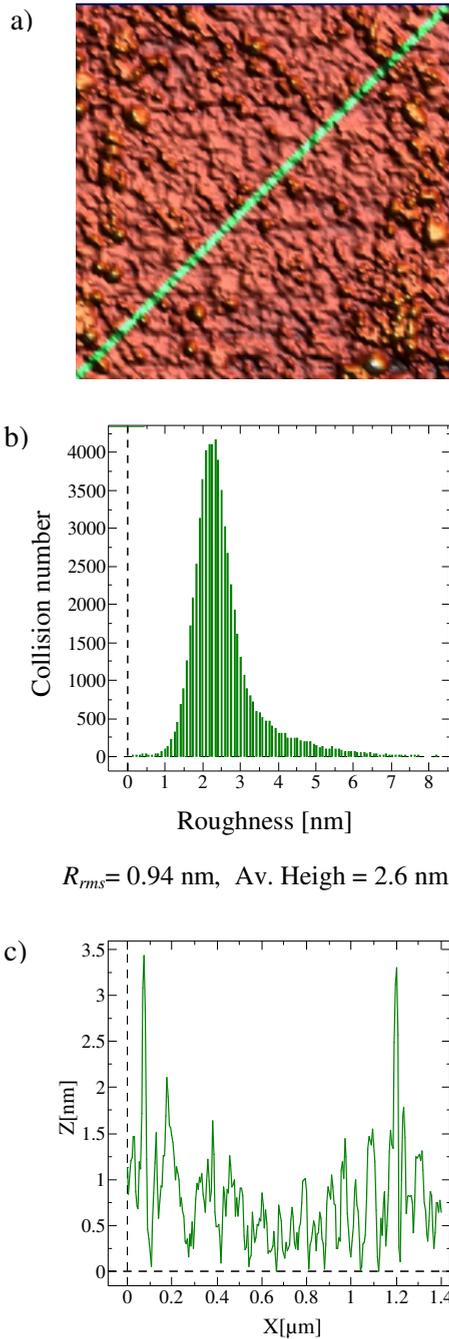
Fig. 3. a) 3D AFM glass mapping (1 μm x 1 μm); b) Roughness distribution of the examined surfaces and R_{rms} and average roughness; c) Surface profile along the line shown in 3D imaging.

The glass surface shown in Figure 3 is characterized by roughness distribution relocated toward higher values. The average roughness is 0.94 nm and R_{rms} = 2.6 nm. The surface profile shows two distinct spikes in the roughness distribution.

Detailed description of the topographical nature of the surface roughness is important because the volume of liquid particles used for the contact angle measurements is significantly different: for diiodomethane 134 Å^3, water 30 Å^3 and formamide 66 Å^3. Therefore, water can more easily penetrate into the surface grooves than the other liquids. However, liquid behaviour on the solid surfaces depends also on its surface tension and polar interactions on the solid.
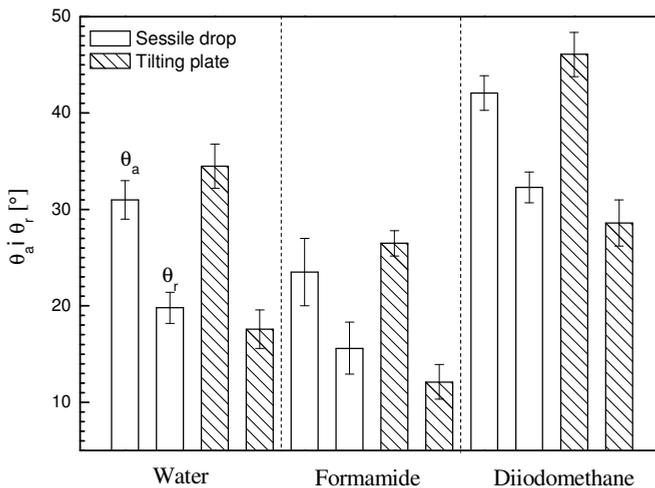

Fig. 4. Advancing (θ_a) and receding (θ_r) contact angles of probe liquids measured on the glass surface using the sessile drop (empty columns) and tilting plate methods (hatched columns).

Advancing and receding contact angles of probe liquids measured by both techniques are shown in Fig. 4. The advancing contact angles measured using the tilting plate method are larger by several degrees in comparison to the contact angles measured by the sessile drop method. The receding contact angles measured using the tilting plate method are mostly lower than those measured using the sessile drop method. The diiodomethane contact angle hysteresis shows large differences between two methods used for contact angle measurements. This is an apolar liquid which interacts with the solid surface practically only by dispersion forces $\gamma_l \approx \gamma_l^d = 50.8$ mJ/m^2, and for water $\gamma_l^d = 21.8$ mJ/m^2, formamide

$\gamma_l^d = 39.0$ mJ/m^2 [15]. Therefore it can be concluded that dispersive interactions are primarily responsible for the differences in the values of hysteresis. Furthermore, a diiodomethane molecule has four times larger volume in comparison to the water molecule and twice to formamide. It can be explained by small diiodomethane hysteresis using the mechanism proposed by Cassie Baster, assuming air-filled voids existence under the droplet. Based on the measured contact angles of probe liquids, it can be seen that there is no simple relationship between the surface roughness and the surface tension of the liquid and its contact angle.

Table 1. Contact angle hysteresis values measured on the glass plates using the sessile drop and tilting plate methods.

| Method	Liquids		
	water	formamide	diiodomethane
Sessile drop	11.2 ± 1.8	7.9 ± 3.1	9.8 ± 1.7
Tilting plate	16.9 ± 2.2	14.4 ± 1.5	17.5 ± 2.4
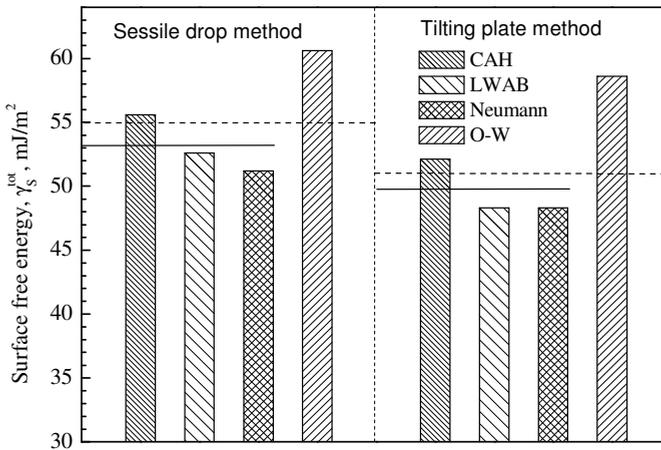
Fig. 5. Surface free energy calculated from different theoretical approaches to the glass surface.

Based on the contact angles measured using both methods shown in Fig. 4 the surface free energy was calculated using the theoretical approaches: contact angle hysteresis (CAH), van Oss, Good, Chaudchury (LWAB), Neumann and Owens-Wendt approaches. The results of surface

free energy estimation are presented in Fig. 5. The dashed horizontal line in the figure indicates the arithmetic average of all used theoretical approaches. However, the Owens - Wendt approach gives the highest surface free energy value, so the horizontal continuous line indicated the arithmetic average of the three approaches: contact angle hysteresis (CAH), van Oss, Good Chaudchury (LWAB) and Neumann. The surface free energy calculated from the contact angle hysteresis is the arithmetic average of the energy calculated for the three probe liquids: water, diiodomethane, formamide. The highest surface free energy values were observed for the surface free energy calculated using the Owens – Wendt and the CAH approaches. Higher contact angle hysteresis values are observed for the contact angles measured using the tilting plate method. Not much higher surface free energy values are observed from the estimation based on the contact angles measured using the sessile drop method but both contact angle measurement techniques: sessile drop and tilting plate, can be widely used for energy calculations from the contact angle hysteresis.

2. CONCLUSIONS

The contact angle of 1 cm^3 droplet was the smallest volume with the biggest standard deviation. The water contact angles measured on the glass surface in the range of 5 – 7 cm^3 are much more representative because the surface area occupied by the droplets is higher. They are not so sensitive to the local surface irregularities. For a 7 cm^3 drop and larger, gravity has much bigger influence on the contact angle measurements. Based on the obtained results 6 cm^3 droplet volume seems to be the optimal for the contact angle measurements. The advancing contact angles measured using the tilting plate method are larger by several degrees in comparison to the contact angles measured by the sessile drop method. On the other hand, the receding contact angles measured using the tilting plate method are mostly lower than those measured using the sessile drop method. Furthermore, the largest surface free energy values were calculated using the Owens-Wendt and the CAH approaches. The surface free energy estimated using the contact angles measured by means of the sessile drop method is 4 mJ/m^2 larger.

REFERENCES

[1] D. K. Owens, R. C. Wendt, *J. Appl. Polymer. Sci.,* **13**, 1741, (1969).
[2] T. Young, *Philos. Trans. R. Soc.* London, **95**, 65, (1895).
[3] C. J. van Oss, R. J. Good, M. K. Chaudhury, *Langmuir,* **4,** 884-891, (1988).
[4] R. J. Good, M. K. Chaudhury, *Plenum Press*, New York, 153, (1991).
[5] M. Żenkiewicz, POLIMERY 52, no. **10**, 764 (2007).
[6] E. Chibowski, VSP, Utrecht 2002, Netherlands.
[7] E. Chibowski, *Advances in Colloid and Interface Science*, **103**, 149–172, (2003).
[8] R. J. Good, M. N. Koo, *J. Colloid Interface Sci.,* **71**, 2, 283, (1979).
[9] J. Drelich, *J. Adhesion,* **63,** 31, (1997).
[10] G. L. Mack, *J. Phys. Chem.,* **40,** 159, (1936).
[11] B. He, J. Lee, N. A. Patankar, *Colloids and Surf. A.,* **248,** 101, (2004).
[12] S. Vafei, M. Z. Podowski, *Nuclear Engineering and Design,* **235,** 1293, (2005).
[13] M. Iwamatsu, *J. Colloid Interface Sci.,* **297,** 772, (2006).
[14] A. B. D. Cassie, Discuss. *Faraday Soc.,* **3,** 11, (1948).
[15] W. Mizerski, *Tablice chemiczne*, Adamant, Warszawa, 2008.

CURRICULUM VITAE

Diana Rymuszka. PhD student of Maria Curie-Skłodowska University in Lublin, Poland, Department of Interfacial Phenomena, Faculty of Chemistry.

Konrad Terpiłowski. Assistant Professor, Department of Interfacial Phenomena, Faculty of Chemistry, Maria Curie Skłodowska University in Lublin, Poland. Author of several dozen publications.

Enhancing the separation of enantiomers in adsorbed overlayers: a Monte Carlo study

Aleksandra Woszczyk[a] and Paweł Szabelski[b]

*Department of Theoretical Chemistry, Maria Curie-Sklodowska University,
M. Curie-Sklodowskiej Sq.3, 20-031 Lublin, Poland*
[a]*ola_w@vega.umcs.lublin.pl*
[b]*szabla@vega.umcs.lublin.pl*

The influence of external factors on the chiral resolution of enantiomers in adsorbed overlayes has been especially interesting form the perspective of creation of chiral surfaces. Chiral segregation of this type can be induced or enhanced, for example, by an external unidirectional fields such as magnetic or electric field. To explore the effect of an external field on the 2D chiral resolution of model enentiomers we performed cannonical Monte Carlo simulations on a square lattice of equivalent adsorption sites. The adsorbed molecules which are sensitive to the external field, were assumed to consist of four identical segments and they were able to adopt four possible orientations on a square lattice. Short-range segment-segment interactions limited to the nearest neighbours on the lattice were allowed to account for the intermolecular interactions. The calculations were performed for two exemplary molecular structures and the strength of the external field was gradually increased in each case. The preliminary results described herein demonstrate that continuously changed external fields can induce chiral resolution of enantiomers of appropriate geometry. The insights from this study can be useful in developing strategies for 2D chiral separations in which external stimuli are used.

Keywords: adsorbed overlayers, chiral resolution, self-assembly, external field

1. INTRODUCTION

Formation of chiral adsorbed overlayers can occur due to adsorption of both chiral and prochiral molecules on solid substrates, leading to the creation of mirror image domains [1]. The spontaneous segregation of enantiomers into homochiral domains has been observed in a number of cases [2-4], but this process is difficult to control and it usually depends on many external parameters (e.g. temperature, concentration etc.). One factor which has been found to enhance the chiral segregation is the unidirectional positioning of the adsorbed molecules which can be imposed by the underlying surface or by external fields. For example, this effect has been observed for the surface-assisted resolution of prochiral derivative of quinacridone adsorbed on Cu (110) whose atomic rows are guiding lines for the adsorbed enantiomers [10]. Similarly, using undirectional magnetic field in combination with liquid crystal imprinting uniaxial arrangement of prochiral molecules adsorbed on graphite surface has been obtained [11]. In order to understand and predict the chiral separation in adsorbed overlayers, one can use theoretical methods such as the Monte Carlo (MC) simulation method. MC simulations have been performed for a variety of simplified molecular chiral structures adsorbed on energetically homogeneous surfaces, including bent needles [5], tripods [6] and other polyatomic molecules [7, 8]. These studies have demonstrated that the main effect on the chiral separation exert: density of the adsorbate [9], geometry of the molecules and intermolecular interactions. Careful manipulating of these factors makes it possible to start-up or enhance the self-organization of adsorbed species. In this contribution we use the MC simulation method to assess the effect of uniaxial external field with continuously changing strength on the 2D segregation of surface enantiomers of a prochiral molecule. To that end we use a modified version of the model proposed previously [10] and we additionally compare the simulated results with those obtained for a molecule with the same composition but different geometry.

2. MODEL AND SIMULATION

We consider four-segment molecules **A** and **B** (Fig. 1) adsorbed on a planar surface represented by a square lattice of equivalent adsorption sites. Note that, molecule **A** is chiral in 2D yet because of the Γ-shaped geometry. In the case of molecule **B**, the source of chirality is the dipole

moment without which this molecule is achiral in 2D. Each enantiomer of the prochiral molecule **A** was allowed to adopt one of the four possible orientations on the lattice. The same orientations were assumed for the molecule **B** shown in the right panel. The molecules were allowed to interact via short-range segment-segment interaction potential limited to the nearest neighbours on a square lattice, as shown in the bottom part of Fig. 1.
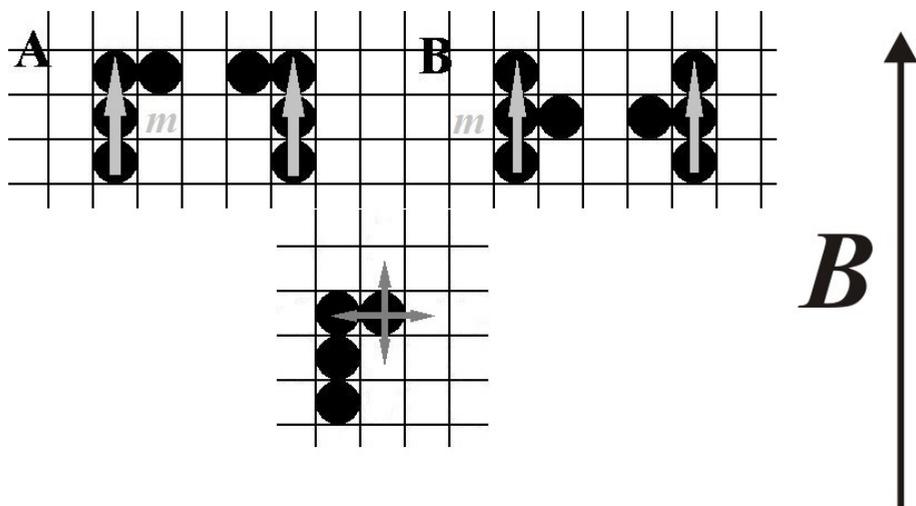

Fig. 1. The molecules **A** and **B** used in the simulations. Molecular (magnetic or electric) moment *m* aligned parallel to the long molecular arm of A and B and the direction of the external field *B* are shown by the grey and black arrows, respectively. The arrows in the bottom part show the range of segment-segment interaction assumed in the model.

The energy of interaction between a pair of neighbouring segments was characterised by the parameter $\varepsilon = -2$ expressed in *kT* units. To take into account sensitivity of the molecule to the external field we assumed that it has a (magnetic or electric) dipole moment parallel to the long molecular axis. Energy of the adsorbed molecule in static field parallel to the surface is given by the scalar product of vectors *m* and *B*:

$$E = -\boldsymbol{m}\cdot\boldsymbol{B} = -mB\cdot cos\theta \tag{1}$$

where *m* is the dipole moment of the molecule (in our studies $m = 1$), *B* is the strength of the field and θ is the angle between *m* and *B*. Although, there are four possible orientations of the molecules, there are only three possible values of the energy *E,* that is: $-mB$ for *m* facing upwards (Fig. 1), mB for *m* facing downwards and zero for *m* aligned horizontally.

The simulations were performed on a 100 by 100 lattice with 900 adsorbed molecules (racemic mixtures) using the conventional canonical ensemble with Monte Carlo method for rigid polyatomic molecules with orientationally biased sampling [11]. Periodic boundary conditions were imposed to eliminate edge effects. The simulation algorithm was organized as follows. At the beginning of the simulation the molecules were randomly distributed over the surface. Next a molecule was chosen randomly and trial displacement was attempted by random choice of new coordinates of the reference segment of that molecule. In a new place four trial orientations were generated by rotating the molecule around the reference segment and for each of these trial orientations potential energy was calculated (sum of segment-segment interactions and coupling with external field). The same calculations were performed in the original position of the molecule. To determine the acceptance probability of the new configuration we defined the Rosenbluth factor for both old (W_o) and new (W_n) position:

$$W_o = \exp[-\beta U_0] + \sum_{i=1}^{3} \exp[-\beta U_i] \tag{2}$$

$$W_n = \sum_{i=1}^{4} \exp[-\beta U_i] \tag{3}$$

U_0 – potential energy in initial orientation, U_i – potential energy in trial orientation i, $\beta = (kT)^{-1}$ where k is the Boltzmann constant

Next, one of the orientations in the new position was selected with the probability:

$$p_j = \frac{\exp[-\beta U_j]}{\sum_{i=1}^{4} \exp[-\beta U_i]} \tag{4}$$

Comparison of the ratio of the Rosenbluth factors in the new and the old position with a random number $r \in (0,1)$ allowed us to decide whether the move should be accepted or rejected. Specifically, if W_n/W_o was greater than r, the new position and orientation of the molecule was accepted. Otherwise the molecule was left in its original position. The simulations were performed using up to 10^8 MC steps, where one MC step is a single trial to move (and rotate) each of N molecules to a new position on the lattice.

3. RESULTS AND DISCUSSION

Figure 2 shows snapshots of the overlayers obtained for molecules **A** and **B** (racemates) without the external field. For clarity the enantiomers of **A** and **B** were coloured differently. As it can bee seen in Fig. 2 both simulated overlayers are compact and strongly disordered with equal occurrence of the four orientations allowed in the model.
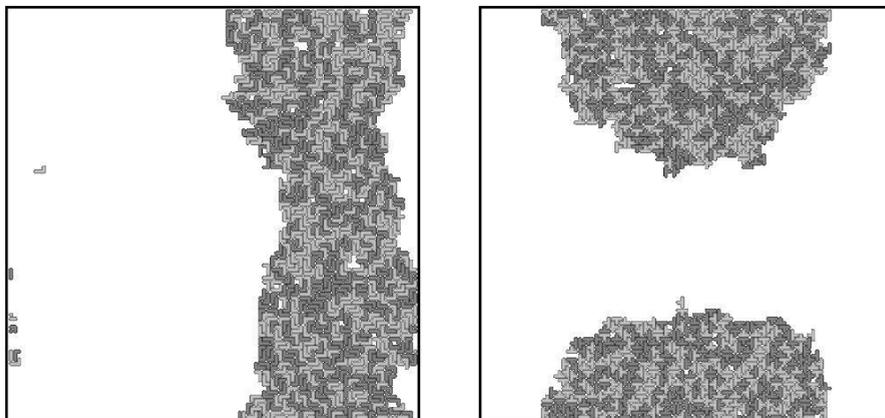

Fig. 2. Snapshots of the overlayers comprising 900 molecules of **A** and **B** (right) simulated under no external field.

When the strength of the external field increases, that is the product *mB* becomes larger, ordering of the adsorbed molecules occurs, so that the molecules are aligned parallel to the field, as shown in Fig. 3.
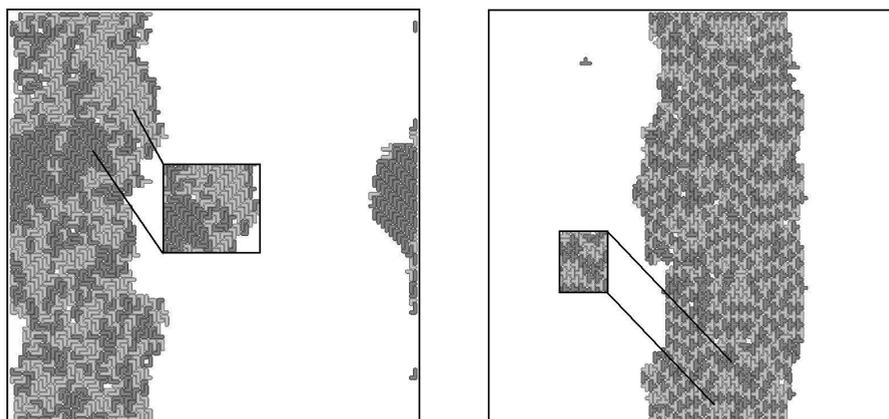
Fig. 3. Snapshots of the overlayers obtained for $mB = 0.76$ (left **A**, right **B**). The insets in both parts are magnified fragments of the corresponding structures.

This tendency is more visible for **B** whose almost all molecules are oriented vertically. For the molecule **A** the external field is responsible for the growth of homochiral domains which are, however, still embedded in a pool of randomly oriented enantiomers.

Further increase of *mB* induces a complete separation of the enantiomers of **A** resulting in the creation of two large homochiral domains, as showed in Fig. 4. In the case of **B** the effect of the external field is only minor compared to the previous situation and it refers to the enhanced formation of alternate rows of molecules whose side segments face the opposite directions (see the inset, Fig. 4).
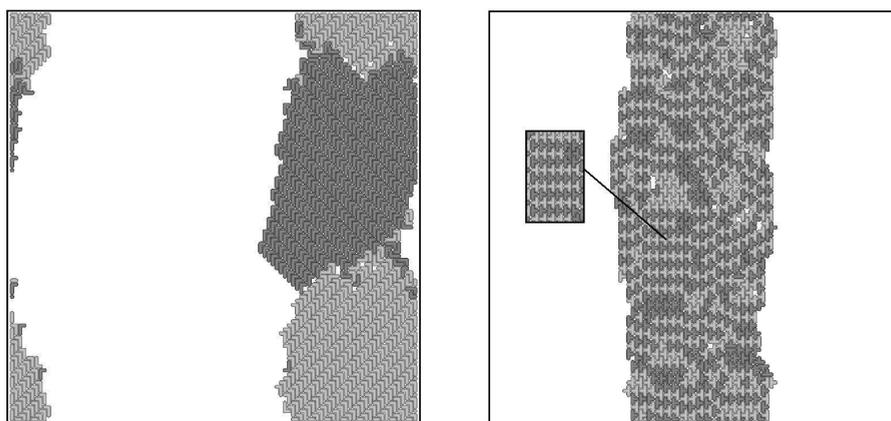

Fig. 4. Snapshots of the overlayers obtained for molecule **A** (left) and molecule **B** (right) for *mB* = 0.82. For molecule **A** two large homochiral domains can be observed. The inset in the right panel shows alternating rows in the domain of **B**.

To quantify the effect of the external field on the structure formation in the systems comprising molecules of **A** and **B** we calculated the average number of heterogenous segment-segment bonds in the simulated overlayers. This quantity means the average number of interactions that a single segment in the enantiomer of given type (colour) forms with foreign neighbouring segment.

As shown in Fig. 5, for the molecule **A** the number of heterogeneous bonds exhibits a rapid decrease at *mB* equal to about 0.8. This effect is a clear manifestation of the chiral resolution which minimizes the number of contacts between different enantiomers of **A**. In consequence above this critical value of *mB* the only contribution to the number of heterogeneous bonds comes from the molecules which are placed at the boundary of the contacting domains. For the molecule **B** we can observe

a different trend, that is the number of heterogeneous bonds increases with the strength of the applied field. In this case, the field is responsible for the formation of locally ordered structures of alternating rows of molecules of different colour. This structure offers more heterogeneous contacts compared to the structure obtained without the field for which numerous clusters comprising randomly oriented molecules of one colour can be identified (see Fig. 2).
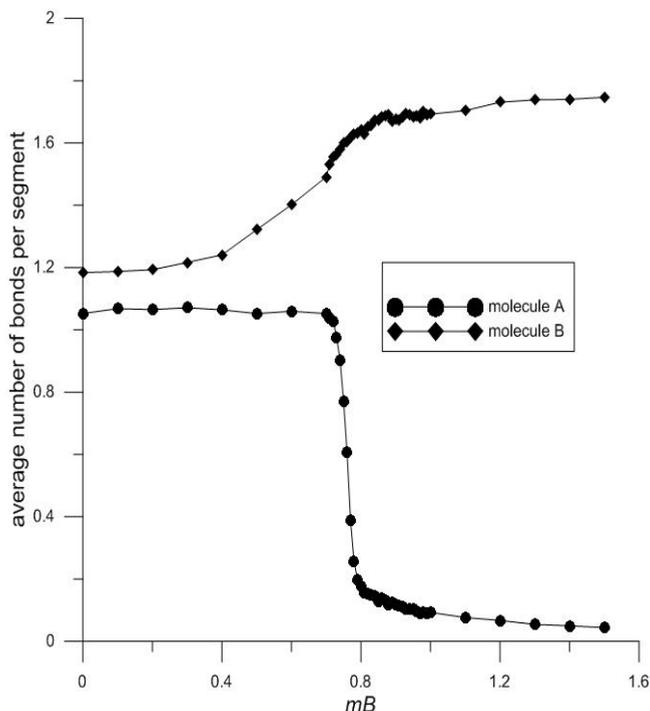

Fig. 5. Changes in the average number of heterogenous bonds per segment as a function of the external field.

4. CONCLUSIONS

The preliminary results of this work demonstrate that the directional external field can greatly promote separation of prochiral molecules into extended enantiopure domains. As we demonstrated, the segregation can be triggered by a substantial adjustment of a continuously changed uniaxial field. The conclusions from this theoretical studies can be useful in developing new experimental techniques in which directional magnetic or electric fields are used to induce controlled resolution of enantiomers

in adsorbed overlayers. To explore the dependency of the resolution on such factors as molecular geometry and density of the adsorbed phase further studies are needed and these factors are the subject of our ongoing research.

REFERENCES

[1]   S. M. Barlow, R. Raval, *Surf. Sci. Rep.,* **50**, 201 (2003).
[2]   J. V. Barth, *Annu. Rev. Phys. Chem*., **58**, 375 (2007).
[3]   J. Barth, G. Costantini , K. Kern, *Nature,* **437**, 671 (2005).
[4]   A. Kühnle, *Curr. Opin. Coll. Int. Sci*., **14**, 157 (2009).
[5]   R. Perusquía, J. Peón, J. Quintana, *Physica A*, **345**, 130 (2005).
[6]   I. Medved', A. Trník, D. A. Huckaby, *Phys. Rev. E*., **80**, 011601 (2009).
[7]   I. Medved', A. Trník, D. A. Huckaby, *J. Stat. Mech*., **12**, P12027 (2010).
[8]   I. Paci, I. Szleifer, M. A. Ratner, *J. Am. Chem. Soc*., **129**, 3545 (2007).
[9]   I. Paci, *J. Phys. Chem. C*, **114***,* 19425 (2010).
[10] P. Szabelski, A. Woszczyk, *Langmuir,* **28**, 11095 (2012).
[11] D. Frenkel, B. Smit, *Understanding Molecular Simulation From Algorithms to Applications,* Academic Press, 2002.
[12] H. Cun, Ye Wang, B. Yang, L. Zhang, S. Du, Yu Wang, K.-H. Ernst, H.-J. Gao, *Langmuir,* **26**, 3402 (2010).
[13] A. M. Berg, D. L. Patrick, *Angew. Chem. Int. Ed*., **44**, 1821 (2005).

CURRICULA VITAE

Aleksandra Woszczyk. Born in 1988. Graduated from the Faculty of Chemistry of Maria Curie-Sklodowska University in Lublin in 2012. After graduation she started Ph. D. studies in Department of Theoretical Chemistry of the same university. Her research interests: adsorption, theoretical modelling of chiral resolution in adsorbed overlayers, computer simulations.

Paweł Szabelski. Born in Lublin, Poland in 1972. In 1996 graduated from the Faculty of Chemistry of Maria Curie-Skłodowska University in Lublin. In 2000 received Ph.D. from the same university. Employed as an assistant lecturer (2000) and next as an assistant professor (2001) in the Department of Theoretical Chemistry, UMCS. Post doctoral studies (2000-2001) at the University of Tennessee, Knoxville, TN, USA. In 2003 and 2004 awarded the stipend for young scientists from the Foundation for Polish Science. In 2006 awarded Fulbright Advanced Research Grant at Carnegie Mellon University, Pittsburgh, PA, USA. Employed as an associate professor since 2012. Main research interests: statistical mechanics of adsorption, computer simulations, chiral surfaces and molecules.

Recenzenci prac zamieszczonych w tym tomie:

1. Piotr Borowski
2. Jacek Goworek
3. Adam Marczewski
4. Jolanta Narkiewicz-Michałek
5. Janusz Ryczkowski
6. Katarzyna Tyszczuk-Rotko